DIFFRACTION AND RADIATION OF WATER WAVES BY TWO COAXIAL VERTICAL CYLINDERS

by

Mohammad Hassan

DEPARTMENT OF MATHEMATICS
INDIAN INSTITUTE OF TECHNOLOGY GUWAHATI,
GUWAHATI-781 039, INDIA

September, 2014

DIFFRACTION AND RADIATION OF WATER WAVES BY TWO COAXIAL VERTICAL CYLINDERS

A thesis submitted
in partial fulfillment of the requirements
for the degree of

DOCTOR OF PHILOSOPHY

by

Mohammad Hassan
(Roll Number: 09612317)

to the

DEPARTMENT OF MATHEMATICS
INDIAN INSTITUTE OF TECHNOLOGY GUWAHATI, INDIA

September, 2014

CERTIFICATE

It is certified that the work contained in the thesis titled **"Diffraction and radiation of water waves by two coaxial vertical cylinders"** by **Mohammad Hassan**, a student in the Department of Mathematics, Indian Institute of Technology Guwahati, for the award of the degree of Doctor of Philosophy has been carried out under my supervision and this work has not been submitted elsewhere for a degree.

September, 2014

Dr. Swaroop Nandan Bora
Professor, Department of Mathematics
Indian Institute of Technology Guwahati, India

Dedicated

to

My Mother

and

the Memory of My Father

Acknowledgement

It has been a great pleasure and privilege to express my deep sense of gratitude and everlasting indebtedness to my thesis supervisor Prof. Swaroop Nandan Bora who introduced me to the area of research in water wave theory and other allied branches of applied mathematics. I am immensely grateful to him for his enthusiasm, continuous encouragement and guidance which have been the main source of inspiration during the preparation of this thesis. I am also thankful to him for making me feel free in expressing my views and for sharing an excellent rapport with me. Without his help this work could not have been accomplished.

I owe my thanks to my doctoral committee members Prof. D. C. Dalal, Prof. Natesan Srinivasan and Dr. Siddhartha P. Chakrabarty for their valuable suggestions and meaningful comments. My sincere thanks go to Prof. R. C. Srivastava, D. D. U. University, Gorakhpur, for his constant encouragement for pursuing research.

I am very much grateful to my late father who was a great blessing and a source of continuous inspiration to me while he was alive and he still continues to be. He would have been the happiest person in this world to see the completion of my degree. Special gratitude goes to my wife Farzana for her support, encouragement, patience and taking care of our lovely son Ayan. I thank my 18-month-old son for easing my pressure at work through his sweet smile and innocence. My heartfelt gratitude is due to my elder sisters and brothers-in-law for their constant encouragement, inspiration, patience and immense affection throughout my research period. I offer my special thankfulness to Mr. Rahmat Ali and Mr. Samsuddin Ahamed for their support, not only for my research work but also for my life till date, which will be treasured in my memory forever.

I would like to offer my special thanks to my friends Vinod, Swargdeep, Abdul and Servesh for their encouragement during my research work. I would also like to thank Gowrisankar, Hanif, Akhilesh, Parvendra, Abu Talat, Dinesh, Himadri, Jitender, Murli, Nasim, Raj Bhawan, Biswajit and other friends here at Indian Institute of Technology Guwahati for their co-operation and pleasant company during my stay.

Finally, I would like to thank Indian Institute of Technology Guwahati for providing me with financial assistance in the form of Junior Research Fellowship and Senior Research Fellowship and the necessary facilities during my stint here.

September, 2014

Mohammad Hassan
Department of Mathematics
Indian Institute of Technology Guwahati

Abstract

The main objective of this thesis is to investigate the wave forces and hydrodynamic coefficients of two coaxial cylindrical structures in water of finite depth within the framework of linear water wave theory. We consider two coaxial vertical cylinders - one a riding hollow cylinder and the other a solid cylinder. This system consisting of two such vertical cylinders is considered as idealization of a buoy and a plate.

In this study, we consider the fluid to be incompressible, homogeneous, inviscid, and the motion irrotational. First, the problem describing wave interaction with two coaxial cylindrical bodies, with one floating and the other submerged, is divided into two parts: one describing the diffraction of water waves by the fixed structure and the other describing the radiation of water waves by the body into otherwise calm water. It is to be noted that the radius of the submerged cylinder (lower solid cylinder) is greater than or equal to that of the floating cylinder (upper hollow cylinder). The radiation problem is further split into a number of parts, each of which corresponds to the moving body in a separate mode of motion. The physical problem involving diffraction or radiation is reduced to a boundary value problem governed by the three-dimensional Laplace's equation. The method of solution is based on the separation of variables and matched eigenfunction expansion technique. In the study of floating structures, an eigenfunction expansion, along with matching technique, is widely used due to its considerable accuracy. By using these techniques, the analytical expressions for the diffracted potentials and radiated potentials are presented, and by applying the appropriate matching conditions, which ensure the continuity of velocity and pressure along the virtual boundaries between two consecutive regions, we obtain a system of linear equations in each case which is solved for the unknown coefficients. The analytical expressions of the diffracted potentials and the radiated potentials, respectively, allow us to obtain the wave forces acting on the fixed cylindrical body and hydrodynamic coefficients, namely, the added mass and damping coefficient, acting on the cylindrical body for different modes of motion such as surge and roll. Since there exists no bottom for the hollow cylinder, we need to consider the translational wave force in the horizontal direction only. We carry out the investigation for two cases: first when the lower cylinder is bottom-mounted and then when it is raised to a finite height above the bottom. We also investigate our problem for the particular base case when the lower cylinder is absent, i.e., the case having only the floating cylinder tethered to the sea-bed. Sets

of values exciting force and hydrodynamic coefficients are obtained for different radii of the cylinders, different gaps between the cylinders, different drafts of the cylinder, etc. It is observed that changes in the radii of the cylinders, the gap between the cylinders and the draft of the upper cylinder have significant effect on the exciting forces and hydrodynamic coefficients. The wave forces and hydrodynamic coefficients are found to be remarkable mostly at lower frequency range. The present problems of diffraction and radiation by these two coaxial cylinders can be considered as equivalent to the corresponding problems for a wave energy device. The energy that is created and transferred finds its use in a number of practical applications. Wave energy devices are used to convert ocean wave energy into electrical energy.

Some of the wave energy device consist of only one structure. Since a hollow cylinder alone also captures the most essential feature of an OWC (oscillating water column), we consider a single floating structure only in deep water case which can be taken as equivalent to a wave energy device. For convenience, a hollow floating cylinder in infinite depth is considered with the arrangement having no bottom cylinder. Henceforth, the last part of this thesis is solely devoted to the investigation of the diffraction and radiation of a train of small amplitude harmonic water waves by a hollow cylindrical body in an infinite water depth. We compute the exciting forces, the hydrodynamic coefficients, free surface elevation and phase angles due to this single cylinder configuration. This arrangement can be considered as a special case of a pair of cylinders. The hydrodynamic influences of various parameters on the the exciting forces, hydrodynamic coefficients and their phase angles are discussed. Higher values of the exciting force occur at lower frequencies of the wave for different values of the radius ratio. The forces diminish at higher frequencies. For all radius ratios, the added mass assumes very high values, both positive and negative, in the neighbourhood of the resonant frequency while the damping coefficient assumes only positive values. Overall it is observed that there is a significant effect of the values of the radii of the cylinders and the gap between them on the hydrodynamic coefficients for radiation of the riding hollow cylinder placed above a coaxial vertical cylinder. From the results, it is clear that the exciting force and the hydrodynamic coefficients depend on a number of factors such as the radii of the cylinders, the gap between them and also on the depth.

The results of this thesis are expected to be helpful in designing a suitable device and also to find a proper position for the device in water so as to extract maximum

energy. The solutions of our problems under consideration are also expected to help the designer/engineer in choosing parameters such as depth, the radii of cylinders, the gap between the cylinders etc. Since tapping of energy from ocean waves is a prime objective of many investigations, our results are likely to throw some new lights in this direction.

Contents

NOMENCLATURE

A :	amplitude of the incident wave
g :	acceleration due to gravity
h_1 :	uniform finite depth of water
h_2 :	gap between the cylinders
$H_m^{(1)}(.)$:	Hankel function of first kind of order m
$H_m^{(2)}(.)$:	Hankel function of second kind of order m
i :	$= \sqrt{-1}$
$I_m(.)$:	modified Bessel function of first kind of order m
$J_m(.)$:	Bessel function of first kind of order m
$K_m(.)$:	modified Bessel function of second kind of order m
k :	wave number (in general)
λ_{11} :	damping coefficient for surge motion
λ_{55} :	damping coefficient for roll motion
λ_n, α_n :	roots of the dispersion relations
μ_{11} :	added mass for surge motion
μ_{55} :	added mass for roll motion
ω :	angular frequency of the incoming water wave
p :	hydrodynamic pressure
Φ :	real-valued velocity potential
ϕ :	complex-valued velocity potential
ϕ_{inc} :	incident velocity potential
ϕ_d :	diffracted velocity potential
$\phi_{rad,j}$:	radiated velocity potential in j-th mode of the motion
ρ :	uniform fluid density
(r, θ, z) :	cylindrical coordinates
t :	time
(x, y, z) :	Cartesian coordinates

List of Figures

List of Tables

Chapter 1

Introduction

1.1 Preamble

Fluid dynamics is that branch of applied mechanics that deals with fluid flow. It finds place in many areas of science and engineering. The analysis of the behaviour of fluids is based upon the fundamental laws of applied mechanics that relate to the conservation of mass, energy and momentum. Fluid dynamics has a wide range of applications, including calculating forces and moments on aircraft, determining the mass flow rate of petroleum through pipelines, predicting weather patterns, designing of ship, dams, bridge etc. The solution to a fluid dynamics problem usually involves calculating various properties of the fluid, such as velocity, pressure, temperature, and density as functions of space and time. In fluid dynamics there are problems that are easily solved by using the simplifying assumption of an inviscid flow. An inviscid flow is the flow in which viscous effects can be neglected. An incompressible flow is defined as one where the mass density of a fluid particle does not change as it moves in the flow field. A flow is irrotational if the curl of the velocity of the fluid is zero. So irrotational flow in a simply-connected domain can be described as a potential flow. If the flow is both irrotational and incompressible, the Laplacian of the velocity potential must be zero. This is referrred to as the continuity equation. A continuity equation is an equation that describes conservation of mass and this equation is the governing equation for the fluid-flow structure problems.

Water wave propagation form a very interesting and useful part of fluid dynamics.

Most of the Earth's surface is covered by water, and waves can develope whenever the surface of water is free to move, providing us with beautiful or terrifying sights. The study of water waves has had practical applications throughout history. The motion of water waves is very complex because of the fundamental property that water, unlike solid structures which allow a limited degree of deformation without breaking, is a fluid capable of unlimited deformation and distortion even under small disturbances. The study of water waves draws freely from various mathematical disciplines. The theory of water waves has profound and fascinating connections to many areas of classical and modern mathematics. Sir Isaac Newton was the first person to attempt to describe a theory of water waves. In Book II, Prop. XLV of Principia (1687), he proposed an unconfirmed analogy with oscillations in a U-tube, correctly deducing that the frequency of deep-water waves must be proportional to the inverse of the square root of the breadth of the wave. Newton's arguments were repeated by many researchers at various later stages.

A wave is a disturbance such that when it propagates through a medium, energy is transmitted to distant points without any displacement of the particle of the medium. The energy from the sun is transmitted by waves in the ether. When some musical instrument is played upon in a room, sound waves spread through the room. If we throw a stone in a pond, we sight waves in the pond which start from the point of striking of the stone and spread in all directions. Such water waves are also produced by the pressure of wind upon the surface of water, by the relative motion of bodies like a ship moving in an ocean and by obstacles in the bed of a stream. These are some easily understood and available examples of wave motion.

The study of water waves is of immense importance for various applications. The practical importance of water waves is evident in areas such as hydro-biology, hydro-acoustics, submerged navigation, hydro-optics and ocean research. Particularly in ocean research, proper knowledge of water waves is required for predicting the behaviour of floating structures (immersed totally or partially) such as ships, submarines and tension-leg platforms, and for describing flows over various bottom topography. Furthermore, the investigation of water wave patterns created by ships and other vehicles in forward

motion is closely related to the calculation of the wave-making resistance and other hydrodynamics characteristics that are used in marine design.

Water waves may be classified into two categories: in one category the wavelength is assumed to be greater than about 20 times the depth of water and the corresponding study is called *shallow water wave theory*. The waves belonging to this category are tidal waves and long waves in shallow water. In the other category the wavelength is assumed to be less than about 2 times the depth of water so that the effect of the disturbance diminishes gradually as one goes downwards away from the free surface. Waves belonging to this category are termed *deep water waves*. In this case, if it is assumed that the amplitude of the wave is small compared to the wavelength, then the theory is called *linearized theory of water waves*. This theory has been derived as an approximation of the general theory on the basis of the assumption that the components of the velocities of water particles, the free surface elevation or depression and their derivatives are small quantities, i.e., the motion is assumed to be very small. Though the ocean waves or surface waves are often nonlinear, the analysis in many physical problems is restricted to small amplitude waves mainly because it has been found that consideration of linear theory is sufficient in offshore engineering and other related studies in handling most of the problems. Due to this reason, majority of the scientists, researchers and ocean technologists use linearized theory of water waves to mathematically model various physical problems related to wave phenomena arising in coastal engineering. In the present thesis, all the problems are formulated and solved on the basis of linearized theory of water waves.

Water wave theory has provided a background for a somewhat rich development of mathematical concepts and techniques, and consequently, it now constitutes an important branch of applied mathematics as well as of mathematical physics. It is most varied and fascinating, and includes a wide range of natural phenomena in ocean, river and lakes. The theory of water waves is mostly concerned with the elucidation of some general aspects of wave motion as well as the prediction of the behaviour of waves in the presence of some special configurations of interest to oceanographers, hydraulic engineers, ship designers etc. One of the most important classes of water wave problems

is concerned with the problems of diffraction and radiation of water waves by obstacles of various geometrical shapes. A number of classes of problems may be considered under the linearised theory of water waves. Mostly, they include diffraction and radiation problems involving bodies of different geometrical shapes placed in water. If a time-harmonic progressive wave train is incident on a structure present in water, a part of it is reflected and the remaining part is transmitted over or around it. The study of ensuing motion and the determination of exciting force is referred to as the diffraction problem. Furthermore, if a structure present in water undergoes some sort of small oscillations, then waves are generated in water region and radiate away from the structure. The study of ensuing motion and determination of hydrodynamic coefficients is referred to as the radiation problem. These two types of problems have considerable practical applications in the ship building industry, offshore structures, construction of harbours etc. The study of diffraction and radiation problems on floating structures can provide fundamental information about the wave force and hydrodynamic properties of added mass and damping of the structure. These two classes of problems of interaction of water waves with floating structures has long been investigated by many researchers with the assumption of linearized water wave theory. An accurate prediction of the hydrodynamic loads on a structure is extremely important. It is evidently clear that a structure in waves will have some motion, however small, which will, in turn, affect the fluid flow in the vicinity. The associated hydrodynamic coefficients play a major role in the motion.

Many physical problems arising in the areas of applied mathematics and mathematical physics can be formulated as mixed boundary value problems governed by elliptic partial differential equations. In the study of diffraction or radiation of surface (or internal) harmonic water waves under the assumption of the linearized theory, the governing partial differential equation happens to be Laplace's equation in either two or three dimensions. Certain other assumptions that are usually considered are that the domain is unbounded, some of the boundary conditions are of mixed type and the behaviour of the velocity potential is not known completely at large distances.

There are different kinds of energy devices used for extracting wave energy from

ocean waves. Some of these devices consist of only one cylinder and some others consist of a pair like our arrangement to be followed in this thesis. The diffraction and radiation problems by this specific pair of two cylinders can be considered to be ones for a wave energy device (oscillating water column). The energy extracted by the buoy is transferred to a liquid pump placed on the solid cylinder which is positioned coaxially below it. Proper positioning of the device will allow the device to capture waves as large as possible. The usefulness and efficiency of wave energy and the estimation of exciting force/hydrodynamic coefficients for the wave energy device usually receive considerable attention from the device designers. An accurate prediction of the wave loads by water waves on the wave energy device is absolutely necessary to design the device. For a designer, it is of utmost importance to design structures with proper parameters so that it will produce maximum benefit. In order to accomplish that, he has to take into account a number of physical actions that the structure/device has to encounter. The solutions of our problems under consideration are also expected to help the designer/engineer in appropriately choosing the parameters such as depth, the radii of cylinders, the gaps between the cylinders etc. This type of energy converter assumes immense significance for offshore structures also. In this age of diminishing natural resources, such devices assume immense importance due to the possibility of using renewable energy.

1.2 Relevant background in the linear theory of water waves

We consider the fluid to be incompressible, homogeneous and inviscid, and the motion irrotational; and the waves are assumed to have small amplitude. Henceforth, linear water wave theory can be adequately applied. We assume that the bottom of the ocean is flat and impermeable.

1.2.1 Diffraction and radiation

If a train of time harmonic progressive waves given by $\mathrm{Re}[\phi_{inc}(x,y,z)e^{-\mathrm{i}\omega t}]$ is incident from negative infinity on a stationary body present in water, then a part of it is reflected

by the body and the remaining part is transmitted over or below depending on the configuration. Then the corresponding diffraction problem is to find the diffracted potential ϕ_d with the help of the incident potential where the incident velocity potential and diffracted velocity potential can, respectively, be written as $\Phi_{inc}(x,y,z,t) = Re[\phi_{inc}(x,y,z)e^{-\mathrm{i}\omega t}]$ and $\Phi_d(x,y,z,t) = Re[\phi_d(x,y,z)e^{-\mathrm{i}\omega t}]$. The total complex-valued velocity potential ϕ can be written as $\phi = \phi_{inc} + \phi_d$. This consideration allows us to employ linear water wave propagation in an ocean of uniform depth h_1. The origin is fixed on the free surface, x is considered positive along the direction of the propagation of waves and z is measured positive vertically upwards. Then the governing equation is given by Laplace's equation

$$\nabla^2 \phi_d = 0. \tag{1.1}$$

The combined linearized free surface condition is given by

$$\frac{\partial \phi_d}{\partial z} - \left(\frac{\omega^2}{g}\right)\phi_d = 0, \qquad \text{at} \quad z = 0. \tag{1.2}$$

The horizontal impermeable bottom condition is

$$\frac{\partial \phi_d}{\partial z} = 0, \qquad \text{at} \qquad z = -h_1. \tag{1.3}$$

The body surface boundary condition states that the normal component of water particle velocity in contact with a boundary surface is equal to the velocity of the surface at that point. In the case of diffraction problem, the body is considered to be at rest. So the normal velocity must be zero, i.e.,

$$\frac{\partial \phi}{\partial n} = 0, \qquad \text{on} \qquad S, \tag{1.4}$$

which is equivalent to

$$\frac{\partial \phi_d}{\partial n} = -\frac{\partial \phi_{inc}}{\partial n}, \tag{1.5}$$

where S is the wetted part of the body and n the outward drawn unit normal to it.

Another boundary condition is imposed on the velocity potential to correspond to the outgoing wave only. This condition is known as the radiation condition or the far-field condition given by

$$\lim_{r\to\infty} \sqrt{r}\left[\frac{\partial \phi_d}{\partial r} - \mathrm{i}k\phi_d\right] = 0. \tag{1.6}$$

If a body present in water is forced to execute a small prescribed motion, a wave motion is set up in the water region which radiates away from the body and is time harmonic with an angular frequency ω. The motion is described by a velocity potential $\Phi_{rad}(x, y, z, t) = Re[\phi_{rad}(x, y, z)\ e^{-\mathrm{i}\omega t}]$, where $\phi_{rad}(x, y, z)$ is the complex-valued radiated velocity potential. Body surface condition is satisfied on the surface of the oscillating body. A floating structure undergoes six degrees of freedom: the translational motions in the x-, y- and z- directions referred to as surge, sway and heave, respectively, and the rotational motions about x-, y- and z-axes referred to as pitch, roll and yaw, respectively. But, under suitable situations, those degrees of freedom can be reduced without loss of generality. For each mode of oscillations, the resulting small periodic motion of angular frequency ω may be expressed in the form $X_j e^{-\mathrm{i}\omega t}$ where X_j is the complex amplitude for the j-th mode of the motion with $j = 1, 2, 3, \ldots, 6$ corresponding to surge, sway, heave, pitch, roll and yaw, respectively. Figure 1.1 represents the motions of a floating structure. In the case of the radiation problem, only body surface condition (1.4) is different from the diffraction problem. The total velocity potential at a point in the fluid in the presence of an oscillating structure in waves may be written as

$$\Phi = Re\left[\left(\phi_{inc} + \phi_d + \sum_{j=1}^{6} X_j\ \phi_{rad,j}\right) e^{-\mathrm{i}\omega t}\right], \tag{1.7}$$

where $\phi_{rad,j}$ is the radiated or forced potentials due to the oscillation of the structure in the j-th mode. Here ϕ_{inc} and $\phi_{rad,j}$ are all functions of x, y and z. In order to understand clearly the body boundary condition for a structure in motion, we elaborate in brief, based on the derivation found in Newman [27].

For the general case, if the translational velocity is $U(t)$ and the body is rotating with angular velocity $\Omega(t)$ about an origin that moves with the body, the velocity potential must satisfy the boundary condition on the body surface,

$$\frac{\partial \phi_{rad}}{\partial n} = U \cdot n + \Omega \cdot (\vec{r} \times \vec{n}), \tag{1.8}$$

where $\vec{r}$ is the position vector of the point measured from the centre of rotation and $U = (X_1, X_2, X_3)$, $\Omega = (X_4, X_5, X_6)$, and

$$\phi_{rad} = X_j\ \phi_{rad,j}. \tag{1.9}$$

The potential defined by equation (1.9) satisfies the body boundary condition (1.8), provided each component $\phi_{rad,j}$ satisfies the corresponding condition

$$\frac{\partial \phi_{rad,j}}{\partial n} = n_j, \quad j = 1, 2, 3, \tag{1.10}$$

$$\frac{\partial \phi_{rad,j}}{\partial n} = \vec{r} \times \vec{n}, \quad j = 4, 5, 6, \tag{1.11}$$

where n_j for $j = 1, 2, 3$ are the x, y, z components of the unit normal outward from the

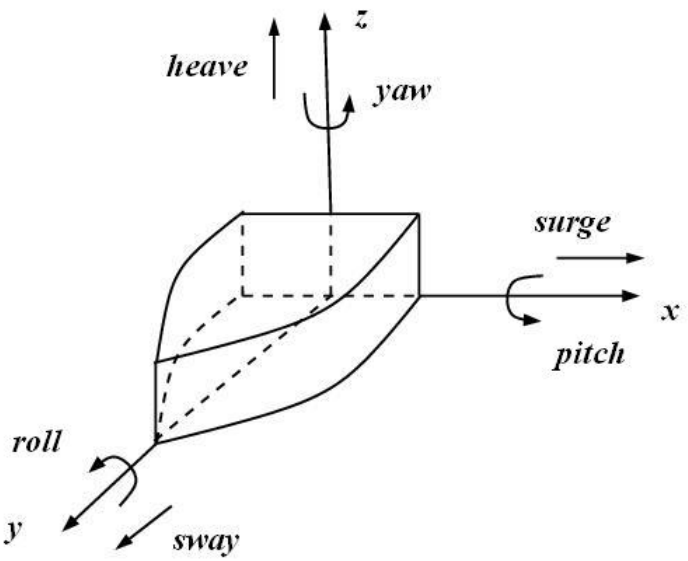

Figure 1.1: Motions of a floating body.

structure, i.e.,

$$n_1 = n_x, \qquad n_2 = n_y, \qquad n_3 = n_z, \tag{1.12}$$

and n_j for $j = 4, 5, 6$ are the corresponding components of $\vec{r} \times \vec{n}$, i.e.,

$$n_4 = (yn_z - zn_y), \qquad n_5 = (zn_x - xn_z), \qquad n_6 = (xn_y - yn_x), \tag{1.13}$$

We introduce cylindrical coordinate system by $x = r\cos\theta$, $x = r\sin\theta$ and $z = z$. Similar to the far-field condition imposed on ϕ_d given by equation (1.6), these radiated potentials also satisfy the same condition.

Once the total velocity potential is known and the pressure on the surface of the structure is known from Bernoulli's equation, the total force $\overrightarrow{F}$ exerted on the body and moment $\overrightarrow{M}$ of this force in vector notation may be obtained from the following formulas:

$$\overrightarrow{F(t)} = -\int\int_S p\,\vec{n}\,ds, \tag{1.14}$$

$$\overrightarrow{M(t)} = -\int\int_S p\,(\vec{r}\times\vec{n})\,ds, \tag{1.15}$$

1.2.2 Wave forces and hydrodynamic coefficients

Wave exciting forces are the forces due to the velocity potentials except radiated velocity potentials. Those velocity potentials are generally composed of the incident velocity potential ϕ_{inc} and the diffracted velocity potential ϕ_d. The hydrodynamic pressure due to the potential is obtained from linearized Bernoulli's equation

$$p = \mathrm{i}\rho\omega\,\phi(r,\theta,z). \tag{1.16}$$

The following formula gives wave forces in the l-th direction:

$$F_l = \mathrm{i}\rho\omega\int_S \phi_{inc}\,n_l\,ds + \mathrm{i}\rho\omega\int_S \phi_d\,n_l\,ds, \tag{1.17}$$

where n_l is the component of the unit normal vector pointing to the cylinder at the cylinder surface.

The hydrodynamic pressure due to the radiated potential is obtained from linearized Bernoulli's equation

$$p_j = \mathrm{i}\rho\omega\,\phi_{rad,j}(r,\theta,z). \tag{1.18}$$

We assume that the motions of the structure are small. As there exists no bottom for the hollow cylinder, there is no need to consider heave motion and therefore we consider surge and roll motions only. If amplitudes of the motion mode j is denoted by A_{jl}, then the radiated potential $\phi_{rad,j}$ can be written as (Wu et al. [38])

$$\phi_{rad,j}(r,\theta,z) = -\mathrm{i}\omega A_{jl}\varphi_{rad,j}(r,z)\cos\theta. \tag{1.19}$$

where j denotes the mode of motion, e.g., surge,... and l denotes direction.
The radiated force is the force due to the motion of the body. It can be computed from the radiated potential whereby the general radiated force on the body due to j-th motion can be written as

$$F_{jl} = -i\rho\omega \int_S \phi_{rad,j}(r,\theta,z)\ \ n_l\ ds, \qquad j,l = 1,2,3,\ldots,6, \tag{1.20}$$

where S is the submerged surface of the body and F_{jl} is the radiated force acting on the body in the l-th direction with amplitude in the j-th direction. Therefore, using equation (1.19) we have

$$F_{jl} \ = \ -\rho\ A_{jl}\ \omega^2 \int_S \varphi_{rad,j}(r,z)\ \cos\theta\ n_l\ ds, \tag{1.21}$$

which can be rewritten as (Rahman [30](Sec. 8.7))

$$F_{jl} = \omega^2 A_{jl}\ \left(\mu_{jl} + \mathrm{i}\frac{\lambda_{jl}}{\omega}\right), \tag{1.22}$$

where the expression of added mass μ_{jl} and damping coefficient λ_{jl} is given by

$$\mu_{jl} + \mathrm{i}\frac{\lambda_{jl}}{\omega} = -\rho \int_S \varphi_{rad,j}\ \cos\theta\ n_l\ ds. \tag{1.23}$$

In physical sense, the added mass is the weight added to a system in a fluid due to the fact that an accelerating or decelerating body must move some volume of surrounding fluid with it as it moves. Damping is an influence within or upon an oscillatory system that has the effect of reducing, restricting or preventing its oscillations. All bodies accelerating in a fluid will be affected by added mass, but since the added mass is dependent on the density of the fluid, the effect is often neglected for dense bodies falling in much less dense fluids. For situations where the density of the fluid is comparable to or greater than the density of the body, the added mass can often be greater than the mass of the body. This property also applies to ships, submarines, and offshore platforms. For ships, the added mass can reach even 3 to 4 times the mass in heave mode and 1-2 times the mass in surge mode. Damping models refer to the energy dissipation during vibrations. These models are important for the stability of structure and its vibration amplitudes. Damping may arise from the structure and from the fluid surrounding it. Fluid damping

is related to viscous dissipation and fluid drag while structural damping is related to properties of the structure itself. Linear and nonlinear wake oscillator models are such examples.

1.3 Brief history

Ocean waves are a huge but largely untapped energy resource and therefore efforts have been undertaken to explore the potential for extracting energy from these waves. Recently, significant progress has been accomplished on the front of interaction of surface waves with floating structures.

Various theoretical investigations have been carried out by researchers in analyzing the wave motion and hydrodynamic forces on a structure. Most of the investigations for water wave diffraction and radiation problems are found to be concerned mainly with a single structure, usually a circular cylinder. Ursell [35] solved the problem for a long and floating horizontal cylinder oscillating with small amplitudes about a mean position in water of infinite depth. By using either a potential or a stream function, he deduced the wave-amplitude at a distance from the cylinder and the added mass of the cylinder due to the fluid motion. Garrett [9] investigated the excitation of waves inside a partially immersed open circular cylinder. The solution was obtained from a variational formulation by using the incoming wave as a trial function. He found that the phase of the solution was independent of depth and resonances at wave-numbers close to those of free oscillations in a cylinder extending to the bottom. Sabuncu and Calisal [34] calculated added mass and damping coefficients for surge, heave and pitch motions for a vertical circular cylinder and presented them in graphical form for different depth to radius and draft to radius ratios. They discussed the limiting values for heave added mass and damping coefficients for zero frequency. Yeung [39] presented a set of added mass and damping coefficients for surge, heave and roll motions of a circular cylinder in finite water depth. He used the method of matched eigenfunctions to solve the hydrodynamic problem in the exterior and interior regions. Miloh [25] considered a floating solar pond in the form of a large partially immersed open circular cylinder in

an open sea of finite depth. He obtained the surge and pitch added mass and damping coefficients by solving the linear radiation problem. He also investigated the resonance conditions for heave and pitch motions and discussed the transmitted wave motion inside the pond. McIver and Evans [20] studied the phenomenon of negative added mass by considering the heave oscillations of a submerged vertical cylinder. Mavrakos [21] solved the linearized diffraction problem of the interaction between regular sinusoidal incident wave and a bottomless cylindrical floating body with a vertical symmetry axis and finite wall thickness. Mavrakos [22] also derived the linearized added mass and damping coefficients for the same structure as in Mavrakos [21] but oscillating in water of finite depth. He considered the forced motions of the cylindrical body in three modes, namely, surge, heave and pitch, and calculated the added mass and damping coefficients for coupled surge-pitch motions also. Rahman and Bhatta [29] investigated the closed form solutions for the added mass and damping coefficient of a large surface-piercing and bottom-mounted vertical circular cylinder undergoing horizontal oscillations in the surge motion and special attention was given to the low-frequency and high-frequency behaviour of the hydrodynamic coefficients. Bhatta and Rahman [3] calculated the wave loading due to scattering and radiation for a floating cylinder in water of finite depth. They decomposed the total velocity potential into four: one due to scattering and the other three due to radiation. For each case, they derived the velocity potential by considering interior and exterior regions. Zhu and Mitchell [44] derived a first order analytical solution for the diffraction problem around a hollow cylinder. They used a new approach to analyze the dependence of the solution upon various parameters as well as the rate of convergence of the series solution. Finnegan et al. [8] derived an analytical solution for surge, heave and pitch wave exciting on a floating cylinder in water of infinite depth. They used the method of separation of variables and Havelock's expansion theorem to derive the velocity potentials throughout the fluid domain and presented the wave exciting forces with respect to incident wave frequencies for various draft to radius ratios.

A number of notable works have also been accomplished by researchers for multiple structures. Berggren and Johansson [2] derived the hydrodynamic coefficients of a wave

energy device consisting of a buoy connected to a submerged plate by using the method of matched eigenfunction expansions and investigated the influence of the plate on the hydrodynamic coefficients of the buoy and vice versa. Further, nonlinear water wave theory was employed by Rahman and Bhatta [28] in which they derived second order wave forces acting on a pair of cylinders placed at some distance apart by considering two coordinate systems and using Graf's addition theorem for Bessel functions. Sahoo [31] investigated the generation of cylindrical surface wave in water of infinite depth for an impermeable circular cylinder surrounded by a coaxial permeable cylinder immersed vertically in the fluid region. He employed Havelock's expansion theorem and various properties of Bessel functions. He also presented the scattering problem when both the cylinders were fixed. Mavrakos [23] presented a solution of the linearized hydrodynamic radiation problem for two concentric, free surface-piercing truncated vertical cylinders that were forced to independently oscillate in heave in finite depth water. He presented the resonant locations of the free surface motion in the inner fluid domain.

Wu et al. ([37], [38]) investigated the problem of diffraction and radiation for two cylinders under different considerations. They obtained the expression for the velocity potential by using the eigenfunction expansion method and investigated the effect of the caisson, approximated by a solid cylinder, on the floating cylinder. Hydrodynamic coefficients and exciting forces were presented for some ratios of the radius of the submerged cylinder to that of the riding one. Zhang et al. [40] studied the diffraction and radiation problems by two vertical truncated cylinders in water of finite depth. They derived the analytical expressions for the diffracted potential and radiated potential, and calculated the hydrodynamic coefficients and wave forces for some specific cases. They also investigated the effect of the cylinders' radii on the hydrodynamic properties. For verification of the results, they used Green's second identity and the symmetry of the matrices for the added mass and damping coefficient. Siddorn and Taylor [33] investigated the diffraction and radiation problems of linear water waves by an array of truncated cylinders and calculated the exciting forces, added mass and damping coefficients for each cylinder.

Some other investigations have been taken up where the structure considered was

not cylindrical. Havelock [11] solved the radiation problem for a floating half-immersed sphere in water of infinite depth. He presented the variation of the virtual inertia coefficient and the equivalent damping coefficient against frequency. Garrett [10] investigated the scattering of surface gravity waves by a circular dock. He presented the results for the horizontal and vertical forces and also for the torque on the dock. He used Galerkin's method to solve the problem numerically. Lee [14] used an approach that converted the nonhomogeneous boundary value problem into two homogeneous boundary value problems, one horizontally and the other vertically, and derived an analytical solution to the heave radiation problem for a rectangular structure. A boundary element method was used to solve the problem, and the added mass and damping coefficients of the structure were presented graphically. Mavrakos [24] presented linearized exciting wave forces and hydrodynamic coefficients of a toroidal body floating in water of finite depth. Chakrabarti and Sahoo [5] solved the problem of diffraction of obliquely incident surface water waves by a vertical cliff for both infinite and finite depths. The method of solution was based on the exploitation of logarithmic singularity of the velocity potential at the corner points where the water surface met the wall in a rather natural manner, while applying Havelock's expansion theorem. Newman [26] investigated the hydrodynamic coefficients for a special toroidal body by using linear water wave theory. He presented added mass, damping and elevation of the free surface in the moon pool for a range of wavenumbers with singular results in the resonant regime. Chakrabarti [6] solved the mixed boundary value problem of scattering of two-dimensional time-harmonic surface water waves by a discontinuity on the surface boundary conditions, separating the clean surface and an ice-covered surface in the case of infinite depth and derived the expressions for the reflection and transmission coefficients. The absolute values of the reflection and transmission coefficients were presented graphically. Mandal and Chakrabarti [18] obtained an integral expansion theorem which is useful for those functions which are in general discontinuous but integrable, having one point of discontinuity and defined on positive real axis. Such expansion theorems have utility in handling wave problems involving multiple layers of inviscid, incompressible and immiscible fluids of different constant densities. Karmakar and Sahoo [12] investigated wave scattering by an artic-

ulated floating elastic plate in infinite water depth within the framework of linearized theory of water waves. They presented phase and group velocities, reflection and transmission coefficients and the vertical displacement response of the plate. Shen et al. [32] analyzed the effect of a bottom sill on the hydrodynamic coefficients, wave force, and the reflection and transmission coefficients of a rectangular structure floating on the free surface. Manam et al. [17] derived an expansion formula based on the orthogonal mode-coupling relations in the case of semi-infinite strips as well as quarter-plane problems in order to tackle a general class of problems of fluid-structure interaction involving higher-order boundary conditions for the governing equation. They investigated the problem of wavemaker by oblique water wave scattering caused by cracks in an ice-sheet in the case of infinite depth. Zheng et al. [41] used the method of separation of variables and eigenfunction expansion matching technique to derive the diffracted velocity potentials when linear waves were scattered by an infinitely long rectangular structure parallel to a vertical wall in oblique seas. They presented the influences of the various parameters on the wave force of the structure. The extension of this work, which includes the radiation and diffraction problems of infinitely long submerged rectangular structure parallel to a vertical wall, was also investigated by Zheng et al. [42]. Martins-Rivas and Mei [19] described linear theory of an oscillating water column installed on a straight coast and calculated the added mass and damping coefficients and chamber pressure. Zhou et al. [43] investigated the radiation and diffraction of water waves by a rectangular body with an opening in its bottom in water of finite depth. They obtained the hydrodynamic coefficients and wave exciting forces. Lovas et al. [15] considered a large circular oscillating water column installed at the tip of a coastal corner in water of uniform depth and solved the diffraction and radiation problems by eigenfunction expansions for an arbitrary apex angle. Bhattacharjee and Soares [4] formulated the diffraction problem of water waves by a floating structure near a wall with a step-type bottom topography and they calculated the wave-induced forces on the structure and on the wall for different water depth ratios. Dong et al. [7] investigated linearized added mass and radiation damping of a submerged hollow sphere with an opening hole in water of finite depth. They analyzed the added mass and radiation damping due to heave motion for different

angles of the opening hole.

1.4 Motivation for the present work

Vertical cylinders are used in different oceanographic applications, e.g., wave energy device, instrumentation platforms for their simplicity in construction and drilling rigs etc. Wave loads and the estimation of hydrodynamic coefficients and the competence of converting cylinders as a wave energy device have received considerable attention from the designers. The problem of diffraction and radiation by two cylinders can be related to the concerned problem of a wave energy device, and the wave energy created by this device can be utilized in a number of applications. The main motivation to use a hollow cylinder is to produce green power generation by an oscillating water column (OWC) device. A hollow cylinder captures the most essential feature of an OWC which can be used to convert ocean wave energy to electricity.

In the present thesis, we specifically study the diffraction and radiation problems of a system consisting of two cylinders: a hollow cylinder which is partially immersed and the other an immersed solid cylinder on an impermeable bed at a finite depth and consider different arrangements of the immersed cylinder. This mathematical model is based on the assumptions of linearized water wave theory. In the study of floating structures, an eigenfunction expansion, along with the matching technique, is being widely used due to its considerable accuracy. Therefore using an eigenfunction expansion approach and separation of variables technique, the analytical solutions for the diffraction and radiation problems are presented. Using the analytical solutions of the problems, the effect of various parameters on the wave force and hydrodynamic coefficients of cylinders is investigated. The obtained results are expected to provide some useful information to the designers. As far as the diffraction and radiation problems involving a riding hollow cylinder and a coaxial solid cylinder below it in water of finite depth is concerned, the authors have not come across any investigation that has employed an analytical approach with an eigenfunction expansion. Later in the thesis, the diffraction and radiation problems for a semi-submerged vertical hollow cylinder in water of infinite

depth is solved.

To produce the maximum benefit out of a structure, it is important to design structures with proper parameters. We evaluate the forces and free surface elevation due to diffraction and the hydrodynamic coefficients due to radiation. It is hoped that the results will be helpful in designing a suitable device and also to find an appropriate position for the device so as to extract maximum energy. The motivation of our present work follows from the number of major applications the aforesaid structures have.

1.5 Outline of the thesis

The work presented in this thesis is concerned with the diffraction and radiation of linear water waves by two coaxial cylindrical structures. We prescribe the incident wave train and its deviation in the still water depth, and seek the additional waves, namely, the diffracted waves and the radiated waves caused by this deviation. A typical problem of this type requires the determination of velocity potentials satisfying Laplace's equation within the fluid, a mixed boundary condition at the free surface and a given normal velocity on the rigid boundaries. If the fluid domain extends to infinity, a radiation condition is required to ensure the uniqueness. The corresponding boundary value problem is established and formally presented in the subsequent chapters. We shall refer to the problem of finding a solution of such boundary value problem as the full linear problem. Analytical solutions for the full linear problem are rare for any deviation from the constant water depth case, that is, for any deviation from a flat ocean-bed. Problems where analytical solutions exist are usually valid for a limited selection of straightforward geometries which include horizontal and/or vertical boundaries. The last part of this thesis is devoted to the diffraction and radiation of water waves by a single cylinder in water of infinite depth.

The mathematical tools utilized in this thesis are (i) Eigenfunction expansion method, (ii) Separation of variables technique, (iii) Fourier sine transform and (iv) Havelock's expansion theorem. The content of the thesis is presented in the form of nine chapters with the present chapter dealing with basic concepts and equations, previous important works

and our motivation to carry out investigations for the present problems. In Chapter 2, we solve the problem of diffraction of incident waves by a pair of coaxial vertical hollow cylinder and bottom-mounted solid cylinder in uniform water depth. Using separation of variables technique and eigenfunction expansion method, the boundary value problem arising out of the physical problem under consideration is solved to find the exciting forces for various parameters. Chapter 3 deals with the corresponding surge radiation problem of water waves by the same structure as in Chapter 2. The hydrodynamic coefficients, namely, the added mass and damping coefficient for surge motion, are obtained by using the same method as was followed in Chapter 2. The particular case of a hollow cylinder over an even sea-bed is also considered and analyzed. Similarly, Chapter 4 deals with the roll radiation problem for the same structure under the same conditions.

Chapters 5 and 6 are devoted to the problems of diffraction and radiation of water waves by two coaxial cylinders with one floating and other submerged at some finite height above the sea-bed. The solution of the boundary value problems are obtained by using the same solution technique as in Chapter 2. Using these solutions, the exciting forces and the added mass and damping coefficient are evaluated corresponding to different parameters.

In Chapters 7 and 8, we solve the diffraction and radiation problems of water waves for a finite hollow circular cylinder in water of infinite depth. Using the separation of variables technique, Fourier Sine transform and suitable application of the Havelock's expansion theorem, we derive and solve the corresponding boundary value problems. The solutions allow us to obtain the exciting forces and the added mass and damping coefficient for different parameters. We also evaluate the free surface elevation and the phase angles of the exciting forces and the radiation forces.

In each chapter, we also depict the graphical representation of the results and conclude about the behaviour of the diffraction and radiation processes. Each chapter contains a sizeable number of graphs validating the analytical results that we derive. As far as possible we also try to consider particular cases and compare our results with available established results.

Finally, Chapter 9 presents a brief summary of results highlighting the contribution

made by this thesis. It also provides information for the scope of future investigations.

It is worthwhile to note here that the numerical values of the various mathematical functions appearing in our calculations throughout this thesis are considered from Abramowitz and Stegun [1] and Matlab. For example, a number of values of the associated functions like Bessel functions, Hankel functions etc, were obtained by using commands in matlab like $\gg besselj(m,x)$ for Bessel function of order m, i.e., $J_m(x)$ and $\gg besselh(m,1,x)$ for Hankel function of first kind of order m, i.e., $H_m^{(1)}(x)$, etc. Various integrals appearing at different places were also evaluated by using commands in Matlab such as $\gg quadl(@(x)cos(\lambda_n * (x+h_1)). * cos(\alpha_n * (x+e_2)), -e_2, 0)$ for $\int_{-e_2}^{0} cos(\lambda_n * (x+h_1))\ \cos(\alpha_n * (x+e_2))dx$.

Chapter 2

Diffraction of water waves by a pair of hollow cylinder and a bottom-mounted cylinder

2.1 Introduction

In this chapter, we consider a system consisting of a buoy floating vertically on the free surface above a bottom-mounted caisson. In order to have a simple modeling of the situation but with a clear understanding, the buoy is idealized as a hollow vertical cylinder and the caisson as a solid circular cylinder. Within the framework of linear water wave theory, we solve the diffraction problem for these two coaxial cylinders. The radius of the bottom-mounted cylinder is greater than or equal to the radius of the hollow cylinder. By using the separation of variables technique and matched eigenfunction expansion approach, the diffracted velocity potential is derived. The analytical expressions of the diffracted velocity potentials allow us to evaluate the exciting forces acting on both the cylinders. We present the exciting forces for various parameters, i.e., for different gaps between the cylinders and for different radii of the cylinders.

2.2 Mathematical formulation of the problem

Let us assume that the fluid is inviscid, homogeneous, incompressible and the motion is irrotational. We consider linear water wave propagation in an ocean of uniform depth h_1. A structure consisting of two coaxial cylinders, one a hollow one of radius R and under it a bottom-mounted solid cylinder of radius $R_p(\geq R)$ is considered. Some part of the hollow cylinder is above the free surface as shown in Figure 2.1. A right-handed Cartesian coordinate system $Oxyz$ is defined with the origin O at the undisturbed free surface and the z-axis measured positive upwards while the direction of propagation of waves is considered along the x-axis. The hollow cylinder, which is hereafter called cylinder 1, occupies the region defined by $r \leq R, \quad 0 \leq \theta \leq 2\pi, \quad -e_1 \leq z \leq 0$. The region of the other cylinder is defined by $r \leq R_p, \quad 0 \leq \theta \leq 2\pi, \quad -h_1 \leq z \leq -e_2$; this cylinder is called cylinder 2 hereafter. Now we introduce a velocity

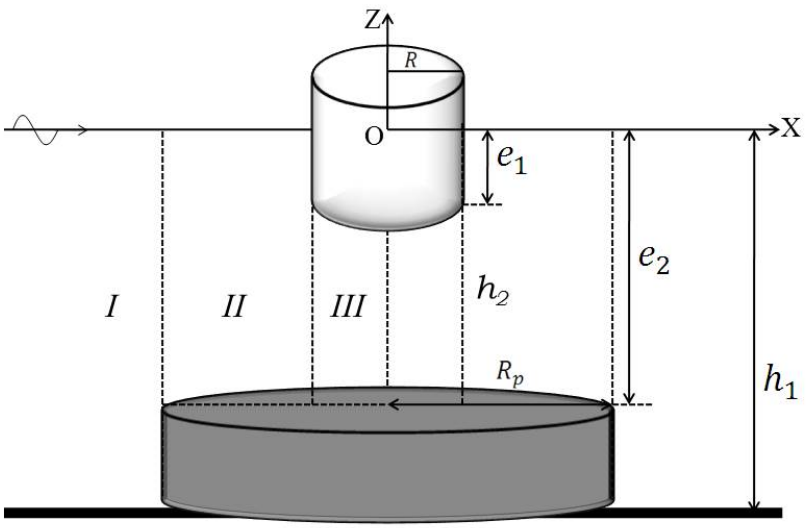

Figure 2.1: Schematic diagram and definition of fluid subdomains.

potential $\Phi(r,\theta,z,t) = Re[\phi(r,\theta,z)e^{-i\omega t}]$ where Re denotes the real part of the quantity in brackets, ω is the angular wave frequency and $\phi(r,\theta,z)$ is the spatial part of the velocity potential which satisfies the Laplace's equation

$$\frac{1}{r}\frac{\partial}{\partial r}\left(r\frac{\partial \phi}{\partial r}\right) + \frac{1}{r^2}\frac{\partial^2 \phi}{\partial \theta^2} + \frac{\partial^2 \phi}{\partial z^2} = 0. \tag{2.1}$$

The velocity potential ϕ can be split into incident velocity potential ϕ_{inc} and diffracted velocity potential ϕ_d due to the diffraction of the wave incident on the cylinders. The solutions for the boundary value problem are obtained in three physical regions. Let ϕ_{d1}, ϕ_{d2} and ϕ_{d3} be the diffracted potentials in the regions I, II and III, respectively. The incident velocity potential of unit amplitude and angular frequency ω propagating along the positive x-direction is given by (MacCamy and Fuchs [16])

$$\phi_{inc} = -\frac{\mathrm{i}g}{\omega}\frac{\cosh k(z+h_1)}{\cosh(kh_1)}\sum_{m=0}^{\infty}\epsilon_m J_m(kr)\cos m\theta, \tag{2.2}$$

where k is the wave number in region I which is determined from the dispersion relation $\omega^2 = gk\tanh(kh_1)$ and ϵ_m is given by

$$\epsilon_m = \begin{cases} 1, & m = 0, \\ 2\mathrm{i}^m, & m \geq 1. \end{cases} \tag{2.3}$$

In this section we set up the boundary value problem with appropriate conditions and find the diffracted potentials.

The governing equation and boundary conditions

The diffracted velocity potential Φ_d can be expressed as Φ_d=$Re[\phi_d(r,\theta,z)e^{-\mathrm{i}\omega t}]$, where the spatial part ϕ_d of the diffracted velocity potential Φ_d is governed by following boundary value problem:

$$\nabla^2\phi_d = 0; \qquad \text{in the respective fluid region,} \tag{2.4}$$

$$\frac{\partial\phi_d}{\partial z} - \frac{\omega^2}{g}\phi_d = 0; \ (z=0), \tag{2.5}$$

$$\frac{\partial\phi_d}{\partial z} = 0; \ (z=-h_1, \ r \geq R_p), \tag{2.6}$$

$$\frac{\partial(\phi_d+\phi_{inc})}{\partial z} = 0; \ (z=-e_2, r<R_p), \tag{2.7}$$

$$\frac{\partial(\phi_d+\phi_{inc})}{\partial r} = 0; \ (-h_1<z<-e_2, \ r=R_p; -e_1<z<0, r=R),$$

with the radiation condition (valid only in unbounded regions)

$$\lim_{r\to\infty}\sqrt{r}\left(\frac{\partial\phi_d}{\partial r} - \mathrm{i}k\phi_d\right) = 0. \tag{2.8}$$

2.3 Method of solution

We apply the separation of variables method in each subdomain in order to obtain an expression for the velocity potential. These expressions are obtained as infinite series of orthogonal functions which are valid in each corresponding subdomain. The analytical expressions for the diffracted velocity potentials in different regions, based on the results of Wu et al. [37], are given by

$$\phi_{d1} = \sum_{m=0}^{\infty}\sum_{n=1}^{\infty} A_{m,n}\frac{R_m(\lambda_n r)}{R_m(\lambda_n R_p)}\cos[\lambda_n(z+h_1)]\cos m\theta, \tag{2.9}$$

$$\phi_{d2} = -\phi_{inc} + \sum_{m=0}^{\infty}\sum_{n=1}^{\infty}\left[B_{m,n}\frac{S_m(\alpha_n r)}{S_m(\alpha_n R)} + C_{m,n}\frac{T_m(\alpha_n r)}{T_m(\alpha_n R)}\right]\cos[\alpha_n(z+e_2)]\cos m\theta, \tag{2.10}$$

$$\phi_{d3} = -\phi_{inc} + \sum_{m=0}^{\infty}\left[D_{m,1}\frac{J_m(k'r)}{J_m(k'R)}\cosh[k'(z+e_2)] + \sum_{n=2}^{\infty} D_{m,n}\frac{I_m(\alpha_n r)}{I_m(\alpha_n R)}\cos[\alpha_n(z+e_2)]\right]\cos m\theta, \tag{2.11}$$

where $A_{m,n}$, $B_{m,n}$, $C_{m,n}$ and $D_{m,n}$ are the unknown coefficients and λ_n and α_n are determined from the following dispersion relations

$$\begin{cases} \lambda_n = -\mathrm{i}k, \quad \omega^2 = gk\tanh(kh_1), & n=1, \\ \omega^2 = -g\lambda_n\tan(\lambda_n h_1), & n=2,3,\ldots, \end{cases} \tag{2.12}$$

$$\begin{cases} \alpha_n = -\mathrm{i}k', \quad \omega^2 = gk'\tanh(k'e_2), & n=1, \\ \omega^2 = -g\alpha_n\tan(\alpha_n e_2), & n=2,3,\ldots, \end{cases} \tag{2.13}$$

where h_2 is the gap between the cylinders and given by $h_2 = e_2 - e_1$; and k' denoting the wave number in regions II and III.

The radial functions $R_m(.)$, $S_m(.)$ and $T_m(.)$ are given by

$$R_m(\lambda_n r) = H_m^{(1)}(kr), \qquad n=1, \tag{2.14}$$

$$R_m(\lambda_n r) = K_m(\lambda_n r), \qquad n=2,3,\ldots, \tag{2.15}$$

$$S_m(\alpha_n r) = H_m^{(1)}(k'r), \qquad n=1, \tag{2.16}$$

$$S_m(\alpha_n r) = K_m(\alpha_n r), \qquad n = 2, 3, \ldots, \tag{2.17}$$

$$T_m(\alpha_n r) = H_m^{(2)}(k' r), \qquad n = 1, \tag{2.18}$$

$$T_m(\alpha_n r) = I_m(\alpha_n r), \qquad n = 2, 3, \ldots. \tag{2.19}$$

Matching conditions and determination of unknown coefficients

In order to determine the unknown coefficients $A_{m,n}$, $B_{m,n}$, $C_{m,n}$ and $D_{m,n}$, we introduce the appropriate matching conditions by means of continuity of pressure and that of velocity along the vertical boundaries as depicted in Figure 2.1. Therefore, using these continuity conditions and also the body boundary conditions at $r = R_p$ and $r = R$, we have

$$\phi_{d1} = \phi_{d2}, \quad \text{for} \quad -e_2 \le z \le 0, \ r = R_p, \tag{2.20}$$

$$\frac{\partial \phi_{d1}}{\partial r} = \begin{cases} \frac{\partial \phi_{d2}}{\partial r}, & \text{for} \quad -e_2 \le z \le 0, \ r = R_p, \\ -\frac{\partial \phi_{inc}}{\partial r}, & \text{for} \quad -h_1 \le z \le -e_2, \ r = R_p, \end{cases} \tag{2.21}$$

$$\phi_{d2} = \phi_{d3}, \quad \text{for} \quad -e_2 \le z \le -e_1, \ r = R, \tag{2.22}$$

$$\frac{\partial \phi_{d2}}{\partial r} = \begin{cases} \frac{\partial \phi_{d3}}{\partial r}, & \text{for} \quad -e_2 \le z \le -e_1, \ r = R, \\ -\frac{\partial \phi_{inc}}{\partial r}, & \text{for} \quad -e_1 \le z \le 0, \ r = R. \end{cases} \tag{2.23}$$

Substituting the expressions of diffracted velocity potentials (equations (2.9)–(2.11)) into equations (2.20)–(2.23) and then using the orthogonality of cosine functions, it follows

$$\sum_{j=1}^{\infty} A_{m,j} E(\lambda_j, \alpha_i; h_1, e_2 : -e_2, 0) - \left[B_{m,i} S_{m,i} + C_{m,i} T_{m,i}\right] N(\alpha_i; e_2 : -e_2, 0) = P_m E(\lambda_1, \alpha_i; h_1, e_2 : -e_2, 0), \tag{2.24}$$

$$A_{m,i} O_{m,i} N(\lambda_i; h_1 : -h_1, 0) - \sum_{j=1}^{\infty} \left[B_{m,j} S'_{m,j} + C_{m,j} T'_{m,j}\right] E(\alpha_j, \lambda_i; e_2, h_1 : -e_2, 0) = P'_m E(\lambda_1, \lambda_i; h_1, h_1 : -h_1, 0), \tag{2.25}$$

$$\sum_{j=1}^{\infty} \left[(B_{m,j} + C_{m,j}) - D_{m,j}\right] E(\alpha_j, \alpha_i; e_2, e_2 : -e_2, -e_1) = U_{m,i}, \tag{2.26}$$

$$\left[B_{m,i} Q_{m,i} + C_{m,i} W_{m,i}\right] N(\alpha_i; e_2 : -e_2, 0) - \sum_{j=1}^{\infty} D_{m,j} L_{m,j} E(\alpha_j, \alpha_i; e_2, e_2 : -e_2, -e_1) = V_{m,i}, \tag{2.27}$$

where,

$$E(\lambda_j, \alpha_i; h_1, e_2 : -e_2, 0) = \int_{-e_2}^{0} \cos[\lambda_j(z+h_1)]\cos[\alpha_i(z+e_2)]dz, \tag{2.28}$$

$$N(\alpha_i; e_2 : -e_2, 0) = \int_{-e_2}^{0} \cos^2[\alpha_i(z+e_2)]dz, \tag{2.29}$$

$$N(\lambda_i; h_1 : -h_1, 0) = \int_{-h_1}^{0} \cos^2[\lambda_i(z+h_1)]dz, \tag{2.30}$$

$$E(\alpha_j, \alpha_i; e_2, e_2 : -e_2, -e_1) = \int_{-e_2}^{-e_1} \cos[\alpha_j(z+e_2)]\cos[\alpha_i(z+e_2)]dz, \tag{2.31}$$

with

$$S_{m,i} = \begin{cases} \frac{H_m^{(1)}(k'R_p)}{H_m^{(1)}(k'R)}, & \text{for } i = 1, \\ \frac{K_m(\alpha_i R_p)}{K_m(\alpha_i R)}, & \text{for } i = 2, 3, \ldots, \end{cases} \tag{2.32}$$

$$T_{m,i} = \begin{cases} \frac{H_m^{(2)}(k'R_p)}{H_m^{(2)}(k'R)}, & \text{for } i = 1, \\ \frac{I_m(\alpha_i R_p)}{I_m(\alpha_i R)}, & \text{for } i = 2, 3, \ldots, \end{cases} \tag{2.33}$$

$$O_{m,i} = \begin{cases} \frac{k\, H_m^{'(1)}(kR_p)}{H_m^{(1)}(kR_p)}, & \text{for } i = 1, \\ \frac{\lambda_i\, K_m'(\lambda_i R_p)}{K_m(\lambda_i R_p)}, & \text{for } i = 2, 3, \ldots, \end{cases} \tag{2.34}$$

$$S'_{m,j} = \begin{cases} \frac{k'\, H_m^{'(1)}(k'R_p)}{H_m^{(1)}(k'R)}, & \text{for } j = 1, \\ \frac{\alpha_j\, K_m'(\alpha_j R_p)}{K_m(\alpha_j R)}, & \text{for } j = 2, 3, \ldots, \end{cases} \tag{2.35}$$

$$T'_{m,j} = \begin{cases} \frac{k'\, H_m^{'(2)}(k'R_p)}{H_m^{(2)}(k'R)}, & \text{for } j = 1, \\ \frac{\alpha_j\, I_m'(\alpha_j R_p)}{I_m(\alpha_j R)}, & \text{for } j = 2, 3, \ldots, \end{cases} \tag{2.36}$$

$$Q_{m,i} = \begin{cases} \frac{k'\, H_m^{'(1)}(k'R)}{H_1^{(1)}(k'R)}, & \text{for } i = 1, \\ \frac{\alpha_i\, K_m'(\alpha_i R)}{K_m(\alpha_i R)}, & \text{for } i = 2, 3, \ldots, \end{cases} \tag{2.37}$$

$$W_{m,i} = \begin{cases} \frac{k'\, H_m^{'(2)}(k'R)}{H_m^{(2)}(k'R)}, & \text{for } i = 1, \\ \frac{\alpha_i\, I_m'(\alpha_i R)}{I_m(\alpha_i R)}, & \text{for } i = 2, 3, \ldots, \end{cases} \tag{2.38}$$

$$L_{m,j} = \begin{cases} \frac{k' J'_m(k'R)}{J_m(k'R)}, & \text{for } j = 1, \\ \frac{\alpha_j I'_m(\alpha_j R)}{I_m(\alpha_j R)}, & \text{for } j = 2, 3, \ldots, \end{cases} \tag{2.39}$$

$$U_{m,i} = V_{m,i} = 0, \tag{2.40}$$

$$P_m = \frac{\mathrm{i}g\epsilon_m J_m(kR_p)}{\omega \cosh(kh_1)}, \tag{2.41}$$

$$P'_m = \frac{\mathrm{i}g\epsilon_m k J'_m(kR_p)}{\omega \cosh(kh_1)}. \tag{2.42}$$

In order to obtain the wave forces, we need to find the unknown coefficients $A_{m,n}$, $B_{m,n}$, $C_{m,n}$ and $D_{m,n}$. Since each expression is an infinite series, there is a need to truncate each series suitably to compute the values of the coefficients. Therefore, all infinite series are truncated after a finite number of terms, $N = 30$. Subsequently, in order to determine the unknown coefficients, we arrive at a linear system of algebraic equations

$$M_l X_l = E_l, \tag{2.43}$$

where $X_l = [A_{l1}, A_{l2}, \ldots, A_{lN}, B_{l1}, B_{l2}, \ldots, B_{lN}, C_{l1}, C_{l2}, \ldots, C_{lN}, D_{l1}, D_{l2}, \ldots, D_{lN}]^T$, M_l the coefficient matrices and E_l the right hand vectors.

That the infinite series can be truncated at $N = 30$ is influenced by the fact that many earlier established results, e.g., those of Berggren and Johansson [2] and Wu et al. ([37],[38]) were obtained with such truncation. Moreover, arriving at desired results by taking $N = 30$ also gave us the idea to consider such truncation. The same is followed in all subsequent problems.

2.4 Wave forces

We proceed to find the wave exciting force acting on the cylinders due to the diffraction taking place on their surfaces. These forces are generally the forces due to the combined action of an incident velocity potential ϕ_{inc} and a diffracted velocity potential ϕ_d on the structures. Let us assume that F_{inc} is the horizontal exciting force for the incident velocity potential and F_d is the diffraction force for the diffracted velocity potential. Therefore the total horizontal exciting force can be written as

$$F_s = F_{inc} + F_d = \mathrm{i}\rho\omega \int_S \phi_{inc}\, n_x ds + \mathrm{i}\rho\omega \int_S \phi_d\, n_x ds, \tag{2.44}$$

where $\overrightarrow{n} = n_x\vec{i} + n_y\vec{j} + n_z\vec{k}$ is the unit normal vector towards the cylinder at the surface of the cylinder. The position vector $\overrightarrow{r}$ is from the origin to the surface element ds. For the horizontal exciting force, $n_x = -\cos\theta$ and when the orthogonality of cosine function is used, the only non-zero value of the integral $\int_0^{2\pi} \cos m\theta \cos\theta$ is the one corresponding to $m = 1$. Therefore, we derive the expression for the horizontal exciting force F_{inc} due to the incident velocity potential as

$$F_{inc} = \mathrm{i}\rho\omega \int_S (\phi_{inc}|_{r=R})\, n_x ds, \tag{2.45}$$

or,

$$F_{inc} = -\frac{2\pi\rho g \mathrm{i} R J_1(kR)}{\cosh(kh_1)} \frac{\sinh(kh_1) - \sinh[k(h_1 - e_1)]}{k}. \tag{2.46}$$

For the diffraction problem, the total velocity potential is the combination of the incident and diffracted velocity potentials. Therefore the total horizontal exciting force (F_{s1}) acting on cylinder 1 can be written as

$$F_{s1} = F_{inc} + F_{d2}, \tag{2.47}$$

where F_{d2} is the horizontal diffraction force due to the diffracted velocity potential ϕ_{d2} acting on cylinder 1 in region II. Now from equations (2.44) and (2.47), we get the total horizontal exciting force acting on cylinder 1 as

$$F_{s1} = -\mathrm{i}\rho\pi\omega R \sum_{n=1}^{\infty} (B_{1,n} + C_{1,n}) \frac{\sin(\alpha_n e_2) - \sin(\alpha_n h_2)}{\alpha_n}. \tag{2.48}$$

The dimensionless horizontal exciting force F_{s1}/w_0, where $w_0 = \rho g \pi R^2$, is given by

$$F_{s1}/w_0 = \frac{-\mathrm{i}\,\omega}{gR} \sum_{n=1}^{\infty} (B_{1,n} + C_{1,n}) \frac{\sin(\alpha_n e_2) - \sin(\alpha_n h_2)}{\alpha_n}. \tag{2.49}$$

The total horizontal exciting force acting on cylinder 2 can be written as

$$F_{s2} = F_{inc} + F_{d1}, \tag{2.50}$$

where F_{d1} is the horizontal diffraction force due to the diffracted velocity potential ϕ_{d1} in region I. Using equations (2.44) and (2.50), we get the total horizontal exciting force

acting on cylinder 2 as

$$F_{s2} = -\mathrm{i}\rho\pi\omega R_p \sum_{n=1}^{\infty} A_{1,n} \frac{\sin[\lambda_n(h_1 - e_2)]}{\lambda_n}. \tag{2.51}$$

The dimensionless horizontal exciting force F_{s2}/w_1, where $w_1 = \rho g \pi R_p^2$, is given by

$$F_{s2}/w_1 = \frac{-\mathrm{i}\,\omega}{gR_p} \sum_{n=1}^{\infty} A_{1,n} \frac{\sin[\lambda_n(h_1 - e_2)]}{\lambda_n}. \tag{2.52}$$

2.5 Numerical results

We use Matlab to solve the system of linear equations. So by the available solution methods in Matlab, for example, Gauss elimination method for the system of equations, one can obtain the solutions. We verify these solutions by some other methods in Matlab like $X_l = M_l \setminus E_l$. Thus the diffracted potentials at any location in each sub-domain can be computed. (Note that for the computation of such potentials, including radiation potentials, in the following chapters also, we use the same methods.) The values of parameters that are kept constant throughout the numerical calculation are $h_1 = 3$ *metre*, $e_2/h_1 = 0.25$ $g = 9.8066$ *metre*/*sec*^{2}. Since we wish to compute the forces for two distinct cases, against the frequency and against the wavenumber, we suitably choose the values of the other parameters. For the former case, we consider $e_1/h_1 = 0.1, R/h_1 = 0.2$; f is the wave frequency: $f = \omega/(2\pi)$. Now we plot F_{s1}/w_0 against f for specific values of R_p, i.e., for $R_p/h_1 = 0.2,\ 0.4,\ 0.9,\ 1.6$ and 2. In Figure 2.2 we observe that no oscillations occur for the first three values of R_p/h_1 when $R_p/h_1 < 1$. We observe oscillations for higher values of R_p/h_1, e.g., $R_p/h_1 = 1.6$ and $R_p/h_1 = 2$ in which case $R_p/h_1 > 1$. It is observed that the oscillations, whenever they occur, happen only at lower frequencies. The exciting force has more than one peak value for those higher values of R_p/h_1. For all values of R_p/h_1, the maximum value of the force occurs within the lower values of f; for $f < 0.75$, to be precise. For higher values of f, the forces steadily diminish reaching almost zero from $f = 2.75$ onwards. It is observed that the peak values occur in the range of $0.274 - 0.4218$. It is to be noted that the highest peak value occurs for $R_p/h_1 = 0.4$, closely followed by those for $R_p/h_1 = 0.9$

and $R_p/h_1 = 1.6$. For clear observation, we produce three figures: Figure 2.2 containing the forces for all values of R_p/h_1; Figure 2.3 containing the forces for $R_p/h_1 = 0.2,\ 0.4$ and $R_p/h_1 = 0.9$; Figure 2.4 containing the forces for $R_p/h_1 = 0.9,\ 1.6$, and 2.0. The main remarkable feature at this point is that the peak values of the exciting force occur at lower frequencies and the forces almost vanish at higher frequencies.

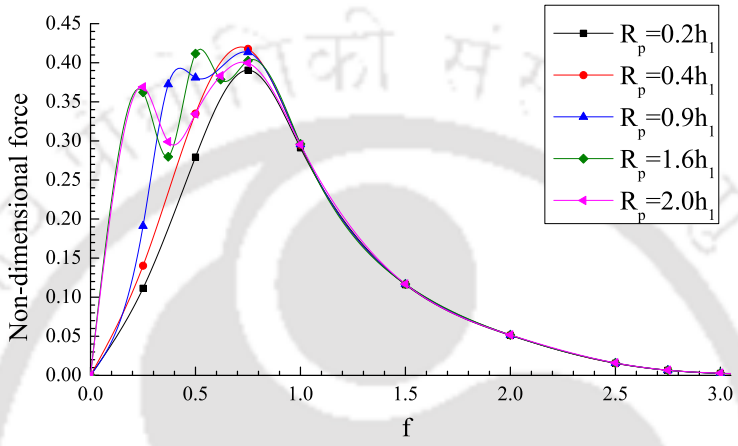

Figure 2.2: Non-dimensional horizontal exciting force F_{s1}/w_0 on hollow cylinder versus wave frequency f for different values of radius (R_p/h_1) of bottom-mounted cylinder with $h_1 = 3\ metre, e_2/h_1 = 0.25, e_1/h_1 = 0.1,\ R/h_1 = 0.2$.

Next we investigate the effect of the gap between the cylinders on the exciting force for cylinder 1. Here we fix the values of R/h_1 and R_p/h_1 by taking $R/h_1 = 0.2$ and $R_p/h_1 = 0.4$. We plot F_{s1}/w_0 against kR for different gaps between the cylinders, $h_2/h_1 = 0.183, 0.150, 0.116, 0.083$. From Figure 2.5, we observe that as the gap decreases, the values of the exciting force increases. Consequently, the higher values of the force are due to $h_2/h_1 = 0.083$. It is to be noted that the force attains higher values corresponding to the lower values of the wavenumber k. For higher values of k, the force diminishes steadily.

Now we examine the horizontal exciting force due to cylinder 2. When we compute the force for different gaps between the cylinders, we choose $R/h_1 = 0.2$ and $R_p/h_1 = 0.2$. We plot F_{s2}/w_1 against kR for different gaps: $h_2/h_1 = 0.217, 0.150, 0.083$. In Figure 2.6 also, it is noticed that as the gap decreases, the exciting force increases, i.e., the higher

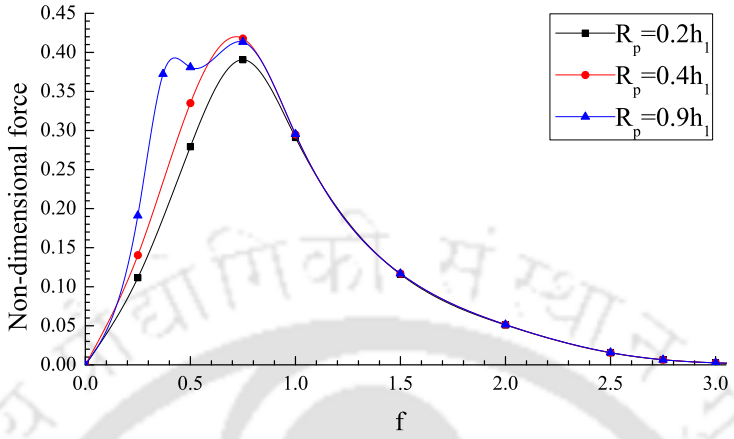

Figure 2.3: Non-dimensional horizontal exciting force F_{s1}/w_0 on hollow cylinder versus wave frequency f for different values of radius (R_p/h_1) of bottom-mounted cylinder with $h_1 = 3\ metre, e_2/h_1 = 0.25, e_1/h_1 = 0.1, R/h_1 = 0.2$.

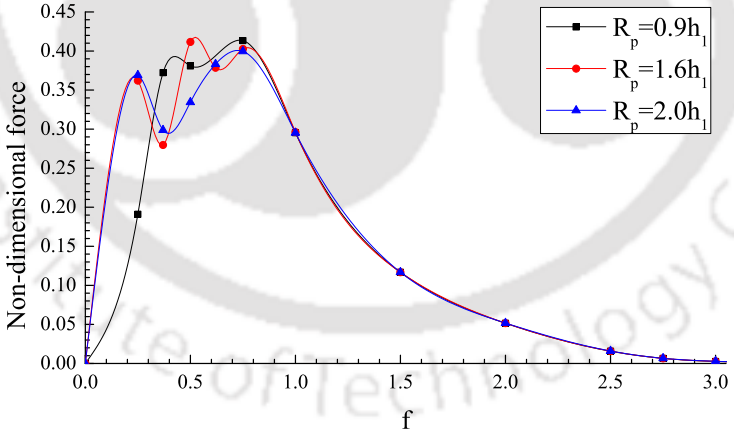

Figure 2.4: Non-dimensional horizontal exciting force F_{s1}/w_0 on hollow cylinder versus wave frequency f for different values of radius (R_p/h_1) of bottom-mounted cylinder with $h_1 = 3\ metre, e_2/h_1 = 0.25, e_1/h_1 = 0.1, R/h_1 = 0.2$.

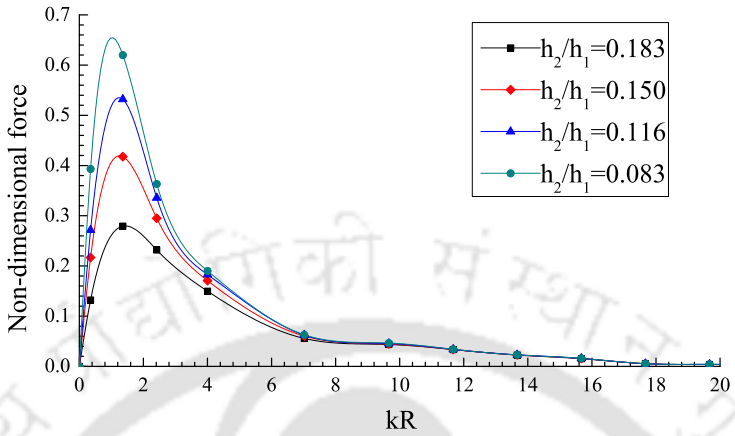

Figure 2.5: Non-dimensional horizontal exciting force F_{s1}/w_0 on hollow cylinder versus kR for different values of gaps between the cylinders with $h_1 = 3\ metre, e_2/h_1 = 0.25, R_p/h_1 = 0.4, R/h_1 = 0.2$.

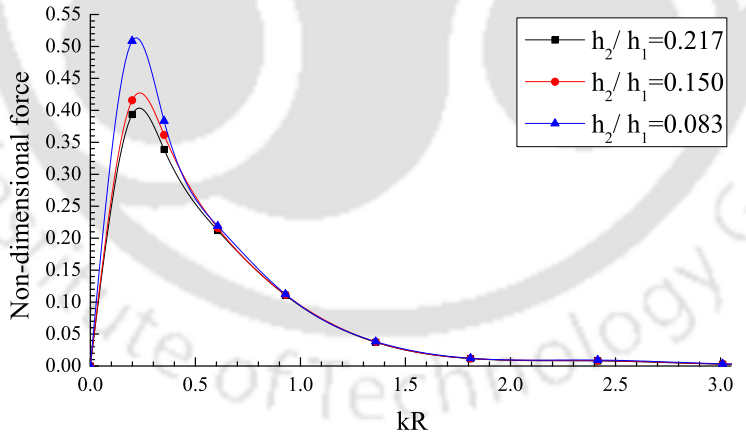

Figure 2.6: Non-dimensional horizontal exciting force F_{s2}/w_1 on bottom-mounted cylinder versus kR for different values of gaps between the cylinders with $h_1 = 3\ metre, e_2/h_1 = 0.25, R_p/h_1 = 0.2, R/h_1 = 0.2$.

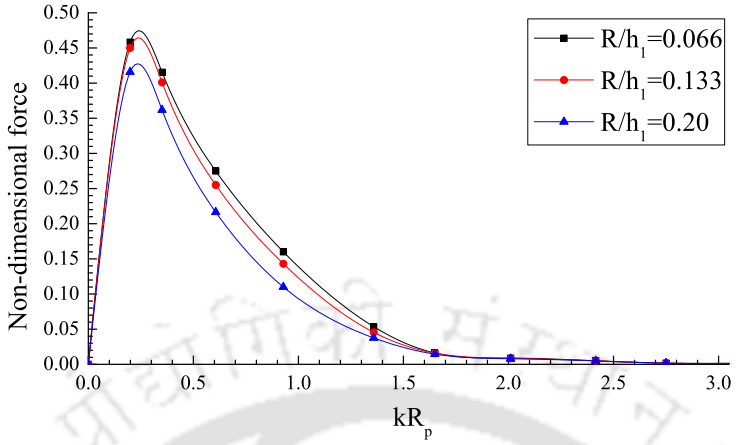

Figure 2.7: Non-dimensional horizontal exciting force F_{s2}/w_1 on bottom-mounted cylinder versus kR_p for different values of radius (R) of upper cylinder with $h_1 = 3\ metre, e_2/h_1 = 0.25, e_1/h_1 = 0.1, R_p/h_1 = 0.2$.

values occur for $h_2/h_1 = 0.083$. The force attains higher values corresponding to the smaller values of the wave number k and diminishing values corresponding to the higher values of k.

For a fixed $R_p/h_1(= 0.2)$, we then investigate the effect of the radius of cylinder 1 on the exciting force for cylinder 2. We plot F_{s2}/w_1 against kR_p for different values of $R/h_1 = 0.066, 0.133, 0.20$. From Figure 2.7, the main observation is that the concerned force attains higher value corresponding to smaller values of R/h_1. The maximum value 0.47711 occurs corresponding to $R/h_1 = 0.066$. Here also, the higher values of the force occur within smaller values of the wavenumber. The force diminishes for higher values of k.

It is reasonable to compare our results with those of Wu et al. [38]. We come up with the same observation regarding the exciting force having higher values at lower frequencies. The difference that we observe is that while the difference in peak values of exciting force for different values of R_p/h_1 is significant in the work of Wu et al. [38], there is no significant deviation of these values for different radius values of cylinder 2 in our case. Additionally, we also calculate the horizontal exciting force for cylinder 2 for different radius values of R/h_1 and different gaps between the cylinders. The

difference between our result and that of Wu et al. [38] may be attributed to the fact that our structure contains a hollow cylinder as the riding one against the solid cylinder considered by them.

2.6 Conclusion

In the present chapter, we derive the velocity potential expressions for the diffraction problem for a hollow cylinder placed over a fixed coaxial bottom-mounted solid cylinder in a uniform water depth by using linear water wave theory. We use an eigenfunction expansion approach and separation of variables technique to solve this problem. In the end, we present the expression for the wave exciting force on the hollow cylinder under the influence of the fixed bottom-mounted solid cylinder and vice versa. We observe that the higher values of the exciting force occur at lower frequencies of the wave for different values of the radius of cylinder 2. The forces diminish quickly at higher frequencies. If the gap between the cylinders is reduced, then the exciting force increases. When exciting force is evaluated for cylinder 1, it is observed that higher value occurs for those values of R_p/h_1 which are less than the uniform depth h_1. While evaluating horizontal force for cylinder 2, we observe that for reduced value of radius of cylinder 1, the exciting force increases. From the results, it is clear that the exciting forces depend on a number of factors such as the radii of the cylinders, the gap between them and also on the depth.

Chapter 3

Surge motion for a radiating hollow cylinder placed above a coaxial bottom- mounted cylinder

3.1 Introduction

In this chapter, we derive the hydrodynamic coefficients due to the horizontal oscillation in surge motion for a floating hollow cylinder placed above a fixed coaxial bottom-mounted cylinder as shown in Figure 2.1. We use the similar method employed in Chapter 2 to obtain the analytical expressions for the corresponding radiated potentials in three clearly identified regions. The analytical expressions of the surge radiated potentials allow us to obtain the corresponding hydrodynamic coefficients, namely, the added mass and damping coefficient, which play a vital role for a structure in motion, however small. Sets of values of added mass and damping coefficient are obtained for different radii of the fixed cylinder and for different gaps (i.e., equivalently also for different drafts of the floating cylinder) between the cylinders for the same fixed radii of the cylinders.

3.2 Mathematical formulation of the problem

We consider the same structure as shown in Figure 2.1 and also use the same formulation as in Chapter 2. Let us consider that the upper floating cylinder is forced to independently oscillate in surge motion with its draft equal to e_1. Since we are going to investigate only the surge motion of the structure, therefore we denote the velocity potential for the radiation problem by $\Phi_{rad,1}(r,\theta,z,t) = Re[\phi_{rad,1}(r,\theta,z)e^{-\mathrm{i}\omega t}]$ where $\phi_{rad,1}(r,\theta,z)$ satisfies Laplace's equation (2.1).

The governing equation and boundary conditions

For the small surge motion of the structure considered here, the radiated potentials with unit amplitude, can be expressed as (substituting $j = 1$ in equation (1.19))

$$\phi_{rad,1}(r,\theta,z) = -\mathrm{i}\omega\varphi_{rad,1}(r,z)\cos\theta, \tag{3.1}$$

where $\varphi_{rad,1}$ denotes the spatial radiated velocity potentials for surge motion. Substitution of equation (3.1) into equation (2.1) gives the following boundary value problem, independent of θ:

$$\frac{1}{r}\frac{\partial\varphi_{rad,1}}{\partial r} + \frac{\partial^2\varphi_{rad,1}}{\partial r^2} + \frac{\partial^2\varphi_{rad,1}}{\partial z^2} - \frac{\varphi_{rad,1}}{r^2} = 0, \tag{3.2}$$

$$\frac{\partial\varphi_{rad,1}}{\partial z} - \frac{\omega^2}{g}\varphi_{rad,1} = 0, \quad (z=0), \tag{3.3}$$

$$\frac{\partial\varphi_{rad,1}}{\partial z} = 0, \quad (z=-h_1, r\geq R_p; z=-e_2, r\leq R_p), \tag{3.4}$$

$$\frac{\partial\varphi_{rad,1}}{\partial r} = 1, \quad (-e_1<z<0, r=R), \tag{3.5}$$

$$\lim_{r\to\infty}\sqrt{r}\left[\frac{\partial\varphi_{rad,1}}{\partial r} - \mathrm{i}k\varphi_{rad,1}\right] = 0. \tag{3.6}$$

Here the solutions for the boundary value problem are to be obtained in three physical regions as shown in Figure 2.1. The added mass and damping coefficient are obtained by solving this radiation problem. In the equations, $\varphi^I_{rad,1}$, $\varphi^{II}_{rad,1}$ and $\varphi^{III}_{rad,1}$ represent the radiated potentials in regions I, II and III, respectively.

3.3 Method of solution

We apply the similar technique as in Chapter 2 in each sub-domain in order to obtain the expression for the velocity potentials. Each expression is obtained as an infinite series of orthogonal functions valid in the respective sub-domain. The analytical expressions for the radiated velocity potentials in different regions, based on the results of Wu et al. [38], are found to be

$$\varphi^{I}_{rad,1} = \sum_{n=1}^{\infty} A_n \frac{R_1(\lambda_n r)}{R_1(\lambda_n R_p)} \cos[\lambda_n(z+h_1)], \tag{3.7}$$

$$\varphi^{II}_{rad,1} = \sum_{n=1}^{\infty} \left[B_n \frac{S_1(\alpha_n r)}{S_1(\alpha_n R)} + C_n \frac{V_1(\alpha_n r)}{V_1(\alpha_n R)} \right] \cos[\alpha_n(z+e_2)], \tag{3.8}$$

$$\varphi^{III}_{rad,1} = D_1 \frac{J_1(k'r)}{J_1(k'R)} \cosh[k'(z+e_2)] + \sum_{n=2}^{\infty} D_n \frac{I_1(\alpha_n r)}{I_1(\alpha_n R)} \cos[\alpha_n(z+e_2)], \tag{3.9}$$

where A_n, B_n, C_n and D_n are unknown coefficients which are to be determined; λ_n and α_n are to be determined from equations (2.12) and (2.13).

The radial functions $R_1(.)$ and $S_1(.)$ can be obtained from equations (2.14)–(2.17) and $V_1(.)$ are given by

$$V_1(\alpha_n r) = H_1^{(2)}(k'r), \qquad n = 1, \tag{3.10}$$

$$V_1(\alpha_n r) = I_1(\alpha_n r), \qquad n = 2, 3, \ldots. \tag{3.11}$$

Matching conditions and body boundary conditions

The appropriate matching conditions are introduced by means of continuity of pressure and that of velocity along the vertical boundaries as depicted in Figure 2.1. Therefore, using these continuity conditions and also the boundary conditions at $r = R_p$ and $r = R$, we have

$$\varphi^{I}_{rad,1} = \varphi^{II}_{rad,1}, \quad \text{for} \quad -e_2 \le z \le 0,\ r = R_p, \tag{3.12}$$

$$\frac{\partial \varphi^{I}_{rad,1}}{\partial r} = \begin{cases} \frac{\partial \varphi^{II}_{rad,1}}{\partial r}, & \text{for} \quad -e_2 \le z \le 0,\ r = R_p, \\ 0, & \text{for} \quad -h_1 \le z \le -e_2,\ r = R_p, \end{cases} \tag{3.13}$$

$$\varphi^{II}_{rad,1} = \varphi^{III}_{rad,1}, \quad \text{for} \quad -e_2 \le z \le -e_1,\ r = R, \tag{3.14}$$

$$\frac{\partial \varphi^{II}_{rad,1}}{\partial r} = \begin{cases} \frac{\partial \varphi^{III}_{rad,1}}{\partial r}, & \text{for} \quad -e_2 \le z \le -e_1,\ r = R, \\ 1, & \text{for} \quad -e_1 \le z \le 0,\ r = R. \end{cases} \tag{3.15}$$

3.4 Hydrodynamic coefficients and numerical results

In order to obtain the hydrodynamic coefficients for the radiating cylinder, we need to find the unknown coefficients appearing in the radiated potentials by applying suitable matching conditions. The resultant infinite series are truncated up to finite number of terms, $N = 30$. In order to determine the unknown coefficients appearing in equations (3.7)–(3.9), we convert the expressions, after using the suitable matching conditions, into a linear system of algebraic equations by the same approach as in Chapter 2. The hydrodynamic pressure is obtained from linearized Bernoulli's equation for the surge motion (putting $j = 1$ in equation (1.18))

$$p_1 = \rho\, \omega^2 \varphi_{rad,1}(r, z) \cos\theta. \tag{3.16}$$

The radiated force is the force due to the motion of the body. It can be computed from the radiated potential whereby the radiated force on the body due to surge motion in horizontal direction can be written as (from equation (1.20))

$$F_{11} = -\int_S p_1\, n_x\, ds, \tag{3.17}$$

where n_x is the component of the unit outward normal vector to the body in the x-direction and S is the submerged surface of the body. Therefore, using equation (3.16) in equation (3.17), we have

$$F_{11} = -\rho\, \omega^2 \int_S \varphi_{rad,1}(R, z) \cos\theta\, n_x ds, \tag{3.18}$$

which can be rewritten as

$$F_{11} = \omega^2 \left[\mu_{11} + \mathrm{i}\frac{\lambda_{11}}{\omega}\right], \tag{3.19}$$

in which

$$\mu_{11} + \mathrm{i}\frac{\lambda_{11}}{\omega} = -\rho \int_S \varphi_{rad,1}(R, z) \cos\theta\, n_x ds, \tag{3.20}$$

where μ_{11} and λ_{11} are the added mass and damping coefficients, respectively, for the surge motion. Therefore, the added mass and damping coefficient expressions for surge motion of the radiating cylinder 1 is given by

$$\mu_{11} + \mathrm{i}\frac{\lambda_{11}}{\omega} = -\rho \int_S (\varphi^{II}_{rad,1}(R,z) - \varphi^{III}_{rad,1}(R,z)) \cos\theta \; n_x \; ds, \tag{3.21}$$

or,

$$\mu_{11} + \mathrm{i}\frac{\lambda_{11}}{\omega} = -\pi\rho R \sum_{n=1}^{\infty} [(B_n + C_n) - D_n] \frac{\sin(\alpha_n e_2) - \sin(\alpha_n h_2)}{\alpha_n}. \tag{3.22}$$

The expression of $\varphi_{rad,1}$ in brackets in equation (3.21) indicates that by considering this expression, the effect of the internal fluid domain III is appropriately taken into account in calculating the hydrodynamics coefficients. The added mass is non-dimensionalized by dividing it by the mass of the water displaced by a semi-immersed sphere with radius R, amounting to $\frac{2}{3}\pi\rho R^3$, and the damping coefficient is non-dimensio- nalized by dividing it by the same factor but multiplied by the angular frequency ω. Thus the non-dimensionalized added mass $\overline{\mu_{11}}$ and damping coefficient $\overline{\lambda_{11}}$ are given by

$$\overline{\mu_{11}} + \mathrm{i}\overline{\lambda_{11}} = -\left(\frac{1}{\frac{2}{3}R^2}\right) \sum_{n=1}^{\infty} [(B_n + C_n) - D_n] \frac{\sin(\alpha_n e_2) - \sin(\alpha_n h_2)}{\alpha_n}. \tag{3.23}$$

The frequency ω is non-dimensionalized by multiplying it by $\sqrt{(R/g)}$, so that the non-dimensionalized frequency $\overline{\omega}$ is represented by $\overline{\omega} = \omega\sqrt{(R/g)}$. Since we wish to compute the hydrodynamic coefficients for two distinct cases for different values of the radius of the cylinder 2 and for different gaps between the cylinders, we suitably choose the values of the other parameters. Figures 3.1 and 3.2, respectively, show the non-dimensional added mass and damping coefficient against non-dimensional frequencies for different values of the ratio of the radius of cylinder 2 to that of cylinder 1, to be precise, for $R_p/R = 1, 2, 4.5, 8$. Here we fix the parameter value $e_1/h_1 = 0.05$, so that a very small portion of the cylinder is submerged. This enables us to study the hydrodynamic coefficients within feasible limits. It is observed from Figure 3.1 that the values of added mass are almost positive and steady at lower frequencies with no occurrence of appreciable oscillating behaviour. However, at particular frequencies near $\overline{\omega} = 4.35$, the added mass

shows very high oscillating behaviour which can be attributed to resonance situation. This peculiar behaviour in the neighbourhood of $\overline{\omega} = 4.35$ is due to the frequencies corresponding to the wavelengths close to those of the free fluid motion. For all radius ratios, the added mass assumes very high values, both positive and negative, in the neighbourhood of the resonant frequency. It is to be noted that the spikes of all the curves are cut in order to have a clear view of the added mass. The same will be followed for all graphs related to added mass, i.e., for Figures 3.3 and 3.5 also. The values of added mass again stabilize after a while and the oscillations diminish. Similar type of phenomenon is also observed in the works of Mavrakos ([22], [23]) and Newman [26]. Figure 3.2 shows the graphs of non-dimensional damping coefficient for the same set of parameters. It shows that the damping coefficient has small oscillation in lower frequency range and the values corresponding to $R_p/R = 2.0, 4.5, 8.0$, converge and are higher than those corresponding to $R_p/R = 1.0$. Same kind of oscillation, as in the case of added mass in Figure 3.1, is noticed in the neighbourhood of $\overline{\omega} = 4.35$ with the only difference being that damping coefficient corresponds to high positive values only as against both high positive and negative values in Figure 3.1.

In Figures 3.3 and 3.4, added mass and damping coefficient are plotted against frequency for different drafts of the upper cylinder for $R_p/R = 1.0$. Figure 3.3 shows that there is no appreciable change of the added mass for all draft values till higher frequency is considered. Higher values (both negative and positive) are observed for added mass for all draft ratios near $\overline{\omega} = 4.35$. Figure 3.4 shows that the damping coefficient varies in the lower frequency range for the higher values of the draft while the values do not change significantly corresponding to the lower draft value. Regarding its behaviour near $\overline{\omega} = 4.35$, the same observation, as noticed in Figure 3.2, is made.

In Figures 3.5 and 3.6, we change the radius ratio to $R_p/R = 2.0$, keeping all other parameter values the same. Figure 3.5 shows that the added mass does not change significantly in the lower range of frequency. However, a sharp change is observed near the neighbourhood of $\overline{\omega} = 4.35$ for all values of the draft. In Figure 3.6, the behaviour of damping coefficient is same as like in Figure 3.4 for lower frequency range, but the coefficient attains only high positive values in the neighbourhood of $\overline{\omega} = 4.35$ for all

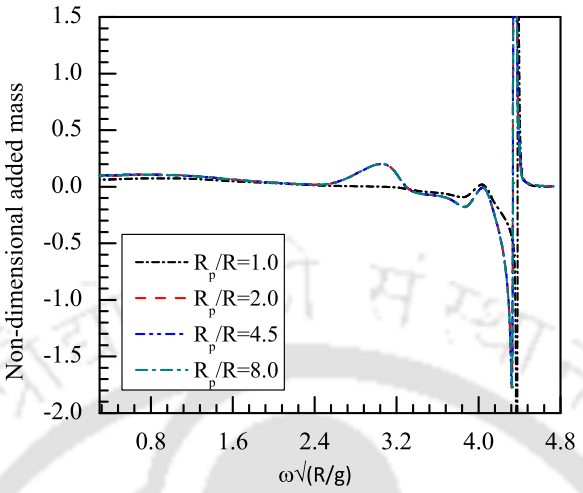

Figure 3.1: Non-dimensional added mass versus non-dimensional frequency $\omega\sqrt{(R/g)}$ for cylinder 1 for different values of radius R_p of bottom-mounted cylinder with $e_2/h_1 = 0.25, e_1/h_1 = 0.05, R/h_1 = 0.2$.

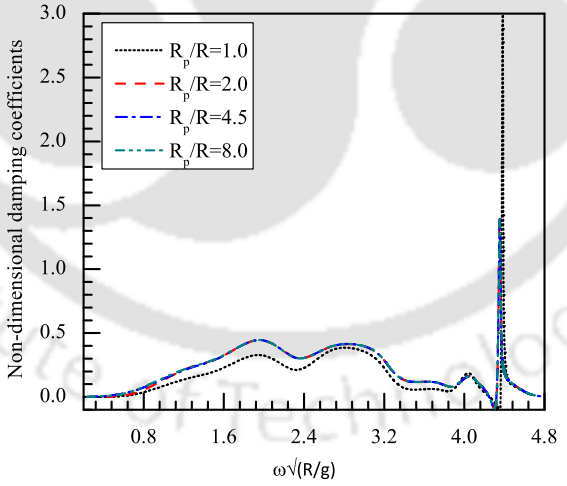

Figure 3.2: Non-dimensional damping coefficient versus non-dimensional frequency $\omega\sqrt{(R/g)}$ for cylinder 1 for different values of radius R_p of bottom-mounted cylinder with $e_2/h_1 = 0.25, e_1/h_1 = 0.05, R/h_1 = 0.2$.

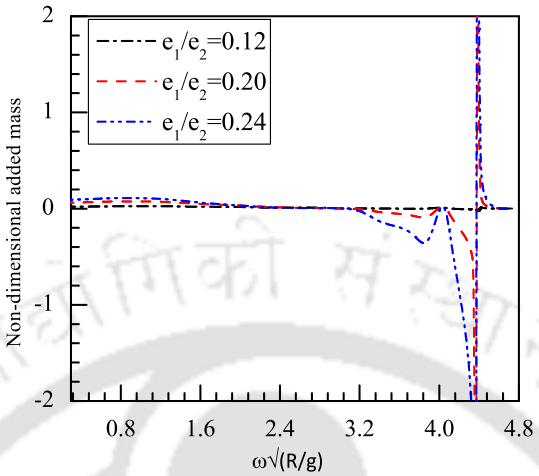

Figure 3.3: Non-dimensional added mass versus non-dimensional frequency $\omega\sqrt{(R/g)}$ for different drafts of cylinder 1 with $e_2/h_1 = 0.25, R_p/R = 1$.

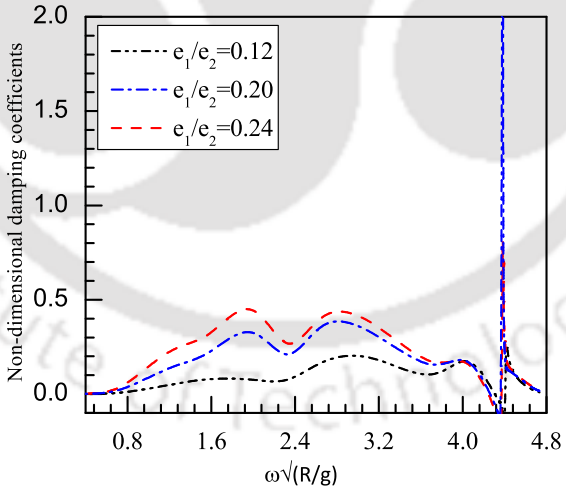

Figure 3.4: Non-dimensional damping coefficient versus non-dimensional frequency $\omega\sqrt{(R/g)}$ for different drafts of cylinder 1 with $e_2/h_1 = 0.25, R_p/R = 1$.

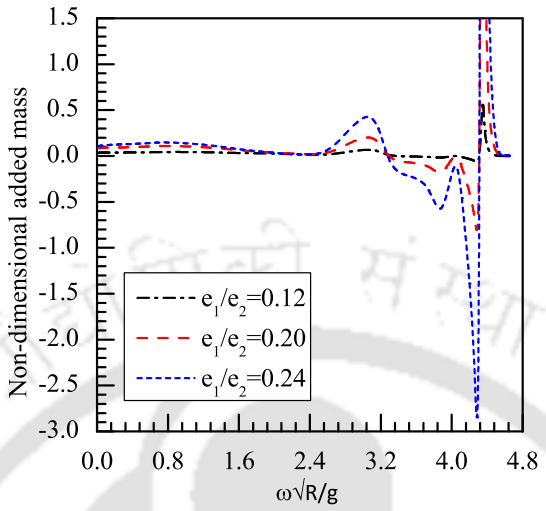

Figure 3.5: Non-dimensional added mass versus non-dimensional frequency $\omega\sqrt{(R/g)}$ for different drafts of cylinder 1 with $e_2/h_1 = 0.25, R_p/R = 2$.

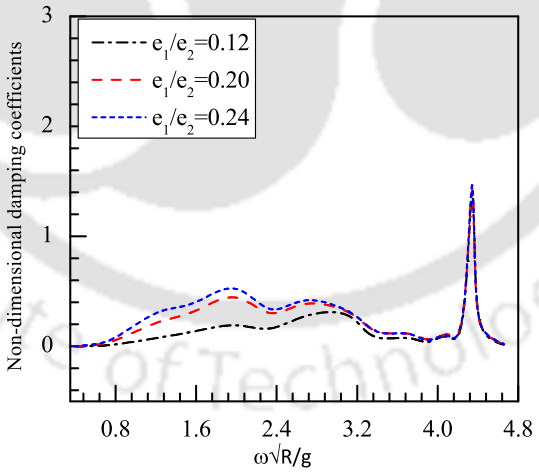

Figure 3.6: Non-dimensional damping coefficient versus non-dimensional frequency $\omega\sqrt{(R/g)}$ for different drafts of cylinder 1 with $e_2/h_1 = 0.25, R_p/R = 2$.

draft values, as compared to small negative values in Figure 3.4. In addition to the

Table 3.1: Fluid velocity $\frac{\partial \varphi^I_{rad,1}}{\partial r}$ at $r = R_p$ with $e_2/h_1 = 0.25, e_1/h_1 = 0.1, R_p/R = 2$.

z	$\left(\mathrm{Re}\left(\frac{\partial \varphi^I_{rad,1}}{\partial r}\right), \mathrm{Im}\left(\frac{\partial \varphi^I_{rad,1}}{\partial r}\right)\right)$ for $\omega\sqrt{(R/g)} = 0.575$	$\left(\mathrm{Re}\left(\frac{\partial \varphi^I_{rad,1}}{\partial r}\right), \mathrm{Im}\left(\frac{\partial \varphi^I_{rad,1}}{\partial r}\right)\right)$ for $\omega\sqrt{(R/g)} = 0.777$
$-0.97h_1$	$(-2.490286 \times 10^{-4}, 9.439556 \times 10^{-4})$	$(-6.053139 \times 10^{-4}, -2.458583 \times 10^{-4})$
$-0.90h_1$	$(3.510383 \times 10^{-4}, 2.496678 \times 10^{-4})$	$(-8.882016 \times 10^{-4}, -1.505102 \times 10^{-4})$
$-0.84h_1$	$(-5.048898 \times 10^{-4}, 9.121897 \times 10^{-5})$	$(-9.191510 \times 10^{-4}, -4.901893 \times 10^{-5})$

Table 3.2: Fluid velocity $\frac{\partial \varphi^{II}_{rad,1}}{\partial r}$ and $\frac{\partial \varphi^{III}_{rad,1}}{\partial r}$ at $r = R$ with $e_2/h_1 = 0.25, e_1/h_1 = 0.1, R_p/R = 2, \omega\sqrt{(R/g)} = 0.575$

z	$\left(\mathrm{Re}\left(\frac{\partial \varphi^{II}_{rad,1}}{\partial r}\right), \mathrm{Im}\left(\frac{\partial \varphi^{II}_{rad,1}}{\partial r}\right)\right)$	$\left(\mathrm{Re}\left(\frac{\partial \varphi^{III}_{rad,1}}{\partial r}\right), \mathrm{Im}\left(\frac{\partial \varphi^{III}_{rad,1}}{\partial r}\right)\right)$
$-0.01h_1$	$(0.993883, 2.228317 \times 10^{-4})$	$(0.992256, 7.385356 \times 10^{-3})$
$-0.02h_1$	$(0.995501, 9.321001 \times 10^{-4})$	$(0.996337, 7.148742 \times 10^{-3})$
$-0.07h_1$	$(1.007167, 1.940581 \times 10^{-4})$	$(1.002769, 7.183632 \times 10^{-3})$

Table 3.3: Fluid velocity $\frac{\partial \varphi^{II}_{rad,1}}{\partial r}$ and $\frac{\partial \varphi^{III}_{rad,1}}{\partial r}$ at $r = R$ with $e_2/h_1 = 0.25, e_1/h_1 = 0.1, R_p/R = 2, \omega\sqrt{(R/g)} = 0.777$

z	$\left(\mathrm{Re}\left(\frac{\partial \varphi^{II}_{rad,1}}{\partial r}\right), \mathrm{Im}\left(\frac{\partial \varphi^{II}_{rad,1}}{\partial r}\right)\right)$	$\left(\mathrm{Re}\left(\frac{\partial \varphi^{III}_{rad,1}}{\partial r}\right), \mathrm{Im}\left(\frac{\partial \varphi^{III}_{rad,1}}{\partial r}\right)\right)$
$-0.01h_1$	$(1.010150, -4.09232 \times 10^{-4})$	$(0.997073, 2.937003 \times 10^{-3})$
$-0.02h_1$	$(1.002121, 7.029969 \times 10^{-4})$	$(0.990895, 2.809269 \times 10^{-3})$
$-0.07h_1$	$(1.010399, 5.696986 \times 10^{-4})$	$(0.999575, 2.628538 \times 10^{-3})$

graphical presentation of the results for the above consideration, a numerical verification is carried out for the body boundary condition (3.5). For parameters considered and admissible draft value, Table 3.1 shows that the values of the fluid velocity corresponding to boundary condition (3.5) in $-h_1 \leq z \leq -0.75h_1, r = R_p$ approach 0, even for two different values of $\omega\sqrt{(R/g)} = 0.575, 0.777$. Tables 3.2 and 3.3, respectively, show that the values of the fluid velocities in both regions II and III corresponding to boundary condition (3.5) in $-0.1h_1 \leq z \leq 0, r = R$ approach 1, for these two different values of $\omega\sqrt{(R/g)}$.

It is reasonable to compare our results with those of Mavrakos ([22], [23]). As observed in Mavrakos' work, occurrence of oscillation in the values of added mass and

damping coefficient due to resonance in the neighbourhood of a particular frequency is also observed in our case though the value of this particular frequency is different. If our work is compared with that of Wu et al. [38], the hydrodynamic coefficients obtained in our work differs from those in the work of Wu et al. [38] in some cases. This again may be due to the fact that Wu et al. [38] considered a solid cylinder as the riding one while we consider a hollow cylinder to be riding in waves.

3.5 Particular case: Single hollow cylinder floating over an even sea bottom

3.5.1 Mathematical formulation

In order to have a comparison with the case in which no bottom-mounted cylinder exists, we consider the base case with only the riding upper cylinder present. This means that now the present device consists of a single floating hollow cylinder only and we divide the whole region into two regions: an interior region ($r \leq R$) and an exterior region ($r \geq R$).

The governing equation and boundary conditions

The governing equation, free surface condition, body surface condition and radiation condition are same as equations (3.2), (3.3), (3.5) and (3.6), respectively. The impermeable bottom condition for this case is given by

$$\frac{\partial \varphi_{rad,1}}{\partial z} = 0, \quad (z = -h_1), \tag{3.24}$$

3.5.2 Radiated potentials

By applying the similar procedure, the expressions of the radiated velocity potentials for the surge motion in the exterior and interior regions are, respectively, given by

$$\varphi^{ext}_{rad,1} = \sum_{n=1}^{\infty} E_n \frac{R_1(\lambda_n r)}{R_1(\lambda_n R)} \cos[\lambda_n (z + h_1)], \tag{3.25}$$

$$\varphi^{int}_{rad,1} = F_1 \frac{J_1(kr)}{J_1(kR)} \cosh[k(z + h_1)] + \sum_{n=2}^{\infty} F_n \frac{I_1(\lambda_n r)}{I_1(\lambda_n R)} \cos[\lambda_n (z + h_1)], \tag{3.26}$$

where E_n and F_n are unknown coefficients.

In order to compare the hydrodynamic coefficients for both the cases, we need to compute those for the present case of single cylinder arrangement. The expressions for dimensionless added mass $\overline{\mu'_{11}}$ and damping coefficient $\overline{\lambda'_{11}}$ for the surge motion of the floating hollow cylinder are given by

$$\overline{\mu'_{11}} + \mathrm{i}\overline{\lambda'_{11}} = -\left(\frac{1}{\frac{2}{3}R^2}\right) \sum_{n=1}^{\infty}[(E_n - F_n)] \frac{\sin(\lambda_n h_1) - \sin(\lambda_n h_2)}{\lambda_n}. \tag{3.27}$$

3.5.3 Numerical results

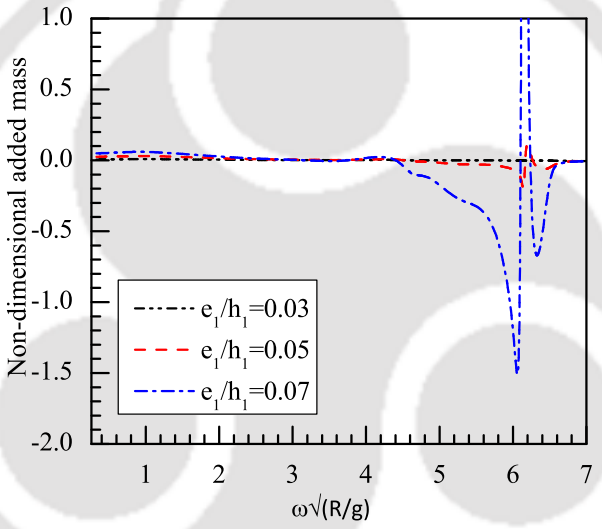

Figure 3.7: Non-dimensional added mass versus non-dimensional frequency $\omega\sqrt{(R/g)}$ for different drafts of the cylinder (for the base case of single hollow cylinder configuration) with $R/h_1 = 0.4$.

Figures 3.7 and 3.8, respectively, show the non-dimensional added mass and damping coefficient against non-dimensional frequencies for the case of single hollow cylinder configuration, i.e., when the height of the bottom-mounted cylinder is zero. By comparing Figure 3.7 with Figure 3.5 and Figure 3.8 with Figure 3.6, it is observed that the variation in the values of added mass and damping coefficient, respectively, in the lower frequency range is less for the single cylinder arrangement. It is to be noted that here

the radius of the cylinder is taken as $R/h_1 = 0.4$ in order to compare the result with the double cylinder arrangement.

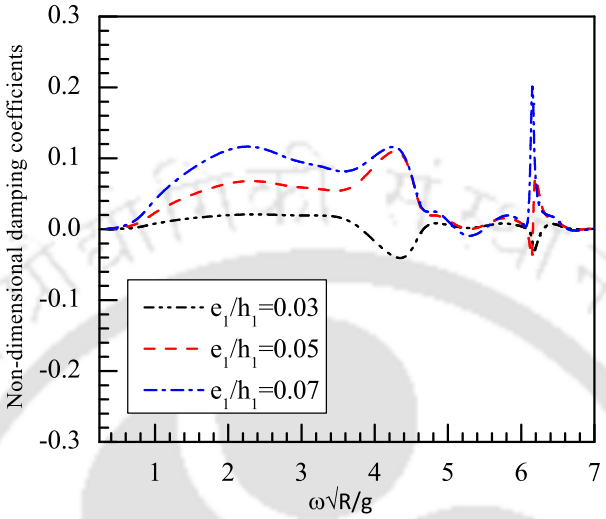

Figure 3.8: Non-dimensional damping coefficient versus non-dimensional frequency $\omega\sqrt{(R/g)}$ for different drafts of the cylinder (for the base case of single hollow cylinder configuration) with $R/h_1 = 0.4$.

3.6 Comparison of present work with available results

For validating our result, we consider the results of Miloh [25] to be compared with our result when the height of the bottom cylinder is zero, i.e., the bottom cylinder is not present. All the parameters considered in our problem are reconsidered according to the ones from Miloh's work in order to have the same physical problem. Consequently, the values of different parameters considered are: $R = 15cm$, $e_1 = 8cm$, $h_1 = 60cm$. So the non-dimensional parameters are $\mu = kR, \nu = h_2/R, \tau = h_1/R, \lambda = e_1/R, \sigma = R\omega^2/g$. Figures 3.9 and 3.10, respectively, represent the comparison of added mass and damping coefficient between these two works. Good agreement can be observed from both the plots in Figures 3.9 and 3.10. While the damping coefficients match for all values of the

wavenumber, the values of added mass match for all values except for a very small range of small wavenumbers. The matching confirms that our model is valid and hence can be employed effectively to investigate various issues related to radiation problems for the type of structures under consideration.

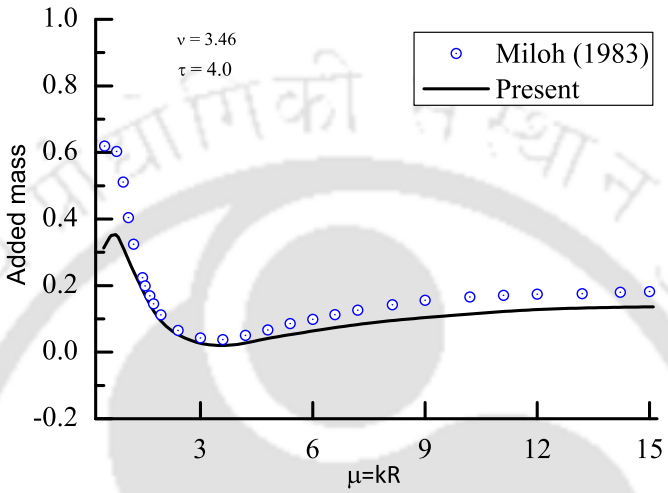

Figure 3.9: Comparison of added mass with result of Miloh (1983) with $R = 15\ cm, e_1 = 8\ cm, h_1 = 60\ cm$

3.7 Conclusion

The radiated potentials, in different sub-domains of the fluid, due to surge motion are obtained for a vertical hollow cylinder placed above a coaxial solid cylinder of greater radius. An eigenfunction approach and separation of variables technique are used to solve this radiation problem governed by Laplace's equation. Non-dimensionalized added mass and damping coefficient are obtained and the effects of the radii of the cylinders and also of the gaps between them are investigated. The added mass is steady and almost positive at lower frequencies for any gap and for any value of the radius of the lower cylinder. But it assumes peculiar behaviour near the non-dimensionalized frequency $\omega\sqrt{(R/g)} = 4.35$. This can be attributed to the resonance situation (Mavrakos [22], Newman [26]). For all radius ratios, the added mass assume very high values, both positive and negative,

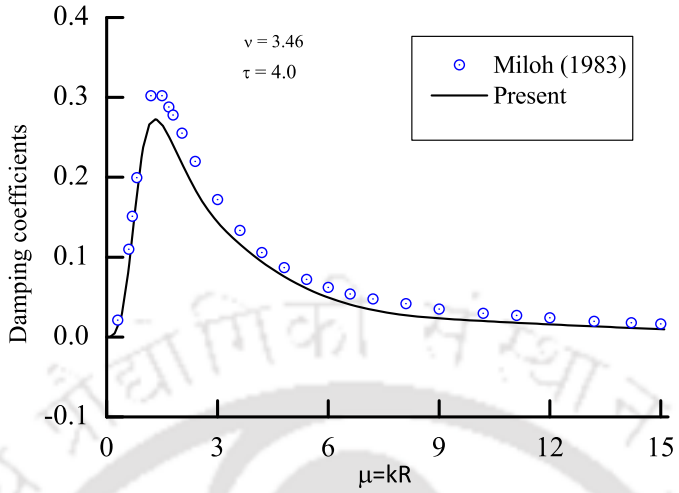

Figure 3.10: Comparison of damping coefficient with result of Miloh (1983) with $R = 15\ cm, e_1 = 8\ cm, h_1 = 60\ cm$

in the neighbourhood of the resonant frequency. The damping coefficient assumes small oscillation in the lower frequency range. Their values increase when the gap between the cylinders is decreased. Here also resonance occurs at $\omega\sqrt{(R/g)} = 4.35$ for different radius ratios and for different gaps of the cylinders. Overall it is observed that there is significant effect of the values of the radii of the cylinders and the gaps between them on the hydrodynamic coefficients for the surge radiation of the riding hollow cylinder placed above a coaxial vertical cylinder. The body boundary condition for both the cylinders is also numerically verified. In order to have a comparison with the case in which no bottom-mounted cylinder exists, we also consider the base case with only the riding upper cylinder present. It is observed that the variation of the values of both added mass and damping coefficient is lower in the lower frequency range when compared to those obtained for the double cylinder arrangement. For validating our result, we compare our result with that of Miloh [25] when the height of the bottom cylinder is zero, i.e., when the bottom cylinder is not present. Good agreement to a large extent can be observed between both results. This confirms that our model is valid and hence can be employed effectively to investigate various issues related to radiation problems

for the type of structures under consideration.

Chapter 4

Roll motion for a radiating coaxial hollow cylinder placed above a coaxial bottom- mounted cylinder

4.1 Introduction

In this chapter, we investigate the hydrodynamic coefficients due to roll motion for a floating hollow cylinder placed above a fixed coaxial bottom-mounted cylinder as shown in Figure 2.1. In order to obtain analytical expressions for the radiated potentials in the clearly identified regions, we apply the same method as in Chapter 3. The added mass and damping coefficient are evaluated for different radii of the fixed cylinder and for different gaps (i.e., also different drafts of the floating cylinder) between the cylinders for the same fixed radii of the cylinders.

4.2 Mathematical formulation of the problem

We consider the same set-up as shown in Figure 2.1 and follow the same mathematical formulation as in Chapter 3. Here, the upper cylinder is forced to independently oscillate in roll motion which is the only motion considered in this chapter.

The governing equation and boundary conditions

Since we are going to investigate only the roll motion of the structure, the corresponding radiated velocity potential $\phi_{rad,5}$ is the only radiated potential to be taken into account. Therefore the radiated velocity potential $\phi_{rad,5}$ for roll motion with unit amplitude, can be expressed as

$$\phi_{rad,5}(r,\theta,z) = -\mathrm{i}\omega\varphi_{rad,5}(r,z)\cos\theta. \tag{4.1}$$

Similarly as in Chapter 3, the substitution of equation (4.1) into equation (2.1) gives the same boundary value problem, independent of θ, for the roll motion except the body boundary condition which is now given by

$$\frac{\partial\varphi_{rad,5}}{\partial r} = z - z_c,\ (-e_1 < z < 0, r = R), \tag{4.2}$$

where $(x_c, y_c, z_c) = (0, 0, z_c)$ is the centre of rotation. The solutions for the boundary value problem are obtained in three physical regions as shown in Figure 2.1. The added mass and damping coefficient are obtained by solving this radiation problem. In the equations, $\varphi^{I}_{rad,5}$, $\varphi^{II}_{rad,5}$ and $\varphi^{III}_{rad,5}$ represent the roll radiated potentials in regions I, II and III, respectively. For the continuity of the flow, we utilize some matching conditions along the virtual vertical boundaries.

4.3 Method of solution

We use the similar method to derive the expression for the velocity potentials in each sub-domain. The analytical expressions for the roll radiated velocity potentials in different regions are found to be

$$\varphi^{I}_{rad,5} = \sum_{n=1}^{\infty} A_n \frac{R_1(\lambda_n r)}{R_1(\lambda_n R_p)} \cos[\lambda_n(z+h_1)], \tag{4.3}$$

$$\varphi^{II}_{rad,5} = \sum_{n=1}^{\infty} \left[B_n \frac{S_1(\alpha_n r)}{S_1(\alpha_n R)} + C_n \frac{V_1(\alpha_n r)}{V_1(\alpha_n R)} \right] \cos[\alpha_n(z+e_2)], \tag{4.4}$$

$$\varphi^{III}_{rad,5} = \sum_{n=1}^{\infty} \left[D_n \frac{E_1(\alpha_n r)}{E_1(\alpha_n R)} \cos[\alpha_n(z+e_2)] \right], \tag{4.5}$$

where A_n, B_n, C_n and D_n are the unknown coefficients, and λ_n and α_n are to be determined from equations (2.12) and (2.13). The radial functions $R_1(.)$, $S_1(.)$ and $V_1(.)$ are given by equations (2.14)–(2.17) and (3.10)–(3.11), respectively, and $E_1(.)$ are given by

$$E_1(\alpha_n r) = J_1(k'r), \qquad n = 1, \tag{4.6}$$

$$E_1(\alpha_n r) = I_1(\alpha_n r), \qquad n = 2, 3, \ldots. \tag{4.7}$$

Matching conditions

We use the similar matching conditions along the interface between the regions and the body boundary conditions as in Chapter 3 in order to find the unknown coefficients of the expressions of radiated potentials.

4.4 Hydrodynamic coefficients and numerical results

In a similar manner like in Chapter 3, the expressions of added mass and damping coefficient for the roll motion of the radiating upper cylinder can be written as (putting $j = 5$ in equation (1.23))

$$\mu_{55} + \mathrm{i}\frac{\lambda_{55}}{\omega} = -\rho \int_S \varphi^{II}_{rad,5}(r,z)\big|_{r=R} \cos\theta\ (z - z_c)\ n_x\ ds, \tag{4.8}$$

or,

$$\mu_{55} + \mathrm{i}\frac{\lambda_{55}}{\omega} = -\pi\rho R \sum_{n=1}^{\infty}(B_n + C_n) \int_{-e_1}^{0} \cos[\alpha_n(z + e_2)](z - z_c)dz, \tag{4.9}$$

where μ_{55} and λ_{55} are the added mass and damping coefficient, respectively. In the similar manner as in Chapter 3, we use the quantity $\frac{2}{3}\pi\rho R^5$ in order to non-dimensionalize added mass and damping coefficient. Therefore, the non-dimensionalized added mass and damping coefficient are, respectively, given by

$$\overline{\mu_{55}} + \mathrm{i}\overline{\lambda_{55}} = -\left(\frac{1}{\frac{2}{3}R^4}\right) \sum_{n=1}^{\infty}(B_n + C_n) \int_{-e_1}^{0} \cos[\alpha_n(z + e_2)](z - z_c)dz. \tag{4.10}$$

4.5 Results and discussion

The frequency ω is non-dimensionalized by multiplying it by $\sqrt{(R/g)}$ and we represent the non-dimensionalized frequency $\overline{\omega}$ by $\overline{\omega} = \omega\sqrt{(R/g)}$. Since we wish to compute the hydrodynamic coefficients for two distinct cases for different values of the radius of the cylinder 2 and for different gaps between the two cylinders, we suitably choose the values of the other parameters. Figures 4.1 and 4.2, respectively, give the plots of added

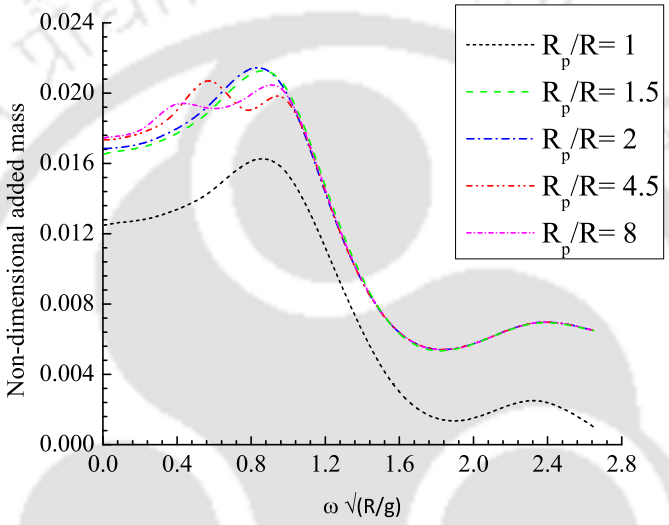

Figure 4.1: Non-dimensional added mass versus non-dimensional frequency $\omega\sqrt{(R/g)}$ for cylinder 1 for different values of radius R_p of bottom-mounted cylinder with $e_2/h_1 = 0.25$, $e_1/h_1 = 0.1$.

mass and damping coefficient for various radius ratios $R_p/R = 1.0$, 1.5, 2.0, 4.5 and 8.0. Figure 4.1 shows that higher values of added mass occur at lower frequencies only ($\omega\sqrt{(R/g)} < 1.2$). It is noticeable that for $R_p/R \neq 1.0$, the values do not show much difference whereas the values corresponding to $R_p/R = 1.0$ are appreciably lower than those for $R_p/R \neq 1.0$. Further, it is observed that oscillations occur for higher radius values $R_p/R > 2$ in the lower frequency range. For the curves in which $R_p/R \neq 1.0$, the higher values correspond to the lower radius ratios. It is also clear that the values diminish at higher frequencies. Figure 4.2 also shows that peak values of the damping

coefficient occur at relatively lower frequencies and they diminish as $\overline{\omega}$ increases. The values are almost same for all $R_p/R \neq 1.0$ whereas the values are somewhat smaller for $R_p/R = 1.0$. No oscillating behaviour is observed for any radius ratio.

Figures 4.3–4.8 show the behaviour of added mass and damping coefficient for various R_p/R due to different gaps between the cylinders. Figures 4.3, 4.5 and 4.7 show the effect of the gaps $(h_2/h_1 = 0.18, 0.15, 0.10)$ on the added mass for different radius ratios: $R_p/R = 1$ for Figure 4.3, $R_p/R = 2$ for Figure 4.5, $R_p/R = 4.5$ for Figure 4.7. For all the cases, higher values occur at lower frequencies and the values diminish as the frequencies increase. It is observed that as the gap decreases, the added mass increases. However, it is apparent from Figure 4.7 that when R_p/R has a greater value at 4.5, there occur oscillations at lower frequencies but only corresponding to the lower values of gaps.

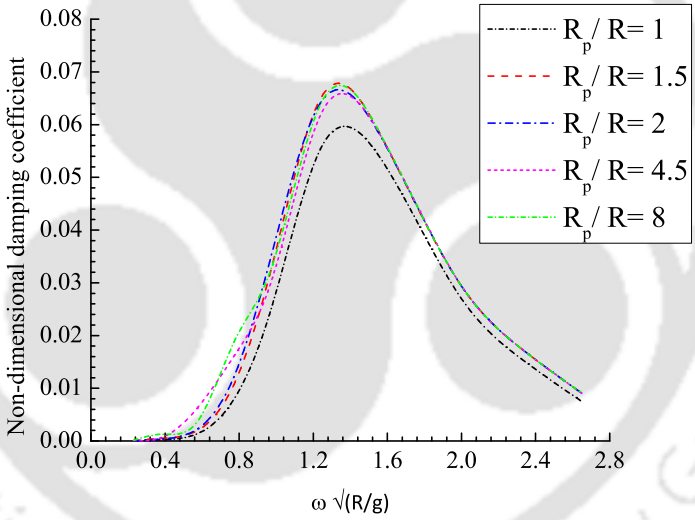

Figure 4.2: Non-dimensional damping coefficient versus non-dimensional frequency $\omega\sqrt{(R/g)}$ for cylinder 1 for different values of radius R_p of bottom-mounted cylinder with $e_2/h_1 = 0.25,\ e_1/h_1 = 0.1$.

Figures 4.4, 4.6 and 4.8 show the effect of the gap between the cylinders on the damping coefficient for different R_p/R. In all cases, it is observed that higher values occur at lower frequencies only and the values are greater when the gap is less. One important observation is that no oscillation occurs for any change of gap for any radius

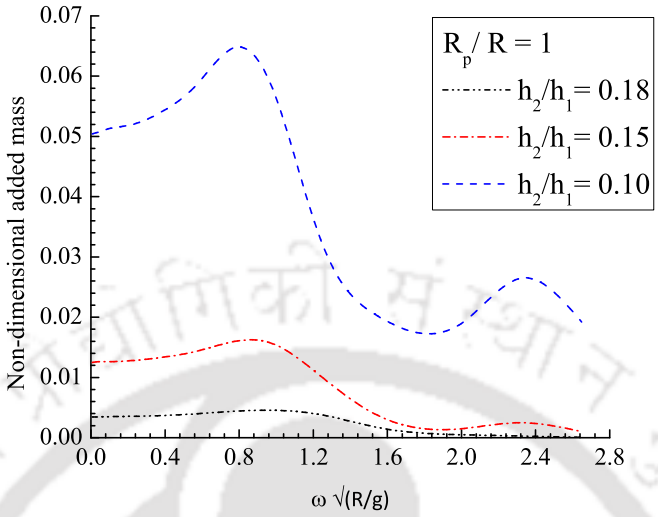

Figure 4.3: Non-dimensional added mass versus non-dimensional frequency $\omega\sqrt{(R/g)}$ for cylinder 1 for different gaps between the cylinders with $e_2/h_1 = 0.25,\ R_p/R = 1$.

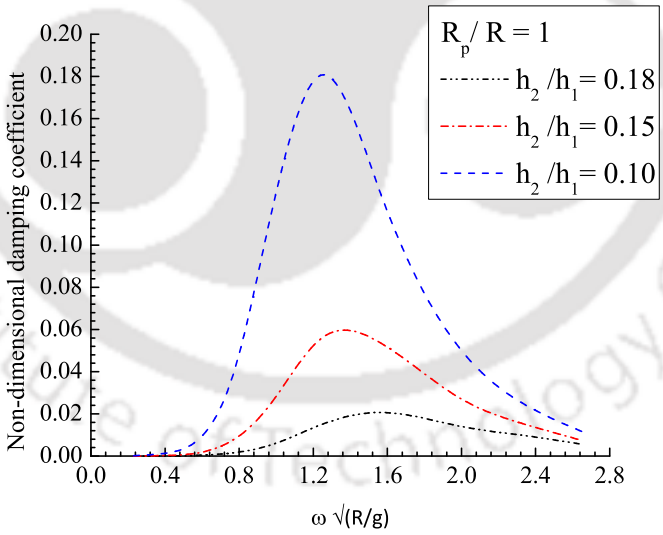

Figure 4.4: Non-dimensional damping coefficient versus non-dimensional frequency $\omega\sqrt{(R/g)}$ for cylinder 1 for different gaps between the cylinders with $e_2/h_1 = 0.25,\ R_p/R = 1$.

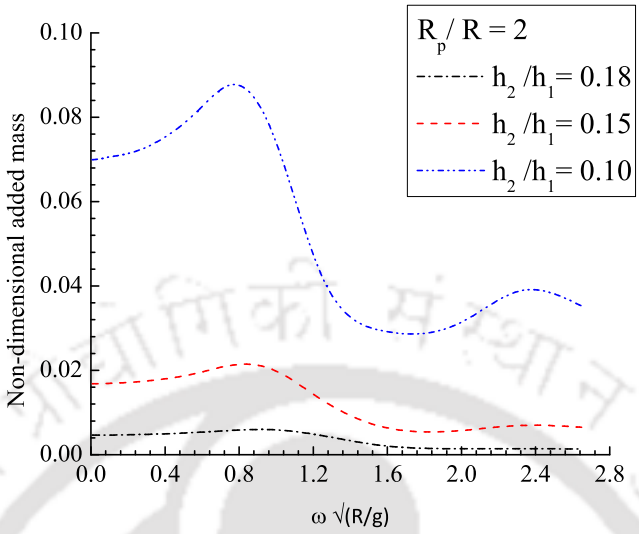

Figure 4.5: Non-dimensional added mass versus non-dimensional frequency $\omega\sqrt{(R/g)}$ for cylinder 1 for different gaps between the cylinders with $e_2/h_1 = 0.25,\ R_p/R = 2$.

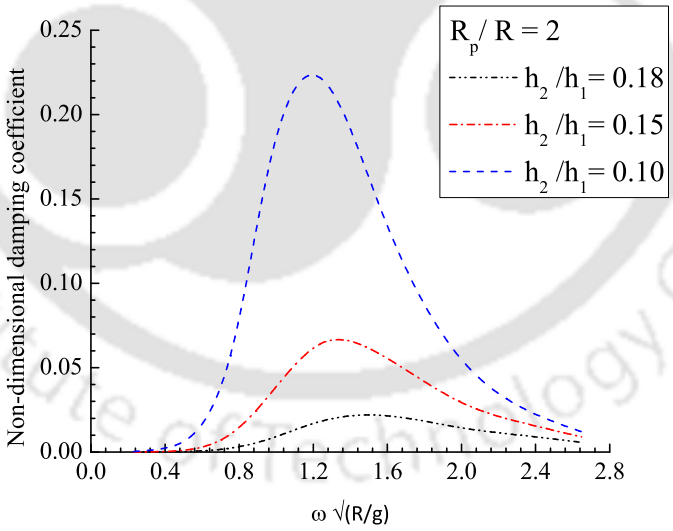

Figure 4.6: Non-dimensional damping coefficient versus non-dimensional frequency $\omega\sqrt{(R/g)}$ for cylinder 1 for different gaps between the cylinders with $e_2/h_1 = 0.25,\ R_p/R = 2$.

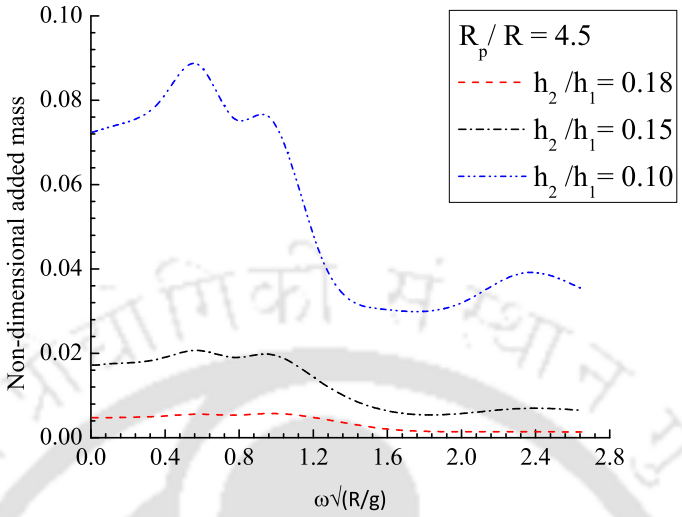

Figure 4.7: Non-dimensional added mass versus non-dimensional frequency $\omega\sqrt{(R/g)}$ for cylinder 1 for different gaps between the cylinders with $e_2/h_1 = 0.25,\ R_p/R = 4.5$.

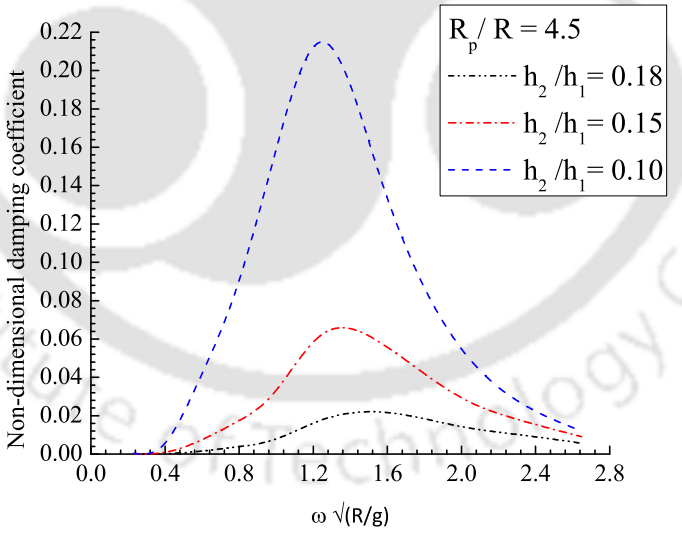

Figure 4.8: Non-dimensional damping coefficient versus non-dimensional frequency $\omega\sqrt{(R/g)}$ for cylinder 1 for different gaps between the cylinders with $e_2/h_1 = 0.25,\ R_p/R = 4.5$.

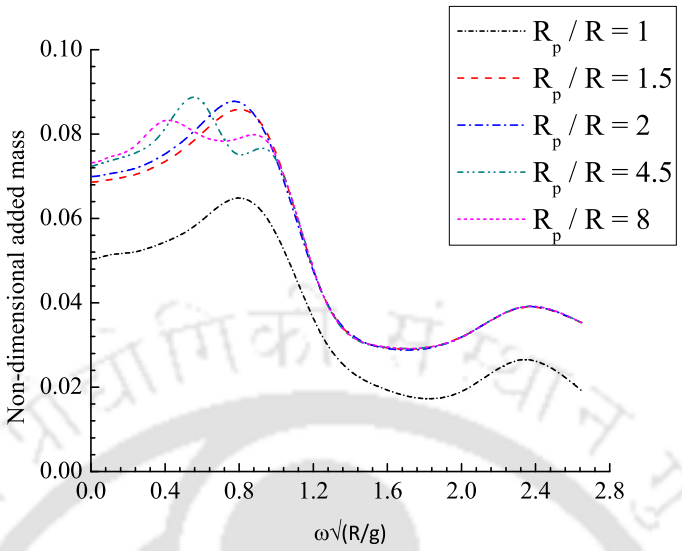

Figure 4.9: Non-dimensional added mass versus non-dimensional frequency $\omega\sqrt{(R/g)}$ for cylinder 1 for different values of radius R_p of bottom-mounted cylinder with $e_2/h_1 = 0.25,\ e_1/h_1 = 0.15$.

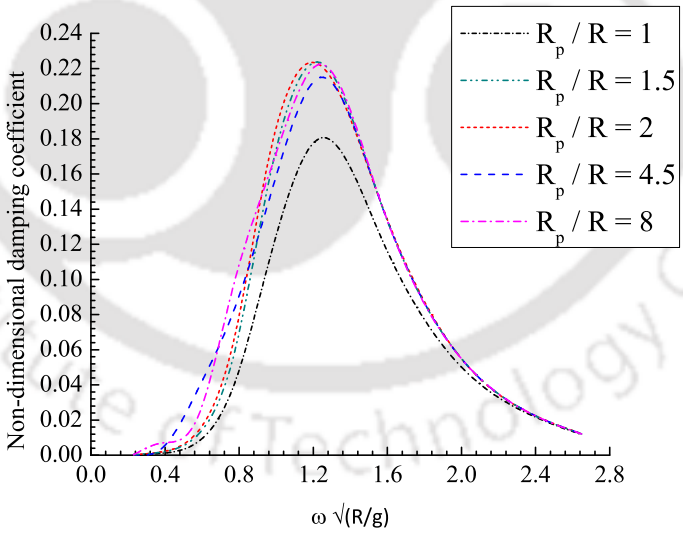

Figure 4.10: Non-dimensional damping coefficient versus non-dimensional frequency $\omega\sqrt{(R/g)}$ for cylinder 1 for different values of radius R_p of bottom-mounted cylinder with $e_2/h_1 = 0.25,\ e_1/h_1 = 0.15$.

ratio. Figures 4.9 and 4.10, respectively, give the plots of added mass and damping coefficient for different radius ratios for the fixed gap $h_2/h_1 = 0.10$. It is to be recalled that in Figures 4.1 and 4.2, the value of h_2/h_1 was taken as 0.15. Now, here we observe the same trend but the values are significantly higher. That is to say that if the values of the gap are smaller, then it produces higher added mass and damping coefficient corresponding to the same radius ratio.

4.6 Conclusion

We derive the radiated potentials in different sub-domains of the fluid due to roll motion. The added mass is higher at lower frequencies for any value of the radius of the lower cylinder and for any gap between the cylinders. Fluctuations are observed for higher radius ratios ($R_p/R > 2$) in the lower frequency range. It is observed that for both added mass and damping coefficient, the values are much lower for $R_p/R = 1$ while the values are higher, but not much different from each other, for all other values of R_p/R. The damping coefficient attains higher values only at relatively lower frequencies and diminish steadily as $\omega\sqrt{(R/g)}$ increases. The values of added mass and damping coefficient increase as the gap between the cylinders decreases. There is no fluctuation observed in the damping coefficient for any change of gap for any radius ratio R_p/R.

Chapter 5

Diffraction of water waves by two coaxial cylinders: one floating and other submerged at some finite height above the sea-bed

5.1 Introduction

In this chapter, we consider a similar system consisting of a buoy floating vertically on the free surface above an immersed solid circular plate which is at some finite height above an impermeable horizontal sea-bed. Here our investigation is related to the diffraction of water waves by these two idealized coaxial vertical cylinders. We use the similar procedure as in Chapter 2 to derive the analytical expressions of the diffracted velocity potential. Sets of exciting force acting on both the cylinders are obtained for different radii of the cylinders and for different gaps between the cylinders. At the end, we consider the base case of no plate arrangement, i.e., the case having only the floating cylinder tethered to the sea-bed and comparison of forces for both the arrangements is carried out.

5.2 Mathematical formulation of the problem

The geometry of the problem is shown in Figure 5.1. The formulation procedure of the problem is on similar lines to that of the problem in Chapter 2. The coaxial lower cylinder of radius R_p, is placed in such a way that its upper surface is at a depth e_2 from the free surface and the lower surface at a depth e_3. Now we introduce a velocity potential $\Phi(r,\theta,z,t) = Re[\phi(r,\theta,z)e^{-i\omega t}]$, where $\phi(r,\theta,z)$ satisfies Laplace's equation (2.1). The velocity potential ϕ can be split into incident velocity potential ϕ_{inc} and diffracted velocity potential ϕ_d due to the diffraction of the incident wave acting on the fixed cylinders. The solutions for the boundary value problem are obtained in four physical regions. Let ϕ_{d1}, ϕ_{d2}, ϕ_{d3} and ϕ_{d4} be the diffracted potentials in the regions I, II, III and IV, respectively, as indicated in Figure 5.1. It is to be noted that in this problem region IV appears (unlike Chapter 2) because of the shifting of the lower cylinder to a finite height. The incident velocity potential is same as in equation (2.2).

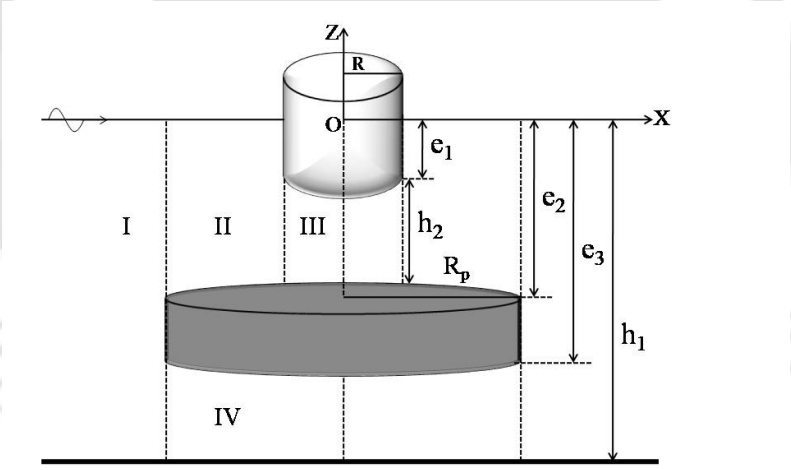

Figure 5.1: Schematic diagram and definition of fluid subdomains.

The governing equation and boundary conditions

The diffracted velocity potential Φ_d can be expressed as Φ_d=$Re[\phi_d(r,\theta,z)e^{-i\omega t}]$, where the spatial part ϕ_d satisfies the following boundary value problem:

$$\nabla^2\phi_d = 0; (0 < r < \infty, -h_1 < z < 0 \text{ or } -e_2 < z < 0 \text{ or } -h_1 < z < -e_3), \quad (5.1)$$

$$\frac{\partial \phi_d}{\partial z} - \frac{\omega^2}{g}\phi_d = 0;\ (z=0), \tag{5.2}$$

$$\frac{\partial \phi_d}{\partial z} = 0;\ (z=-h_1), \tag{5.3}$$

$$\frac{\partial (\phi_d + \phi_{inc})}{\partial z} = 0;\ (z=-e_2,\ r<R_p;\ z=-e_3,\ r<R_p), \tag{5.4}$$

$$\frac{\partial (\phi_d + \phi_{inc})}{\partial r} = 0;\ (-e_3<z<-e_2,\ r=R_p;\ \ -e_1<z<0,\ r=R). \tag{5.5}$$

The radiation condition that is to be satisfied only for region I, which is unbounded, is

$$\lim_{r\to\infty} \sqrt{r}\left(\frac{\partial \phi_d}{\partial r} - \mathrm{i}k\phi_d\right) = 0. \tag{5.6}$$

Here the solutions for the boundary value problem are obtained in four physical regions as shown in Figure 5.1. The exciting forces are obtained by solving this diffraction problem.

5.3 Method of solution

By applying the same method as in Chapter 2, the analytical expression for the diffracted velocity potentials in different regions are obtained as

$$\phi_{d1} = \sum_{m=0}^{\infty}\sum_{n=1}^{\infty} A_{m,n}\frac{R_m(\lambda_n r)}{R_m(\lambda_n R_p)}\cos[\lambda_n(z+h_1)]\cos m\theta, \tag{5.7}$$

$$\phi_{d2} = -\phi_{inc} + \sum_{m=0}^{\infty}\sum_{n=1}^{\infty}\left[B_{m,n}\frac{S_m(\alpha_n r)}{S_m(\alpha_n R)} + C_{m,n}\frac{T_m(\alpha_n r)}{T_m(\alpha_n R)}\right]\cos[\alpha_n(z+e_2)]\cos m\theta, \tag{5.8}$$

$$\phi_{d3} = -\phi_{inc} + \sum_{m=0}^{\infty}\sum_{n=1}^{\infty}\left[P_{m,n}\frac{U_m(\alpha_n r)}{U_m(\alpha_n R)}\cos[\alpha_n(z+e_2)]\right]\cos m\theta, \tag{5.9}$$

$$\phi_{d4} = -\phi_{inc} + \sum_{m=0}^{\infty}\left[Q_{m,1}r^m + \sum_{n=2}^{\infty} Q_{m,n}\frac{I_m(\gamma_n r)}{I_m(\gamma_n R_p)}\cos[\gamma_n(z+h_1)]\right]\cos m\theta, \tag{5.10}$$

where $A_{m,n}, B_{m,n}, C_{m,n}, P_{m,n}$ and $Q_{m,n}$ are unknown coefficients; λ_n and α_n are determined from equations (2.12) and (2.13), and γ_n is given by

$$\gamma_n = \frac{(n-1)\pi}{h_3}, \qquad n = 1, 2, 3, \ldots, \tag{5.11}$$

with $h_2 = e_2 - e_1$; $h_3 = h_1 - e_3$.

The radial functions $R_m(.)$, $S_m(.)$, $T_m(.)$ are given by equations (2.14)–(2.19) and $U_m(.)$ are given by

$$U_m(\alpha_n r) = J_m(k'r), \qquad n = 1, \tag{5.12}$$

$$U_m(\alpha_n r) = I_m(\alpha_n r), \qquad n = 2, 3, \ldots. \tag{5.13}$$

Matching conditions

We arrive at the appropriate matching conditions by means of continuity of pressure and that of the horizontal velocity along the virtual boundaries as depicted in Figure 5.1. Along the virtual boundary $r = R_p$, between regions I and II and regions I and IV, we have

$$\phi_{d1} = \phi_{d2}, \quad (-e_2 \le z \le 0), \tag{5.14}$$

$$\phi_{d1} = \phi_{d4}, \quad (-h_1 \le z \le -e_3), \tag{5.15}$$

$$\frac{\partial \phi_{d1}}{\partial r} = \frac{\partial \phi_{d2}}{\partial r}, \quad (-e_2 \le z \le 0), \tag{5.16}$$

$$\frac{\partial \phi_{d1}}{\partial r} = \frac{\partial \phi_{d4}}{\partial r}, \quad (-h_1 \le z \le -e_3), \tag{5.17}$$

Along the virtual boundary $r = R$, between regions II and III, we have

$$\phi_{d2} = \phi_{d3}, \quad (-e_2 \le z \le -e_1), \tag{5.18}$$

$$\frac{\partial \phi_{d2}}{\partial r} = \frac{\partial \phi_{d3}}{\partial r} \quad (-e_2 \le z \le -e_1). \tag{5.19}$$

These matching conditions are indispensable for determining the diffracted potentials.

5.4 Wave forces

Having determined the velocity potentials, we now proceed to find the horizontal wave exciting force acting on both the cylinders due to diffraction taking place on their surfaces. By the similar manner of Chapter 2, the total horizontal exciting force is given by,

$$F_s = F_{inc} + F_d = \mathrm{i}\rho\omega \int_S \phi_{inc} n_x ds + i\rho\omega \int_S \phi_d n_x ds, \tag{5.20}$$

The expression for the horizontal exciting force F_{inc1} on cylinder 1 due to the incident velocity potential can be written as (Wu et al. [38])

$$F_{inc1} = -\frac{2\pi\rho g \mathrm{i} R J_1(kR)}{\cosh(kh_1)} \frac{\sinh(kh_1) - \sinh[k(h_1 - e_1)]}{k}. \tag{5.21}$$

The total horizontal exciting force (F_{s1}) acting on cylinder 1 can be written as

$$F_{s1} = -\mathrm{i}\rho\pi\omega R \sum_{n=1}^{\infty} (B_{1,n} + C_{1,n}) \frac{\sin(\alpha_n e_2) - \sin(\alpha_n h_2)}{\alpha_n}. \tag{5.22}$$

The dimensionless horizontal exciting force F_{s1}/w_0, where $w_0 = \rho g \pi R^2$, is given by

$$F_{s1}/w_0 = \frac{-\mathrm{i}\,\omega}{gR} \sum_{n=1}^{\infty} (B_{1,n} + C_{1,n}) \frac{\sin(\alpha_n e_2) - \sin(\alpha_n h_2)}{\alpha_n}. \tag{5.23}$$

Similarly the horizontal exciting force F_{inc2} on cylinder 2 due to the incident velocity potential can be written as

$$F_{inc2} = -\mathrm{i}2\rho\pi g R_p \frac{J_1(kR_p)}{\cosh(kh_1)} \frac{\sinh[k(h_1 - e_2)] - \sinh(kh_3)}{k}. \tag{5.24}$$

The total horizontal exciting force acting on cylinder 2 can be written as

$$F_{s2} = F_{inc2} + F_{d1}, \tag{5.25}$$

where F_{d1} is the horizontal diffraction force due to the diffracted velocity potential ϕ_{d1} in region I. Using equations (5.20), (5.24) and (5.25), we get the total horizontal exciting force acting on cylinder 2 as

$$\begin{aligned} F_{s2} = & -\mathrm{i}2\rho\pi g R_p \frac{J_1(kR_p)}{\cosh(kh_1)} \frac{\sinh[k(h_1 - e_2)] - \sinh(kh_3)}{k} \\ & -\mathrm{i}\rho\pi\omega R_p \sum_{n=1}^{\infty} A_{1,n} \frac{\sin[\lambda_n(h_1 - e_2)] - \sin(\lambda_n h_3)}{\lambda_n}. \end{aligned} \tag{5.26}$$

The dimensionless horizontal exciting force F_{s2}/w_1, where $w_1 = \rho g \pi R_p^2$, is given by

$$\begin{aligned} F_{s2}/w_1 = & -\mathrm{i}\frac{2}{R_p} \frac{J_1(kR_p)}{\cosh(kh_1)} \frac{\sinh[k(h_1 - e_2)] - \sinh(kh_3)}{k} \\ & -\mathrm{i}\frac{\omega}{gR_p} \sum_{n=1}^{\infty} A_{1,n} \frac{\sin[\lambda_n(h_1 - e_2)] - \sin(\lambda_n h_3)}{\lambda_n}. \end{aligned} \tag{5.27}$$

5.5 Numerical results

In order to obtain the exciting force acting on the cylinders, we need to find the unknown coefficients $A_{m,n}$, $B_{m,n}$, $C_{m,n}$, $P_{m,n}$ and $Q_{m,n}$ that appear in the diffracted potentials, given by equations (5.7)–(5.10), by applying the similar technique as in Chapter 2. The values of parameters that are kept constant throughout the numerical calculation are $h_1 = 3\ metre, g = 9.8066\ metre/sec^2, e_2/h_1 = 0.25, e_3/h_1 = 0.35$. The frequency ω is non-dimensionalized by dividing it by $\sqrt{(g/R)}$. We represent the non-dimensionalized frequency by $\overline{\omega} = \omega/\sqrt{(g/R)}$. Since we wish to compute the forces for two distinct cases for different values of the radius of the cylinders and for different gaps between the cylinders, we suitably choose the values of the other parameters.

Figure 5.2 shows the non-dimensional exciting force against non-dimensional frequencies for different values of the radius of cylinder 2: to be precise, for $R_p/R = 1, 2, 3.6, 4.5, 8$. Here we fix the parameter values $e_1/h_1 = 0.1, R/h_1 = 0.2$. We observe from Figure 5.2 that no fluctuations occur for the first two radius ratios, i.e., for $R_p/R \leq 2$ and the peak value occurs at relatively higher frequencies, but still within the range of lower frequencies only. We observe fluctuations for higher radius ratios, i.e., for $R_p/R \geq 3.6$. It is also observed that the fluctuations, in the event of their occurrence, occur only at lower frequencies. The exciting force has more than one peak value for those higher radius ratios. For all values of radius ratio, the maximum value of the force occurs within the lower values of $\overline{\omega}$, to be precise, for $\overline{\omega} < 1.3$. Among the lower ratios $R_p/R \leq 2$, the peak value is higher when the radius ratio is higher. For the higher values of $\overline{\omega}$, the forces corresponding to all radius ratios converge to the same value and steadily diminish. It is to be noted that the highest peak value occurs for the radius ratio $R_p/R = 8$, closely followed by those for $R_p/R = 3.6$ and $R_p/R = 2.0$.

We further investigate the effect of the gap between the cylinders on the exciting force for cylinder 1. Figures 5.3–5.6 show the non-dimensional horizontal exciting force F_{s1}/w_0 against the non-dimensional frequency $\overline{\omega}$ for different gaps between the cylinders, $h_2/h_1 = 0.01, 0.07, 0.11, 0.15, 0.18$ and 0.24.

For Figure 5.3, we fix $R_p/R = 1$ and we observe that as the gap decreases, the value

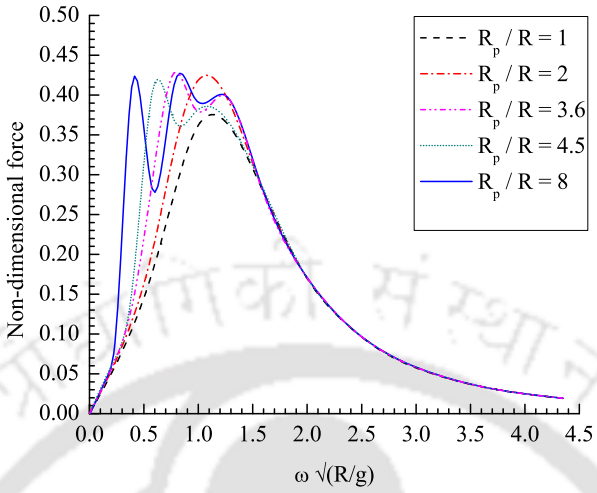

Figure 5.2: Non-dimensional horizontal exciting force F_{s1}/w_0 on the upper cylinder versus non-dimensional frequency $\omega\sqrt{(R/g)}$ for different values of radius (R_p) of submerged cylinder with $h_1 = 3\ metre, e_1/h_1 = 0.1, e_2/h_1 = 0.25, e_3/h_1 = 0.35, R/h_1 = 0.2$

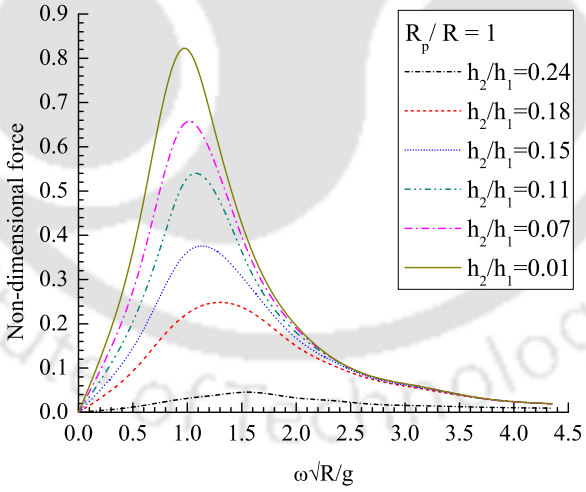

Figure 5.3: Non-dimensional horizontal exciting force F_{s1}/w_0 on the upper cylinder versus non-dimensional frequency $\omega\sqrt{(R/g)}$ for different values of gaps between the cylinders with $h_1 = 3\ metre, e_2/h_1 = 0.25, e_3/h_1 = 0.35, R/h_1 = 0.2$.

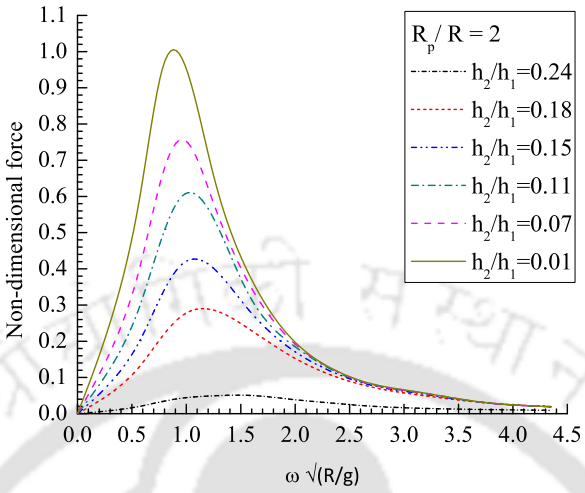

Figure 5.4: Non-dimensional horizontal exciting force F_{s1}/w_0 on the upper cylinder versus non-dimensional frequency $\omega\sqrt{(R/g)}$ for different values of gaps between the cylinders with $h_1 = 3\ metre, e_2/h_1 = 0.25, e_3/h_1 = 0.35, R/h_1 = 0.2$.

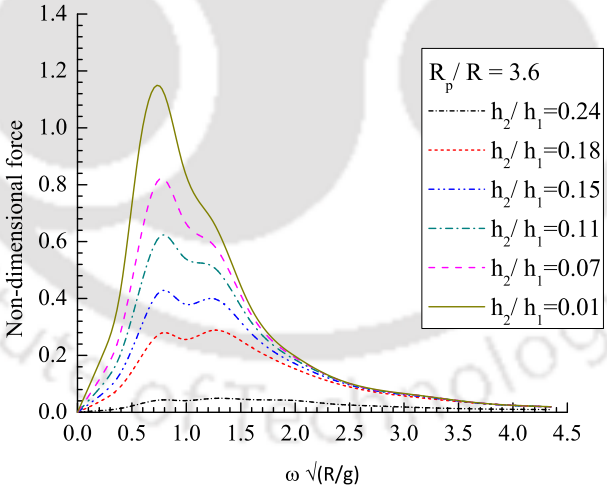

Figure 5.5: Non-dimensional horizontal exciting force F_{s1}/w_0 on the upper cylinder versus non-dimensional frequency $\omega\sqrt{(R/g)}$ for different values of gaps between the cylinders with $h_1 = 3\ metre, e_2/h_1 = 0.25, e_3/h_1 = 0.35, R/h_1 = 0.2$.

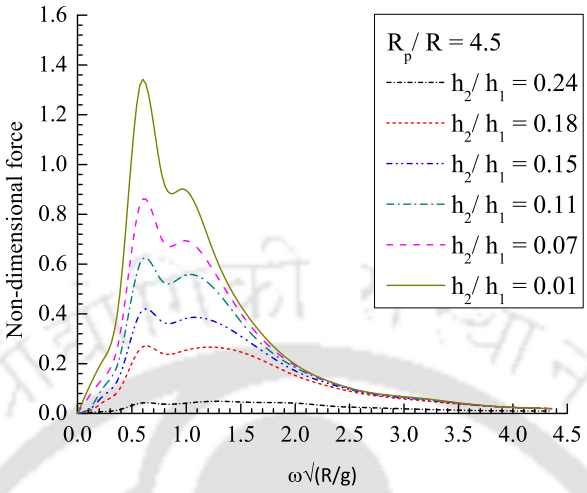

Figure 5.6: Non-dimensional horizontal exciting force F_{s1}/w_0 on the upper cylinder versus non-dimensional frequency $\omega\sqrt{(R/g)}$ for different values of gaps between the cylinders with $h_1 = 3\ metre, e_2/h_1 = 0.25, e_3/h_1 = 0.35, R/h_1 = 0.2$.

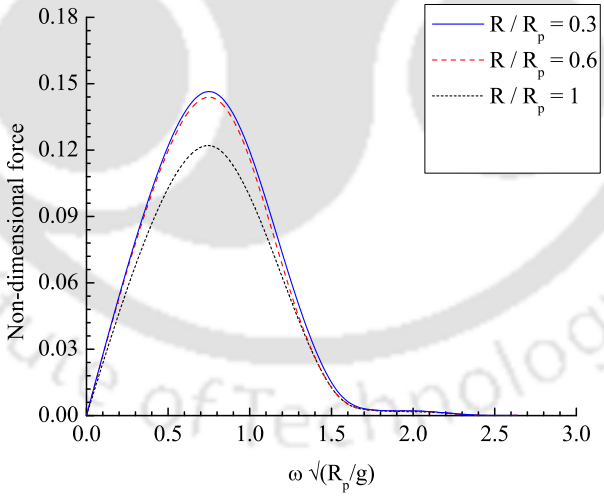

Figure 5.7: Non-dimensional horizontal exciting force F_{s2}/w_1 on submerged cylinder versus non-dimensional frequency $\omega\sqrt{(R_p/g)}$ for different values of radius (R) of the upper cylinder with $h_1 = 3\ metre, e_1/h_1 = 0.1, e_2/h_1 = 0.25, e_3/h_1 = 0.35, R_p/h_1 = 0.2$

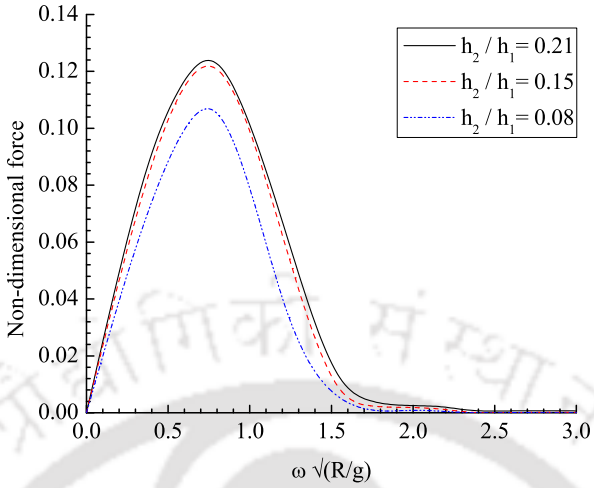

Figure 5.8: Non-dimensional horizontal exciting force F_{s2}/w_1 on submerged cylinder versus non-dimensional frequency $\omega\sqrt{(R/g)}$ for different values of gaps between the cylinders with $h_1 = 3\ metre, e_2/h_1 = 0.25, e_3/h_1 = 0.35, R/h_1 = 0.2, R_p/R = 1$

of the exciting force increases. Consequently, the higher values of the force are due to $h_2/h_1 = 0.01$. The force attains higher values corresponding to the lower values of the frequency $\overline{\omega}$. For higher values of $\overline{\omega}$, the force steadily diminishes. Figure 5.4, in which $R_p/R = 2.0$, shows the same trend as observed in Figure 5.3. Now even when the radius ratio increases to $R_p/R = 3.6$, with other parameters remaining the same, Figure 5.5 indicates the fluctuations starting and the peak value shifting towards the lower frequencies. Here also, as the gap decreases, the value of the exciting force increases and the maximum value of the exciting force occurs at $h_2/h_1 = 0.01$. In order to check whether this fluctuating nature of the exciting force continues for higher radius values, we consider the forces corresponding to $R_p/R = 4.5$, and subsequently observe from Figure 5.6 that the fluctuations do occur, which validates our result. It is observed from Figure 5.7 that as the radius of cylinder 1 increases, the value of the exciting force decreases, i.e., the higher value occurs for $R/R_p = 0.3$, the force attains higher values corresponding to smaller values of frequency. For higher values of frequency, exciting force diminishes for all radius ratios R/R_p. From Figure 5.8, it is clear that as the gap

decreases, the value of the exciting force also decreases, i.e., higher value occurs for the gap $h_2/h_1 = 0.21$.

5.6 Particular case: Single hollow cylinder configuration over an even sea bottom

In order to produce a comparison with the no bottom plate case, we consider the base case when the lower submerged cylinder is not present. Therefore we consider a vertical hollow cylinder of radius R and draft e_1 in water of finite depth. It is to be noted that some part of the cylinder is above the free surface as shown in Figure 5.9. Now the present device consists of a single floating hollow cylinder only. We follow the technique of Yeung [39], Bhatta and Rahman [3] and Zhu and Michell [44] of dividing the whole region into two regions. Therefore the problem consists of two regions: an interior region defined by $r \leq R,\ \ 0 \leq \theta \leq 2\pi,\ \ -h_1 \leq z \leq 0$ and an exterior region defined by $r \geq R,\ \ 0 \leq \theta \leq 2\pi,\ \ -h_1 \leq z \leq 0$.

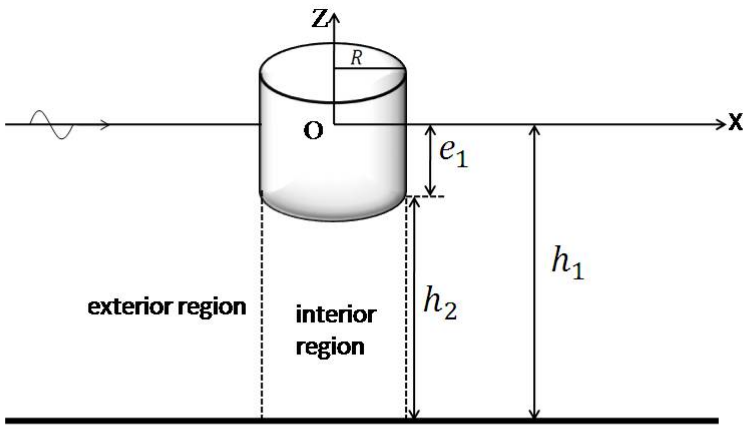

Figure 5.9: Schematic diagram and definition of fluid subdomains.

5.6.1 Boundary value problem

The diffracted velocity potential Φ_d can be written as Φ_d=$Re[\phi_d(r,\theta,z)e^{-i\omega t}]$, where the spatial part ϕ_d satisfies the following boundary value problem:

(i) governing equation and body surface condition:

$$\nabla^2\phi_d = 0, \quad \text{in the respective fluid region,} \tag{5.28}$$

$$\frac{\partial(\phi_d + \phi_{inc})}{\partial r} = 0; \ (-e_1 < z < 0, \ r = R), \tag{5.29}$$

(ii) linearized free surface condition is same as equation (5.2).

(iv) bottom boundary condition is same as equation (5.3).

(v) radiation condition is same as equation (5.6).

5.6.2 Diffracted potentials

The solutions for the boundary value problem are obtained in these two regions. Therefore, the velocity potential ϕ is decomposed into two potentials defined on $r \leq R$ and $r \geq R$, respectively:

$$\phi = \begin{cases} \phi^{int}, & r \leq R, \\ \phi^{ext}, & r \geq R, \end{cases} \tag{5.30}$$

where ϕ^{int} and ϕ^{ext} denote the velocity potential in the interior and exterior regions, respectively. By applying the similar solution technique as in Chapter 2 to derive the expressions of the diffracted velocity potentials in the exterior and interior regions, we have,

$$\phi_d^{ext} = \sum_{m=0}^{\infty}\sum_{n=1}^{\infty} D_{m,n}\frac{R_m(\lambda_n r)}{R_m(\lambda_n R)}\cos[\lambda_n(z+h_1)]\cos m\theta, \tag{5.31}$$

$$\phi_d^{int} = -\phi_{inc} + \sum_{m=0}^{\infty}\sum_{n=1}^{\infty}\left[E_{m,n}\frac{U_m(\lambda_n r)}{U_m(\lambda_n R)}\cos[\lambda_n(z+h_1)]\right]\cos m\theta, \tag{5.32}$$

where $D_{m,n}$ and $E_{m,n}$ are unknown coefficients and λ_n is given by equation (2.12); radial functions $R_m(.)$ and $U_m(.)$ are given by equations (2.14)–(2.15) and (5.12)–(5.13), respectively.

5.6.3 Matching conditions

In order to compute the unknown coefficients $D_{m,n}$ and $E_{m,n}$, we introduce the appropriate matching conditions in the same way. At $r = R$, the conditions which are to be

satisfied at the interface between the regions are:

$$\phi^{ext} = \phi^{int}, \quad (-h_1 \leq z \leq -e_1), \tag{5.33}$$

$$\frac{\partial \phi^{ext}}{\partial r} = \frac{\partial \phi^{int}}{\partial r}, \quad (-h_1 \leq z \leq -e_1). \tag{5.34}$$

5.6.4 Wave force and numerical results

In order to compare the exciting force for both the cases, we need to compute the exciting force of the cylinder for the present case of the single cylinder arrangement. Therefore the total horizontal exciting force acting on the hollow cylinder can be written as

$$F_{s3} = F_{inc1} + F_e, \tag{5.35}$$

where F_e is the horizontal diffraction force due to the diffracted velocity potential ϕ_d^{ext}. Now by using equations (5.21) and (5.35), we get the total horizontal exciting force acting on the hollow cylinder as

$$\begin{aligned} F_{s3} = & -\frac{2\pi\rho g i R J_1(kR)\{\sinh(kh_1) - \sinh[k(h_1 - e_1)]\}}{k\cosh(kh_1)} \\ & -i\rho\pi\omega R \sum_{n=1}^{\infty} D_{1,n} \frac{\sin(\lambda_n h_1) - \sin[\lambda_n(h_1 - e_1)]}{\lambda_n}. \end{aligned} \tag{5.36}$$

The dimensionless horizontal exciting force F_{s3}/w_0 is given by

$$\begin{aligned} F_{s3}/w_0 = & -\frac{2\mathrm{i} J_1(kR)\{\sinh(kh_1) - \sinh[k(h_1 - e_1)]\}}{kR\cosh(kh_1)} \\ & -\frac{i\omega}{gR} \sum_{n=1}^{\infty} D_{1,n} \frac{\sin(\lambda_n h_1) - \sin[\lambda_n(h_1 - e_1)]}{\lambda_n}. \end{aligned} \tag{5.37}$$

However, when the forces are calculated for a fixed draft and varying radius, they are non-dimensionalized by $w_2 = \rho g \pi e_1^2$. Figures 5.10 and 5.11, respectively, study the forces for different drafts and different radii of the riding hollow cylinder with no plate below it, i.e., it is now a single-cylinder configuration. Figure 5.10 shows that higher values of the force are attained corresponding to the higher values of the draft. By comparing this figure with Figure 5.3, we can conclude that a no-plate arrangement gives rise to values of the force which are a little higher than those for the original arrangement. Similar conclusion can be made from Figure 5.11 by comparing it with Figure 5.2.

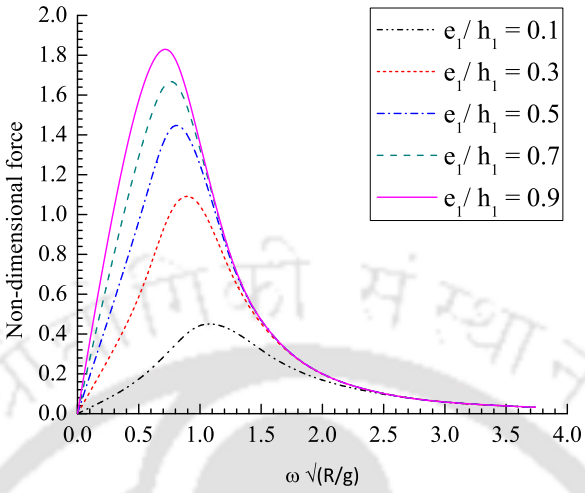

Figure 5.10: Non-dimensional horizontal exciting force F_{s3}/w_0 on the cylinder (for the base case of no plate) versus non-dimensional frequency $\omega\sqrt{(R/g)}$ for different values of draft of the cylinder with $h_1 = 3\ metre, R/h_1 = 0.2$.

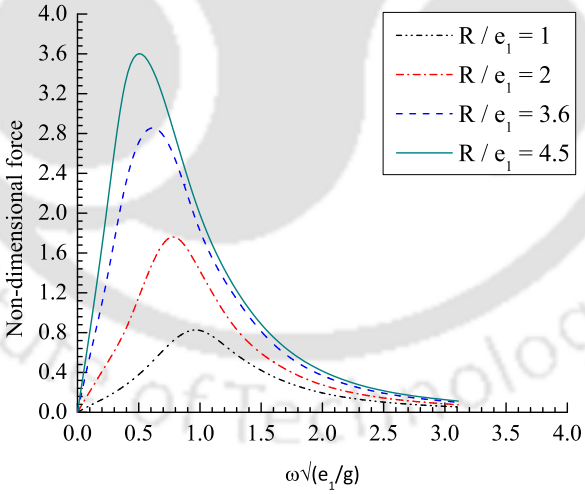

Figure 5.11: Non-dimensional horizontal exciting force F_{s3}/w_2 on the cylinder (for the base case of no plate) versus non-dimensional frequency $\omega\sqrt{(e_1/g)}$ for different values of radius of the cylinder with $h_1 = 3\ metre, e_1/h_1 = 0.2$.

5.7 Conclusion

By using linear water wave theory, we derive the velocity potential expressions for the diffraction problem for a hollow cylinder placed over a solid cylinder which is raised by some distance from the bottom in uniform water depth. We present the expression for the wave exciting force on the hollow cylinder under the influence of the solid cylinder and vice versa. For higher values of the radius of the lower cylinder for a fixed radius of the upper cylinder, the exciting force on the upper cylinder exhibits a fluctuating behaviour but the peak values occur at lower frequencies only. We observe no fluctuation for smaller values of radius ratios, i.e., for $R_p/R \leq 2.0$. With regard to the effect of the gap between the cylinders, it is observed clearly that, for fixed values of the radii, the exciting force increases as the gap decreases. It is also noticed that for higher radius ratios, the exciting force exhibits a fluctuating nature. In this case also, the values of the exciting force are significant mainly at lower frequencies. With respect to the exciting force on the lower cylinder, keeping the radius of the lower cylinder fixed, it increases as the value of the radius of the upper cylinder decreases. On the other hand, for fixed values of the radii of the cylinders, the exciting force increases as the gap increases. We also compare our two-cylinder configuration with the base case of only the floating hollow cylinder present and tethered to the sea-bed. Force evaluated for different radius ratios and different drafts reveals that a single cylinder arrangement is likely to be more efficient than a two-cylinder arrangement.

Chapter 6

Surge motion by two coaxial cylinders: one floating and other submerged at some finite height above the sea-bed

6.1 Introduction

In this chapter, we consider the same structure as in Chapter 5 but this chapter is concerned with the surge radiation problem. We use the similar procedure as in Chapter 3 to derive the analytical expressions of the surge radiated velocity potential. The hydrodynamic coefficients, namely, added mass and damping coefficient, are obtained for different radii of the cylinders and for different gaps between the cylinders.

6.2 Mathematical formulation of the problem

Here, we consider the same geometry as shown in Figure 5.1. The cylinders are forced to independently oscillate in small surge motion only. We introduce a radiated velocity potential $\Phi^m_{rad,1}(r,\theta,z,t) = Re[\phi^m_{rad,1}(r,\theta,z)e^{-\mathrm{i}\omega t}]$ where $\phi^m_{rad,1}(r,\theta,z)$ satisfies Laplace's equation (2.1).

The governing equation and boundary conditions

Since we investigate only the surge motion of the structure, let $\phi^m_{rad,1}$ be the radiated potential with amplitude ξ^m corresponding to the surge motion which can be expressed as

$$\phi^m_{rad,1}(r,\theta,z) = -\mathrm{i}\omega\xi^m\varphi^m_{rad,1}(r,z)\cos\theta, \tag{6.1}$$

where $m = 1$ and 2 refer to the upper cylinder and lower cylinder, respectively. Substitution of equation (6.1) into equation (2.1) gives the following boundary value problem:

$$\frac{1}{r}\frac{\partial\varphi^m_{rad,1}}{\partial r} + \frac{\partial^2\varphi^m_{rad,1}}{\partial r^2} + \frac{\partial^2\varphi^m_{rad,1}}{\partial z^2} - \frac{\varphi^m_{rad,1}}{r^2} = 0, \tag{6.2}$$

$$\frac{\partial\varphi^m_{rad,1}}{\partial z} - \frac{\omega^2}{g}\varphi^m_{rad,1} = 0, \quad (z=0), \tag{6.3}$$

$$\frac{\partial\varphi^m_{rad,1}}{\partial z} = 0, \quad (z=-h_1; z=-e_2, z=-e_3, r\le R_p), \tag{6.4}$$

$$\frac{\partial\varphi^m_{rad,1}}{\partial r} = 1, \quad (-e_1<z<0, r=R; \; -e_3<z<-e_2, r=R_p), \tag{6.5}$$

$$\lim_{r\to\infty}\sqrt{r}\left[\frac{\partial\varphi^m_{rad,1}}{\partial r} - \mathrm{i}k\varphi^m_{rad,1}\right] = 0. \tag{6.6}$$

It is to be noted that radiation condition 6.6 is valid only for the unbounded region I.

6.3 Method of solution

We obtain the surge radiation potentials $\varphi^{m,j}_{rad,1},\ j = I, II, III, IV$, as follows:

$$\varphi^{m,I}_{rad,1} = \sum_{n=1}^{\infty} A_{m,n}\frac{R_1(\lambda_n r)}{R_1(\lambda_n R_p)}\cos[\lambda_n(z+h_1)], \tag{6.7}$$

$$\varphi^{m,II}_{rad,1} = \sum_{n=1}^{\infty}\left[B_{m,n}\frac{S_1(\alpha_n r)}{S_1(\alpha_n R)} + C_{m,n}\frac{T_1(\alpha_n r)}{T_1(\alpha_n R)}\right]\cos[\alpha_n(z+e_2)], \tag{6.8}$$

$$\varphi^{m,III}_{rad,1} = \sum_{n=1}^{\infty}\left[P_{m,n}\frac{U_1(\alpha_n r)}{U_1(\alpha_n R)}\right]\cos[\alpha_n(z+e_2)], \tag{6.9}$$

$$\varphi^{m,IV}_{rad,1} = Q_{m,1}r + \sum_{n=2}^{\infty}\left[Q_{m,n}\frac{I_1(\gamma_n r)}{I_1(\gamma_n R_p)}\right]\cos[\gamma_n(z+h_1)], \tag{6.10}$$

where $A_{m,n}, B_{m,n}, C_{m,n}, P_{m,n}$ and $Q_{m,n}$ are unknown coefficients, the radial functions $R_1(.), S_1(.), T_1(.)$ are given by equations (2.14)–(2.19), and $U_1(.)$ given by equations (5.12)–(5.13).

Matching conditions

We apply the same matching conditions as in Chapter 4.

6.4 Hydrodynamic coefficients and numerical results

Added mass (μ_{11}) and damping coefficient (λ_{11}) of the upper cylinder by an oscillation of lower cylinder in surge mode can be obtained as

$$\mu_{11} + \frac{\mathrm{i}\lambda_{11}}{\omega} = -\rho\pi R \sum_{n=1}^{\infty}(B_{1,n} + C_{1,n})\frac{\sin(\alpha_n e_2) - \sin(\alpha_n h_2)}{\alpha_n}. \tag{6.11}$$

The added mass is non-dimensionalized by dividing it by the mass of the water displaced by a semi-immersed sphere with radius R, amounting to $\frac{2}{3}\pi\rho R^3$, and the damping coefficient is non-dimensionalized by dividing it by the same factor but multiplied by the angular frequency ω. Thus the non-dimensionalized added mass $\overline{\mu_{11}}$ and damping coefficient $\overline{\lambda_{11}}$ are given by

$$\overline{\mu_{11}} + \mathrm{i}\overline{\lambda_{11}} = -\left(\frac{1}{\frac{2}{3}R^2}\right) \sum_{n=1}^{\infty}(B_{1,n} + C_{1,n})\frac{\sin(\alpha_n e_2) - \sin(\alpha_n h_2)}{\alpha_n}. \tag{6.12}$$

Similarly the added mass (μ'_{11}) and damping coefficient (λ'_{11}) of the lower cylinder by an oscillation of upper cylinder in surge mode can be obtained from

$$\mu'_{11} + \frac{\mathrm{i}\lambda'_{11}}{\omega} = -\rho\pi R_p \sum_{n=1}^{\infty} A_{2,n}\frac{\sin[\lambda_n(h_1 - e_2)] - \sin(\lambda_n h_3)}{\lambda_n}. \tag{6.13}$$

The corresponding non-dimensionalized added mass and damping coefficient are given by

$$\overline{\mu'_{11}} + \mathrm{i}\overline{\lambda'_{11}} = -\left(\frac{1}{\frac{2}{3}R_p^2}\right) \sum_{n=1}^{\infty} A_{2,n}\frac{\sin[\lambda_n(h_1 - e_2)] - \sin(\lambda_n h_3)}{\lambda_n}. \tag{6.14}$$

Figures 6.1–6.2 present the non-dimensional added mass and damping coefficient,

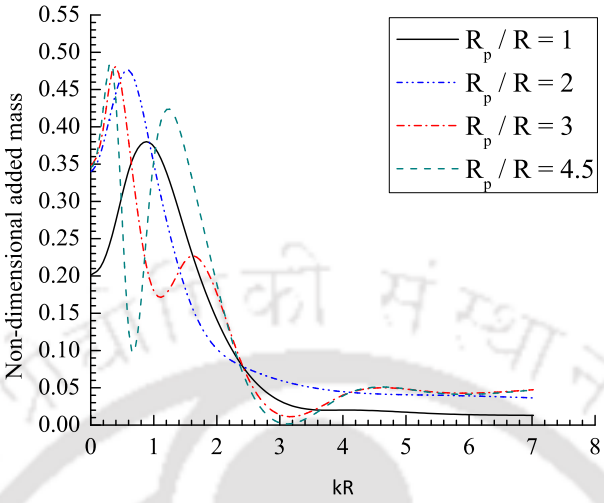

Figure 6.1: Non-dimensional added mass for the upper cylinder for different values of radius of the lower cylinder with $h_1 = 3$ *metre*, $e_1/h_1 = 0.1, e_2/h_1 = 0.25, e_3/h_1 = 0.35, R/h_1 = 0.2$.

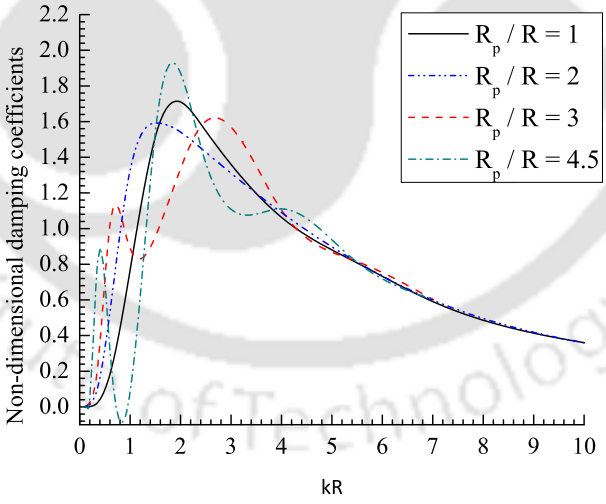

Figure 6.2: Non-dimensional damping coefficient for the upper cylinder for different values of radius of the lower cylinder with $h_1 = 3$ *metre*, $e_1/h_1 = 0.1, e_2/h_1 = 0.25, e_3/h_1 = 0.35, R/h_1 = 0.2$.

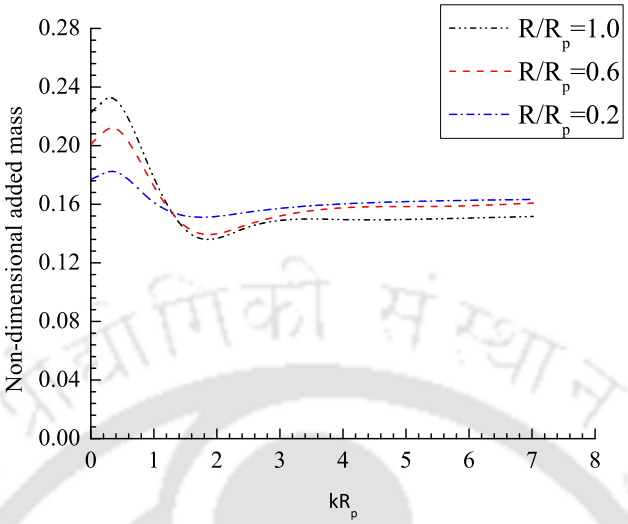

Figure 6.3: Non-dimensional added mass for the lower cylinder for different values of radius of the upper cylinder with $h_1 = 3\ metre, e_1/h_1 = 0.1, e_2/h_1 = 0.25, e_3/h_1 = 0.35, R_p/h_1 = 0.2$.

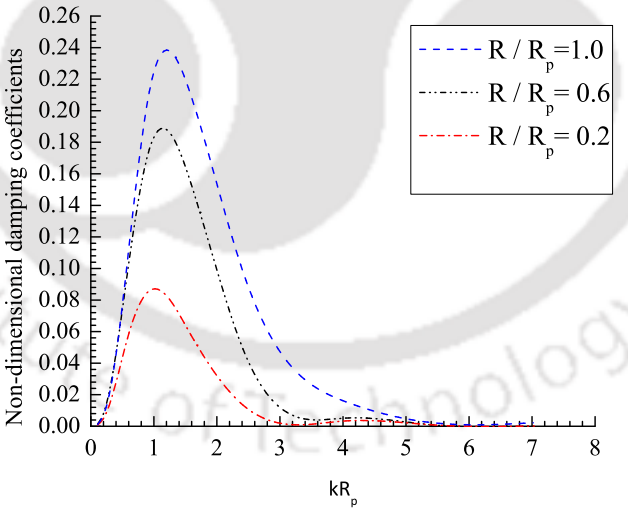

Figure 6.4: Non-dimensional damping coefficient for the lower cylinder for different values of radius of the upper cylinder with $h_1 = 3\ metre, e_1/h_1 = 0.1, e_2/h_1 = 0.25, e_3/h_1 = 0.35, R_p/h_1 = 0.2$.

respectively, of the upper cylinder with different radius ratios $R_p/R = 1.0, 2, 3, 4.5$. We observe that the higher values of the coefficient, as well as the fluctuations, if any, occur for higher radius ratio within the lower range of wavenumbers. Further, irrespective of the ratios, the added mass diminish for higher wavenumbers but they have almost the same values for higher radius ratios. The multiple peaks observed in the values of hydrodynamic coefficients for the upper cylinder are due to the influence of the lower plate with larger radius which allows for more fluid to interact.

Figures 6.3–6.4 present the non-dimensional added mass and damping coefficient, respectively, for the lower cylinder with different radius ratios $R/R_p = 0.2, 0.6, 1.0$. Figure 6.3 shows that the higher values of added mass correspond to the higher values of the radius ratio for small wavenumbers whereas there is not much difference in the values for higher wavenumbers. Figure 6.4 shows that higher values of damping coefficient correspond to higher radius ratios in the lower range of wavenumbers. For higher wavenumbers, there is no significant difference in the values and they converge to zero. No oscillation is observed in the values of hydrodynamic coefficients for the lower cylinder due to the fact that increasing value in the radius of the upper cylinder creates a situation where both the cylinders are of the same size thereby practically making region II vanish.

6.4.1 Effect of interior region

Added mass (μ''_{11}) and damping coefficient (λ''_{11}) of the upper cylinder in surge mode in the presence of an oscillating lower cylinder can be obtained as (as in Chapter 3)

$$\mu''_{11} + \frac{\mathrm{i}\lambda''_{11}}{\omega} = -\rho\pi R \sum_{n=1}^{\infty}[(B_{1,n} + C_{1,n}) - P_{1,n}]\frac{\sin(\alpha_n e_2) - \sin(\alpha_n h_2)}{\alpha_n}. \quad (6.15)$$

Similarly, the non-dimensionalized added mass $\overline{\mu''_{11}}$ and damping coefficient $\overline{\lambda''_{11}}$ are given by

$$\overline{\mu''_{11}} + \mathrm{i}\overline{\lambda''_{11}} = -\left(\frac{1}{\frac{2}{3}R^2}\right) \sum_{n=1}^{\infty}[(B_{1,n} + C_{1,n}) - P_{1,n}]\frac{\sin(\alpha_n e_2) - \sin(\alpha_n h_2)}{\alpha_n}. \quad (6.16)$$

From Figures 6.5 and 6.6, we observe similar kind of results as was observed in Chapter 3 for the added mass and damping coefficient. Similarly the hydrodynamic coefficients of the lower cylinder in the presence of an oscillating upper cylinder can be obtained.

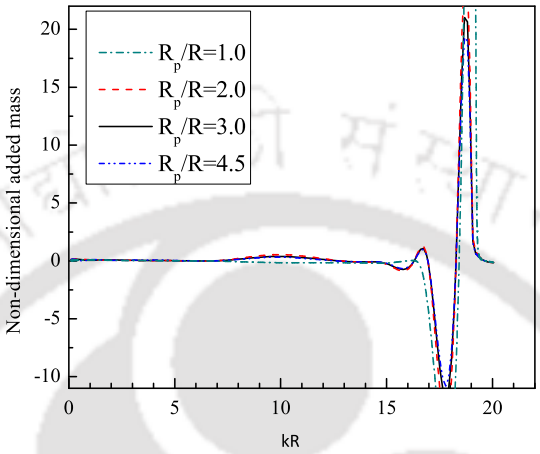

Figure 6.5: Non-dimensional added mass for the upper cylinder for different values of radius of the lower cylinder with $h_1 = 3$ *metre*, $e_1/h_1 = 0.05, e_2/h_1 = 0.25, e_3/h_1 = 0.35, R/h_1 = 0.2$.

Having formulated and solved the present problem for a structure which may represent a wave energy converter (WEC), it is also important to analyze how the structure will be moored. A number of works in this connection have been carried out such as the one by Vicente et al. [36]. The mooring connections may significantly modify the energy absorption properties of the structure by interacting with its oscillations. Therefore, when designing a mooring system for a WEC, various initial parameters, such as cable material, thickness, distance to the mooring point on the structure and so on, are to be taken into account. Different arrangements give us different displacements from the equilibrium position of the converter, load-demand on the mooring and the power absorbed. We may use slack chain lines mooring system to moor the structure to the anchor point on the bottom because slack chain lines rely on their weight to provide the necessary horizontal restoring force. Proper location of the WEC is also important for extracting maximum energy. The horizontal distance between the anchor point and

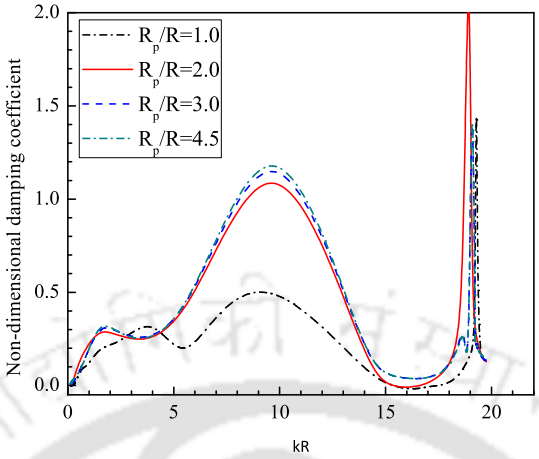

Figure 6.6: Non-dimensional damping coefficient for the upper cylinder for different values of radius of the lower cylinder with $h_1 = 3\ metre, e_1/h_1 = 0.05, e_2/h_1 = 0.25, e_3/h_1 = 0.35, R/h_1 = 0.2$.

structure, water depth, vertical distance from the sea-bed to the lower cylinder, etc. are to be taken into account for designing a suitable wave energy converter.

6.5 Conclusion

We present the radiated potentials in different sub-domains of the fluid due to surge motion of a structure consisting of a pair of coaxial cylinders with the upper one floating and the lower one raised to a finite height above the sea-bed. An eigenfunction approach and separation of variables technique are used to solve this radiation problem governed by Laplace's equation. Non-dimensionalized added mass and damping coefficient are evaluated and the effects of the radii of the cylinders are investigated. The added mass and damping coefficient for the upper cylinder show fluctuations for higher radius ratios in the lower range of wavenumbers. The damping coefficient for the lower cylinder increases as the radius of the upper cylinder increases. We also take into account the interior region in the formulation of the hydrodynamic coefficients and the results are presented through graphs.

Note: In a similar manner, the roll radiation problem can be considered for this configuration in a similar way as was done in Chapter 4.

Chapter 7

Diffraction of water waves by a vertical hollow cylinder in water of infinite depth

7.1 Introduction

Within the framework of linear water wave theory, the diffraction of water waves by a hollow circular cylinder in an infinite ocean depth is considered. Since a single structure also represents a particular form of energy devices and a hollow cylinder alone also captures the most essential feature of an OWC (oscillating water column), we proceed to investigate a single cylinder floating in water and the associated diffraction. The whole fluid domain is divided into two regions: interior and exterior. Using separation of variables technique, Fourier sine transform and Havelock's expansion theorem, the diffracted potentials in each region are obtained, and consequently the exciting forces and its phase angles are evaluated for different draft and different radius of the cylinder. The free surface elevation for both exterior and interior regions is also discussed.

7.2 Mathematical formulation of the problem

We consider a vertical hollow cylinder of radius R and draft e_1 in water of infinite depth. It is to be noted that some part of the cylinder is above the free surface as shown in

Figure 7.1. A right-handed Cartesian coordinate system is defined with $z = 0$ coincident with the centre of the cylinder on the undisturbed free surface, the x-direction pointing in the direction of incoming wave and the z-direction pointing vertically downwards. We follow the same technique of dividing the whole region into two regions as in Chapter 5. Therefore the problem consists of an interior region defined by $r \leq R,\ \ 0 \leq \theta \leq 2\pi,\ \ 0 \leq z < \infty$ and an exterior region defined by $r \geq R,\ \ 0 \leq \theta \leq 2\pi,\ \ 0 \leq z < \infty$. The motion is described by the velocity potential $\Phi(r, \theta, z, t) = Re[\phi(r, \theta, z)e^{-i\omega t}]$ where Re denotes the real part, ω the angular wave frequency and $\phi(r, \theta, z)$ the spatial part of the velocity potential. The incident velocity potential of amplitude A and angular frequency ω propagating along the positive x-direction in deep water is given by (Kim[13])

$$\phi_{inc} = -\frac{igA}{\omega}\ e^{-Kz} \sum_{m=0}^{\infty} \epsilon_m\ J_m(Kr) \cos m\theta, \tag{7.1}$$

where K is the infinite depth wave number defined by $K = \omega^2/g$ and ϵ_m is given by equation (2.3).

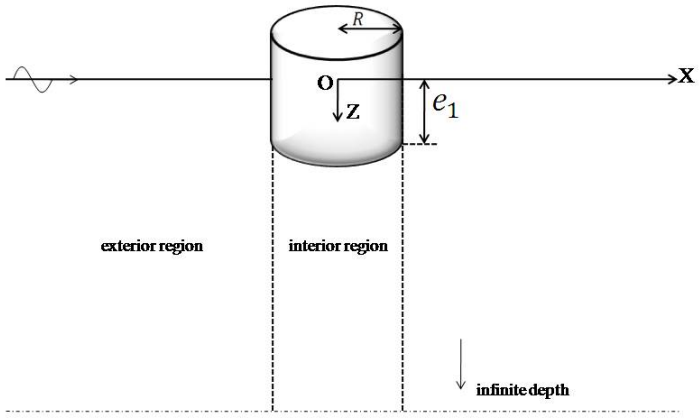

Figure 7.1: Schematic diagram and definition of fluid subdomains.

The governing equation and boundary conditions

The diffracted velocity potential Φ_d can be written as Φ_d=$Re[\phi_d(r, \theta, z)e^{-i\omega t}]$, where the spatial part ϕ_d satisfies the following boundary value problem:

(i) Governing equation:

$$\frac{1}{r}\frac{\partial}{\partial r}\left(r\frac{\partial \phi_d}{\partial r}\right)+\frac{1}{r^2}\frac{\partial^2 \phi_d}{\partial \theta^2}+\frac{\partial^2 \phi_d}{\partial z^2}=0, \quad \text{in the fluid region,} \tag{7.2}$$

(ii) Linearized free surface condition:

$$\frac{\partial \phi_d}{\partial z}+K\phi_d=0, \quad (z=0), \tag{7.3}$$

(iv) Bottom condition:

$$\phi_d,\ |\nabla \phi_d| \to 0, \ \text{ as } \ z\to\infty, \tag{7.4}$$

(v) Radiation condition:

$$\lim_{r\to\infty}\sqrt{r}\left(\frac{\partial \phi_d}{\partial r}-\mathrm{i}K\phi_d\right)=0. \tag{7.5}$$

7.3 Method of solution

The solutions for the boundary value problem are obtained in the exterior and interior regions. Therefore the velocity potential ϕ is decomposed into two potentials defined on $r \le R$ and $r \ge R$, respectively, (Zhu and Mitchell [44]):

$$\phi=\begin{cases}\phi^{int}, & r\le R,\\ \phi^{ext}, & r\ge R,\end{cases} \tag{7.6}$$

where ϕ^{int} and ϕ^{ext} denote the velocity potential in the interior and exterior regions, respectively. For the continuity of the flow, some matching conditions along the interface between the regions are to be considered.

Diffracted potentials

The velocity potential in the exterior region is the sum of the incident and diffracted velocity potentials, i.e, $\phi^{ext}=\phi_{inc}+\phi_d^{ext}$. We apply the method separation of variables and Fourier sine transform to derive the expressions of diffracted velocity potentials. The Fourier sine transform of $\phi(r,z)$ with respect to z is defined by

$$\mathcal{F}_s\{\phi(r,z)\}=\bar{\phi}(r,\xi)=-\int_0^\infty \phi(r,z)\sin\xi z\, dz, \tag{7.7}$$

and its inverse transform by

$$\phi(r,z) = -\frac{2}{\pi}\int_0^\infty \bar{\phi}(r,\xi)\sin\xi z\, d\xi. \tag{7.8}$$

Application of Fourier sine transform to the boundary value problem is justified since the diffracted velocity potential ϕ_d vanishes as $z \to \infty$ (Condition (7.4)). By applying Fourier sine transform, the boundary value problem in $\phi(r,z)$ is transformed to one in $\bar{\phi}(r,\xi)$. Inverting appropriately, we obtain the expressions for the diffracted potentials in interior and exterior regions, based on the result of Manam et al. [17], as

$$\phi^{int} = \sum_{m=0}^{\infty}\left[a_m\frac{J_m(Kr)}{J_m(KR)}e^{-Kz} + \frac{2}{\pi}\int_0^\infty \frac{A_m(\xi)I_m(r\xi)L(\xi,z)\,d\xi}{I_m(\xi R)\,(\xi^2+K^2)}\right]\cos m\theta, \tag{7.9}$$

$$\phi^{ext} = \sum_{m=0}^{\infty}\frac{-gA}{\omega}\epsilon_m i^{m+1}\left[\left(J_m(Kr) + b_m\frac{H_m^{(1)}(Kr)}{H_m^{(1)}(KR)}\right)e^{-Kz} + \frac{2}{\pi}\int_0^\infty \frac{B_m(\xi)K_m(r\xi)L(\xi,z)\,d\xi}{K_m(\xi R)\,(\xi^2+K^2)}\right]\cos m\theta, \tag{7.10}$$

where $L(\xi,z) = \xi\cos\xi z - K\sin\xi z$. Here a_m and b_m are unknown constant coefficients while $A_m(\xi)$ and $B_m(\xi)$ are unknown functions to be determined.

7.3.1 Determination for the unknown coefficients

We introduce the appropriate matching conditions by means of continuity of pressure and velocity potentials along the vertical boundary $r = R$ and also the body surface condition. These conditions are used to find the unknown coefficients. At $r = R$, the conditions which are to be satisfied at physical boundary and interface between the regions are:

$$\frac{\partial\phi^{ext}}{\partial r} = 0, \qquad 0 \le z \le e_1, \tag{7.11}$$

$$\phi^{ext} = \phi^{int}, \qquad e_1 \le z < \infty, \tag{7.12}$$

$$\frac{\partial\phi^{ext}}{\partial r} = \frac{\partial\phi^{int}}{\partial r}, \qquad e_1 \le z < \infty. \tag{7.13}$$

We use the following procedure of Fennigan et al. [8] to derive an analytical expression for exterior and interior velocity potentials. In order to derive expressions for b_m and

$B_m(\xi)$, large draft values of the cylinder are considered, i.e., $e_1 \to \infty$ in the boundary condition (7.11), which corresponds to evaluating the velocity potential in the exterior region for a cylinder of infinite draft. Now from the boundary condition (7.11) and equation (7.10), we have

$$K\left[J'_m(KR) + b_m \frac{H_m^{(1)'}(KR)}{H_m^{(1)}(KR)}\right] e^{-Kz} + \frac{2}{\pi}\int_0^\infty B_m(\xi)\frac{\xi K'_m(\xi R)L(\xi,z)}{K_m(\xi R)(\xi^2+K^2)}d\xi = 0 \quad (7.14)$$

or,

$$b_m \frac{KH_m^{(1)'}(KR)}{H_m^{(1)}(KR)}e^{-Kz} + \frac{2}{\pi}\int_0^\infty B_m(\xi)\frac{\xi K'_m(\xi R)L(\xi,z)}{K_m(\xi R)(\xi^2+K^2)}d\xi = -KJ'_m(KR)e^{-Kz}, \quad (7.15)$$

where $'$ denotes differentiation with respect to r. Note that the Havelock's expansion theorem (Chakrabarti and Sahoo[5], Chakrabarti[6]) states that if

$$g(z) = C_0 e^{-Kz} + \frac{2}{\pi}\int_0^\infty \frac{C(\xi)[\xi\cos(\xi z) - K\sin(\xi z)]d\xi}{\xi^2+K^2}, \qquad 0 < \xi < \infty, \quad (7.16)$$

then,

$$C_0 = 2K\int_0^\infty g(z)e^{-Kz}dz, \quad (7.17)$$

$$C(\xi) = \int_0^\infty g(z)[\xi\cos(\xi z) - K\sin(\xi z)]dz, \quad (7.18)$$

where C_0 and K are constant, and $g(z)$ and its derivative are continuous and integrable in the range $(0,\infty)$.

Utilizing this result, we have from equation (7.15):

$$\frac{b_m\, H_m^{(1)'}(KR)}{H_m^{(1)}(KR)} = -2KJ'_m(KR)\int_0^\infty e^{-2Kz}dz, \quad (7.19)$$

which implies

$$b_m = -J'_m(KR)\frac{H_m^{(1)}(KR)}{H_m^{(1)'}(KR)}, \quad (7.20)$$

and,

$$B_m(\xi) = -\frac{KJ'_m(KR)K_m(\xi R)}{\xi\, K'_m(\xi R)}\int_0^\infty e^{-Kz}(\xi\cos\xi z - K\sin\xi z)dz \quad (7.21)$$

giving $$B_m(\xi) = 0. \tag{7.22}$$

The result (7.22) is due to

$$\int_0^\infty e^{-Kz}(\xi\cos\xi z - K\sin\xi z)dz = 0. \tag{7.23}$$

Now using these values of b_m and $B_m(\xi)$ in equation (7.10) and then applying equation (7.12),

$$\frac{-gA\epsilon_m \mathrm{i}^{m+1}}{\omega}\left[J_m(KR) - J_m'(KR)\frac{H_m^{(1)}(KR)}{H_m^{(1)'}(KR)}\right]e^{-Kz} = a_m e^{-Kz} + \frac{2}{\pi}\int_{e_1}^\infty A_m(\xi)\frac{L(\xi,z)}{\xi^2+K^2}d\xi. \tag{7.24}$$

From the Wronskian of Bessel function

$$J_m(KR)H_m^{(1)'}(KR) - J_m'(KR)H_m^{(1)}(KR) = -\frac{2}{\mathrm{i}\pi KR}. \tag{7.25}$$

Therefore from equation (7.24), we have

$$\frac{2gA\epsilon_m \mathrm{i}^m}{\omega\pi KRH_m^{(1)'}(KR)}\ e^{-Kz} = a_m e^{-Kz} + \frac{2}{\pi}\int_{e_1}^\infty A_m(\xi)\frac{L(\xi,z)}{\xi^2+K^2}d\xi. \tag{7.26}$$

From Havelock's expansion theorem,

$$A_m(\xi) = \frac{2gA\epsilon_m \mathrm{i}^m}{\omega\pi KRH_m^{(1)'}(KR)}\int_{e_1}^\infty e^{-Kz}(\xi\cos(\xi z) - K\sin(\xi z))dz, \tag{7.27}$$

since

$$\int_{e_1}^\infty e^{-Kz}(\xi\cos(\xi z) - K\sin(\xi z))dz = -e^{-Ke_1}\sin(\xi e_1). \tag{7.28}$$

Therefore,

$$A_m(\xi) = \frac{-2gA\epsilon_m \mathrm{i}^m}{\omega\pi KRH_m^{(1)'}(KR)}e^{-Ke_1}\sin(\xi e_1), \tag{7.29}$$

and

$$a_m = \frac{4KgA\epsilon_m \mathrm{i}^m}{\omega\pi KRH_m^{(1)'}(KR)}\int_{e_1}^\infty e^{-2Kz}dz. \tag{7.30}$$

After simplifying and using Wronskian of Bessel function from equation (7.25),

$$a_m = \frac{2\,\epsilon_m\,\mathrm{i}^m\,gA\;\;e^{-2Ke_1}}{\omega\pi KR\,H_m^{(1)'}(KR)}. \tag{7.31}$$

Therefore, from equations (7.9), (7.29) and (7.31), the velocity potential in the interior region is obtained as

$$\phi^{int} = \sum_{m=0}^{\infty} \frac{2\epsilon_m \mathrm{i}^m gAe^{-Ke_1}}{\omega\pi KRH_m^{(1)'}(KR)} \left[\frac{J_m(Kr)e^{-Ke_1}e^{-kz}}{J_m(KR)} - \frac{2}{\pi}\int_0^{\infty} \frac{I_m(r\xi)L(\xi,z)\sin(\xi e_1)\,d\xi}{I_m(\xi R)\,(\xi^2+K^2)}\right] \times \cos m\theta. \tag{7.32}$$

From equations (7.10), (7.20) and (7.22), the velocity potential in the exterior region is obtained as

$$\phi^{ext} = \sum_{m=0}^{\infty} \frac{-gA}{\omega}\epsilon_m \mathrm{i}^{m+1}\left[\left(J_m(Kr) - \frac{J_m'(KR)H_m^{(1)}(Kr)}{H_m^{(1)'}(KR)}\right)e^{-Kz}\right]\cos m\theta. \tag{7.33}$$

7.4 Wave force

The horizontal exciting force F_c acting on the cylinder can be calculated by

$$F_c = \mathrm{i}\rho\omega\int_S (\phi^{ext}(R,\theta,z) - \phi^{int}(R,\theta,z))\;\; n_x ds, \tag{7.34}$$

where S is wetted surface of the cylinder and n_x is the x-component of the unit normal to the surface of the cylinder. As considered in Chapter 2, here also the value of m is taken to be $m = 1$ for evaluating horizontal exciting force.

Therefore the horizontal exciting force F_c from equation (7.34), with the use of the Wronskian of Bessel function from equation (7.25), is given by

$$F_c = \frac{4\rho gA}{KH_1^{(1)'}(KR)}\left[\frac{(1-e^{-Ke_1})}{K} - e^{-Ke_1}\left\{\frac{e^{-Ke_1}(1-e^{-Ke_1})}{K} - \frac{2}{\pi}\int_0^{\infty}\frac{\sin(\xi e_1)(\xi\sin(\xi e_1)+K\cos(\xi e_1)-K)d\xi}{\xi^3+\xi K}\right\}\right]. \tag{7.35}$$

The dimensionless horizontal exciting force F_c/w_2, where $w_2 = \rho g\pi R^2 A$, is given by

$$F_c/w_2 = \frac{4}{\pi R^2 KH_1^{(1)'}(KR)}\left[\frac{(1-e^{-Ke_1})}{K} - e^{-Ke_1}\left\{\frac{e^{-Ke_1}(1-e^{-Ke_1})}{K} - \frac{2}{\pi}\int_0^{\infty}\frac{\sin(\xi e_1)(\xi\sin(\xi e_1)+K\cos(\xi e_1)-K)d\xi}{\xi^3+\xi K}\right\}\right]. \tag{7.36}$$

However, when forces are calculated for a fixed draft and varying radius, the parameter used for nondimensionalizing is taken as $w_3 = \rho g \pi e_1^2 A$.
Free surface elevation in the exterior region is given by

$$\eta = Re\left[\frac{\mathrm{i}\omega}{g}\phi^{ext}e^{-\mathrm{i}\omega t}\right]. \tag{7.37}$$

Therefore the non-dimensional free surface elevation corresponding to $m = 1$, in the exterior region, can be obtained as

$$\eta/A = Re\left[2\mathrm{i}\left(J_1(Kr) - \frac{J_1'(KR)}{H_1^{(1)'}(KR)}H_1^{(1)}(Kr)\right)e^{-\mathrm{i}\omega t}\right]\cos\theta. \tag{7.38}$$

In a similar manner, free surface elevation in the interior region corresponding to $m = 1$ is obtained as

$$\eta/A = Re\left[\frac{-4e^{-Ke_1}}{\pi KRH_1^{(1)'}(KR)}\left(\frac{J_1(Kr)e^{-Ke_1}}{J_1(KR)} - \frac{2}{\pi}\int_0^\infty \frac{I_1(r\xi)L(\xi,z)\sin(\xi e_1)\,d\xi}{I_1(\xi R)\,(\xi^2+K^2)}\right)e^{-\mathrm{i}\omega t}\right]\cos\theta. \tag{7.39}$$

The phase angle of the exciting force F_c/w_p is defined by

$$\theta = \tan^{-1}[Im(F_c/w_p)/Re(F_c/w_p)] \qquad p = 2, 3. \tag{7.40}$$

7.5 Numerical results and discussion

Having obtained the unknown coefficients $a_m, b_m, A_m(\xi)$ and $B_m(\xi)$ appearing in equations (7.9)–(7.10) and consequently in equation (7.34), we proceed to study the horizontal exciting force acting on the cylinder and also the corresponding phase angle and free surface elevation. We investigate various effects of different parameters on the force and wave elevation for this infinite depth problem.

Figure 7.2 shows the non-dimensional horizontal exciting force F_c/w_2 on the cylinder against KR with different values of the draft of the cylinder: to be precise, for $e_1/R = 0.5,\ 1.0,\ 3.0$. It is observed that the exciting force increases within the lower values of wavenumbers as the draft of the cylinder increases and that for higher values of wave

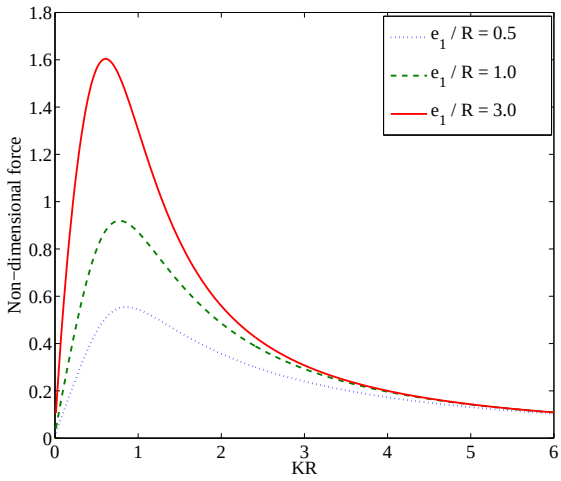

Figure 7.2: Non-dimensional horizontal exciting force (F_c/w_2) versus KR for different values of draft of the cylinder with fixed radius $R = 1.2$ metre.

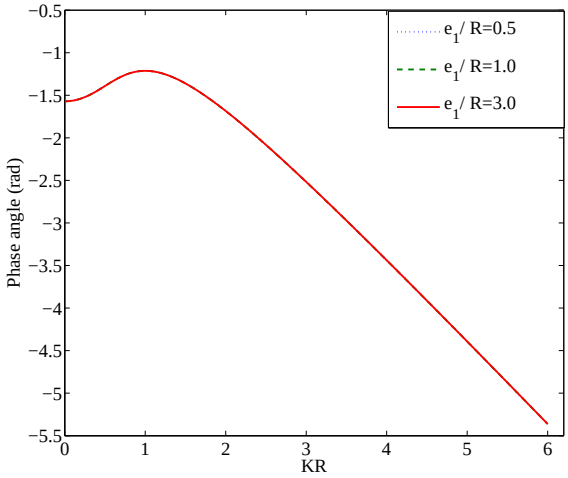

Figure 7.3: Phase angle of the force F_c/w_2, versus wavenumber for different values of draft of the cylinder with fixed radius of the cylinder $R = 1.2$ metre.

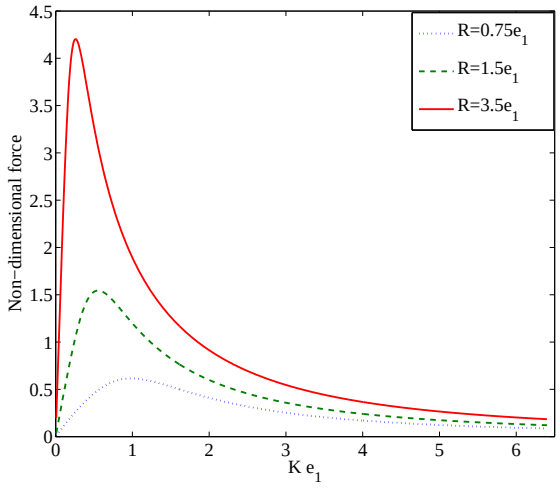

Figure 7.4: Non-dimensional force F_c/w_3, versus wavenumber for different values of the radius of the cylinder with fixed draft $e_1 = 0.8$ metre.

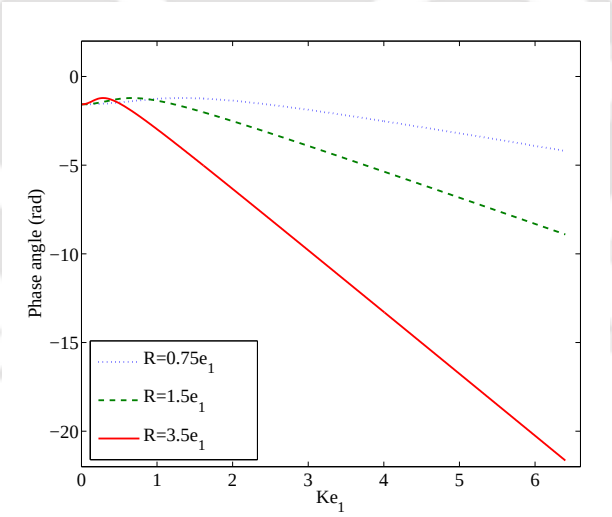

Figure 7.5: Phase angle of the force F_c/w_3, versus wavenumber for different values of the radius of the cylinder with fixed draft $e_1 = 0.8$ metre.

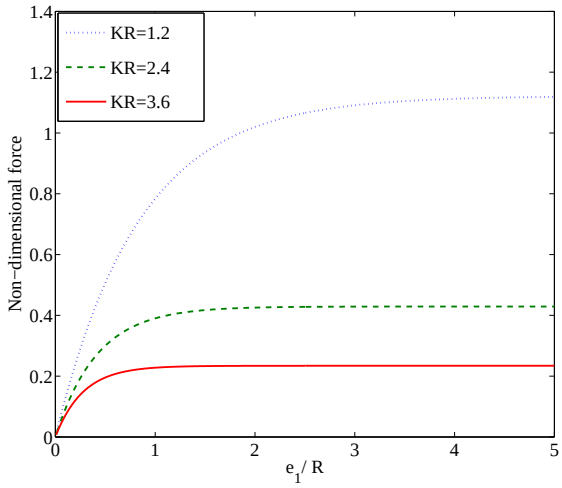

Figure 7.6: Non-dimensional exciting force versus draft of the cylinder for different values of wavenumbers with fixed radius of the cylinder $R = 1.2$ metre.

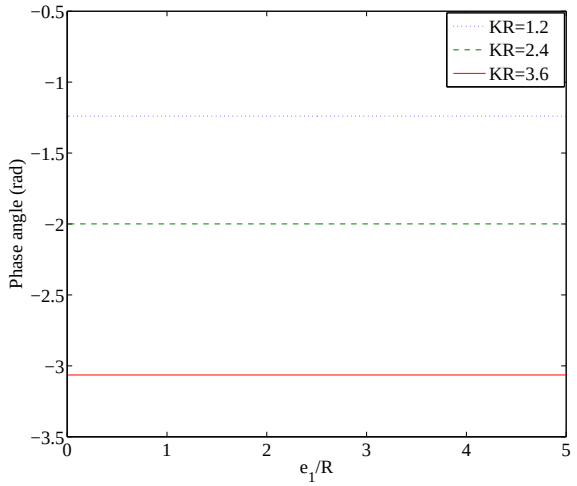

Figure 7.7: Phase angle of the force against e_1/R for different values of wavenumber with fixed $R = 1.2$ metre.

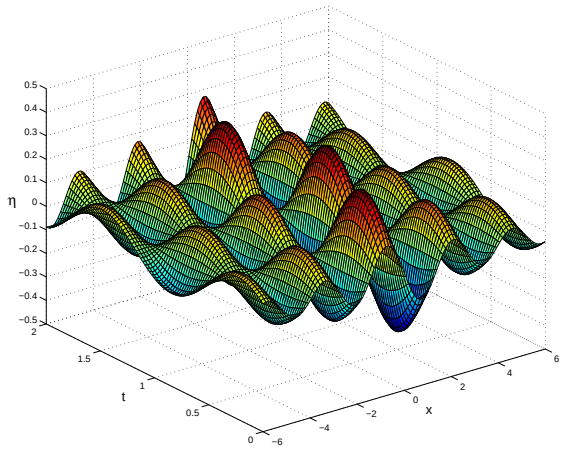

Figure 7.8: Surface plot for elevation in the interior region for different wavenumbers with $R/e_1 = 6.25, e_1 = 0.8\ metre, \theta = 0, m = 1$.

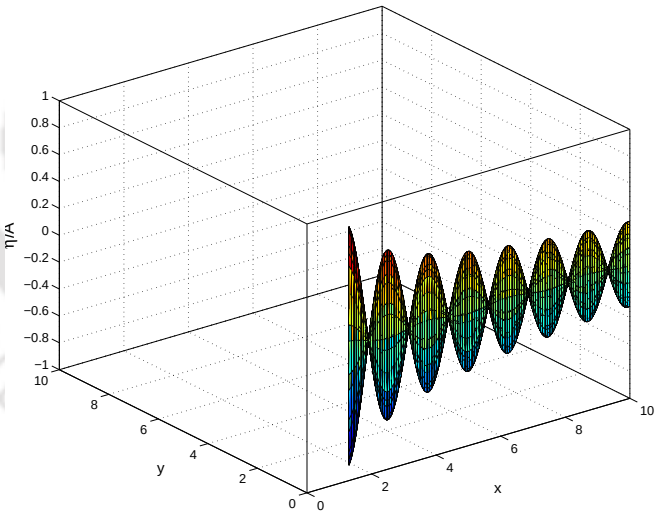

Figure 7.9: Surface plot for wave elevation in exterior region with $m = 1$, $\theta = 0$, $K = 2.5493\ metre^{-1}$.

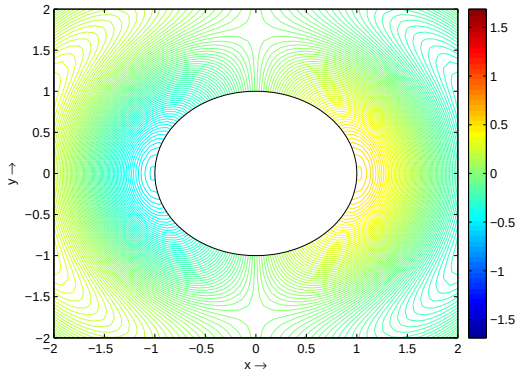

Figure 7.10: Contour plot for wave elevation in exterior region with $R = 1.0$ metre, $K = 2.5493\ metre^{-1}, t = 1.2566s, \theta = 0, m = 1$.

number, the values of the exciting force steadily diminish. Consequently, the peak value occurs for the highest draft value: $e_1/R = 3.0$, to be precise.

Figure 7.3 shows the phase angle of the exciting force F_c/w_2 for different drafts of the cylinder for a fixed radius, $R = 1.2$ metre, corresponding to the exciting force in Figure 7.2. It is observed that, irrespective of the draft values of the cylinder, the phase angle reduces rapidly as wave number increases. Moreover, the phase angle has the same values for all drafts considered. Figures 7.4 and 7.5 show the non-dimensional exciting force F_c/w_3 and its corresponding phase angles against the wavenumber for different values of the radius of the cylinder for a fixed draft $e_1 = 0.8$ metre. In Figure 7.4, it is observed that the exciting force increases as the radius of cylinder increases in the lower range of the wavenumber. For higher range, the force decreases steadily and each force tends to a fixed value later on. For higher radius values, the exciting force attains higher values. Also, as the values of the radius increases, the peak value shifts towards left. Figure 7.5 shows that the absolute value of the phase angle is higher for higher radius value. As the wavenumber increases, the phase angle decreases and there is no appreciable change in the values of the phase angle for very low wavenumbers, i.e., for long waves.

Figures 7.6 and 7.7 show the non-dimensional exciting force F_c/w_2 and its phase angle against the draft of the cylinder for different values of wavenumbers for a fixed

radius $R = 1.2$ metre. It is observed from Figure 7.6 that the exciting force increases as the draft increases and each force attains a constant value for very high draft values. It is also seen that the values of the force are higher corresponding to lower values of wavenumber. It is also interesting to note that the greater variation of increase takes place for smaller values of e_1/R. Further, this increase is much more noticeable for long waves. For shallow water, the change in force is much more significant than those for intermediate and deep water depth. Figure 7.7 shows that the phase angle is constant for each wavenumber. It does not depend on the draft of the cylinder and it is further observed that the absolute value of the phase angle is higher for higher wavenumbers. Figure 7.8 shows the surface plot of wave elevation inside the cylinder for a fixed draft and a fixed radius. Figures 7.9 and 7.11 give us the surface plot and contour plot, respectively, for the free surface elevation in the exterior region.

7.5.1 Comparison with the case of finite depth

In this section we compare the results of exciting forces for the case of infinite depth to the case of finite depth for the single hollow cylinder configuration. In order to compare, we consider the expression of exciting force for finite depth from Chapter 5 for single cylinder case. In this expression, we consider the parameters, higher depth $h_1 = 10$ metres and draft of the cylinder $e_1 = 0.8$ metre as considered in Chapter 5. So Figure 7.11 shows the exciting force with draft $e_1 = 0.8$ metre and depth $h_1 = 10, 20$ metres. From Chapter 5 and Figure 7.11, we observe that as depth increases, the corresponding force is going to converge to the force in the infinite depth case.

7.6 Conclusion

The diffraction problem of water waves by a semi-submerged hollow cylinder is formulated and solved to analyze wave motion/force in water of infinite depth under the assumptions of linearized theory of water waves. The whole fluid domain is divided into two regions: interior and exterior ones. We derive the expressions for the diffracted potentials in each region by using the method of separation of variables and Fourier sine

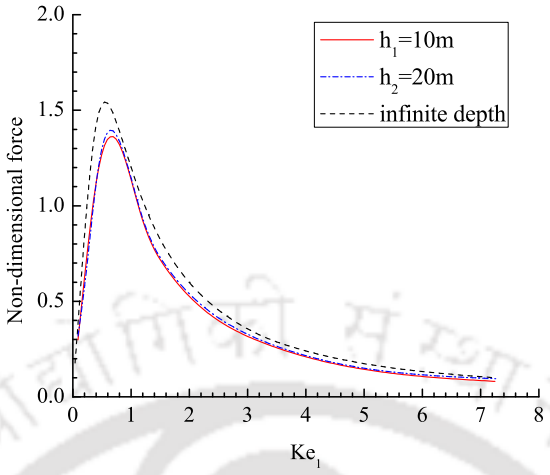

Figure 7.11: Comparison of exciting forces with finite depth and infinite depth cases with $R = 1.2$ metre, $e_1 = 0.8$ metre.

transform. In order to determine the unknown coefficients, which are present in the expressions of diffracted potentials, Havelock's expansion theorem and matching conditions along the virtual boundary are utilized. The hydrodynamic influences of various parameters on exciting force, its phase angles and free surface elevation are discussed. With regard to the effect of the draft of the cylinder, it is observed that the exciting force increases as the draft of the cylinder increases and the peak value occurs only for the lower values of wavenumbers. The same observation is noticed for various values of the radius of the cylinder for a fixed draft. With regard to the phase angle of the exciting force, we observe that the phase angle decreases as the wavenumber increases for a fixed radius. We also graphically present the free surface elevation in the interior and exterior regions. It is observed that, in the exterior region, as the distance from the surface of the cylinder increases, the amplitude of the oscillation decreases. We also compare the present case of single cylinder in infinite depth with previously obtained result for finite depth in Chapter 5. The comparison suggests that as depth increases, the corresponding force is going to converge to the force in the infinite depth case.

Chapter 8

Surge radiation of water waves by a vertical hollow cylinder in water of infinite depth

8.1 Introduction

From the point of view of radiation, a circular cylinder is considered to be the most efficient structure used in ocean engineering applications. For this floating structure, the moving bodies may act as wave-makers in all of the motion modes in deep water. In this chapter, we take up the radiation problem for the hollow cylinder in infinite depth for the same setup as in Chapter 7, and consider the surge motion. We use the similar method of solution as in Chapter 7 to derive radiated potentials in both interior and exterior regions. The added mass, damping coefficient and phase angle are evaluated for various parameters.

8.2 Mathematical formulation of the problem

We consider the same geometry and formulation as in Chapter 7.

The governing equation and boundary conditions

For the small motion due to the surge mode of the structure considered here, if the amplitude of the oscillation is denoted by ζ, the radiated velocity potential $\phi_{rad,1}$ can be expressed as (from equation (1.19))

$$\phi_{rad,1}(r,\theta,z) = -\mathrm{i}\omega\zeta\varphi_{rad,1}(r,z)\cos\theta, \tag{8.1}$$

where $\varphi_{rad,1}$ denotes the spatial part of the radiated velocity potential which satisfies the following governing equation and boundary conditions. Using equation (8.1) in equation (2.1), we obtain

$$\frac{1}{r}\frac{\partial\varphi_{rad,1}}{\partial r} + \frac{\partial^2\varphi_{rad,1}}{\partial r^2} + \frac{\partial^2\varphi_{rad,1}}{\partial z^2} - \frac{\varphi_{rad,1}}{r^2} = 0, \qquad \text{in the fluid region,} \tag{8.2}$$

$$\frac{\partial\varphi_{rad,1}}{\partial z} + K\varphi_{rad,1} = 0, \quad (z=0), \tag{8.3}$$

$$\frac{\partial\varphi_{rad,1}}{\partial r} = 1, \quad (0<z<e_1,\ r=R), \tag{8.4}$$

$$\varphi_{rad,1},\ |\nabla\varphi_{rad,1}| \to 0, \quad \text{as} \quad z\to\infty, \tag{8.5}$$

$$\lim_{r\to\infty}\sqrt{r}\left(\frac{\partial\varphi_{rad,1}}{\partial r} - \mathrm{i}K\varphi_{rad,1}\right) = 0. \tag{8.6}$$

8.3 Method of solution

The solutions for the boundary value problems are obtained in the exterior and interior regions. Therefore the velocity potential $\varphi_{rad,1}$ is decomposed into two potentials defined on $r \le R$ and $r \ge R$, respectively:

$$\varphi_{rad,1} = \begin{cases} \varphi^{int}_{rad,1}, & r \le R, \\ \varphi^{ext}_{rad,1}, & r \ge R, \end{cases} \tag{8.7}$$

where $\varphi^{int}_{rad,1}$ and $\varphi^{ext}_{rad,1}$ denote the velocity potentials in the interior and exterior regions, respectively. For the continuity of the flow, some matching conditions along the interface between the regions are to be considered.

Radiated potentials

By applying the same method of solution as in Chapter 7, we obtain the expressions for the radiated potentials in the interior and exterior regions as

$$\varphi^{int}_{rad,1} = a_1 \frac{J_1(Kr)}{J_1(KR)} e^{-Kz} + \frac{2}{\pi} \int_0^\infty \frac{A_1(\xi) I_1(r\xi) L(\xi, z)\, d\xi}{I_1(\xi R)\,(\xi^2 + K^2)}, \tag{8.8}$$

$$\varphi^{ext}_{rad,1} = b_1 \frac{H^{(1)}_1(Kr)}{H^{(1)}_1(KR)} e^{-Kz} + \frac{2}{\pi} \int_0^\infty \frac{B_1(\xi) K_1(r\xi) L(\xi, z)\, d\xi}{K_1(\xi R)\,(\xi^2 + K^2)}, \tag{8.9}$$

where $L(\xi, z) = \xi \cos \xi z - K \sin \xi z$. Here a_1 and b_1 are unknown constant coefficients while $A_1(\xi)$ and $B_1(\xi)$ are unknown functions to be determined.

8.3.1 Determination of the unknown coefficients

We introduce the appropriate matching conditions by means of continuity of pressure and velocity potentials along the vertical boundary $r = R$ and also the body surface condition. At $r = R$, the conditions which are to be satisfied at physical boundary and interface between the regions are:

$$\frac{\partial \varphi^{ext}_{rad,1}}{\partial r} = 1, \qquad (0 \le z \le e_1), \tag{8.10}$$

$$\varphi^{ext}_{rad,1} = \varphi^{int}_{rad,1}, \qquad (e_1 \le z < \infty), \tag{8.11}$$

$$\frac{\partial \varphi^{ext}_{rad,1}}{\partial r} = \frac{\partial \varphi^{int}_{rad,1}}{\partial r} \qquad (e_1 \le z < \infty). \tag{8.12}$$

We employ the procedure followed in Chapter 7 to derive an analytical expression for the exterior and interior velocity potentials. Now from the boundary condition (8.10) and equation (8.9), we have

$$b_1 K \frac{H^{(1)'}_1(KR)}{H^{(1)}_1(KR)} e^{-Kz} + \frac{2}{\pi} \int_0^\infty B_1(\xi) \frac{\xi K'_1(\xi R) L(\xi, z)}{K_1(\xi R)(\xi^2 + K^2)} d\xi = 1, \tag{8.13}$$

where $'$ denotes differentiation with respect to r. Using Havelock's expansion theorem, we get the following from equation (8.13):

$$\frac{b_1 K\ H^{(1)'}_1(KR)}{H^{(1)}_1(KR)} = 2K \int_0^\infty e^{-Kz} dz, \tag{8.14}$$

which implies

$$b_1 = \frac{2H_1^{(1)}(KR)}{KH_1^{(1)'}(KR)}, \tag{8.15}$$

and the choice of $B_1(\xi) = 0$ has been made to remove the Dirac delta function from the exterior velocity potential. Now using these values of b_1 and $B_1(\xi)$ in equation (8.9) and then applying it to equation (8.11), we obtain

$$a_1 e^{-Kz} + \frac{2}{\pi}\int_{e_1}^{\infty} \frac{A_1(\xi)L(\xi,z)\,d\xi}{(\xi^2+K^2)} = \frac{2H_1^{(1)}(KR)}{KH_1^{(1)'}(KR)} e^{-Kz}. \tag{8.16}$$

From Havelock's expansion theorem

$$a_1 = \frac{2H_1^{(1)}(KR)}{KH_1^{(1)'}(KR)} e^{-2Ke_1}, \tag{8.17}$$

and

$$A_1(\xi) = \frac{2H_1^{(1)}(KR)}{KH_1^{(1)'}(KR)} \int_{e_1}^{\infty} e^{-Kz}(\xi\cos(\xi z) - K\sin(\xi z))dz, \tag{8.18}$$

since

$$\int_{e_1}^{\infty} e^{-Kz}(\xi\cos(\xi z) - K\sin(\xi z))dz = -e^{-Ke_1}\sin(\xi e_1). \tag{8.19}$$

Therefore,

$$A_1(\xi) = \frac{-2H_1^{(1)}(KR)}{KH_1^{(1)'}(KR)e^{-Ke_1}} \sin(\xi e_1). \tag{8.20}$$

Hence, from equations (8.8), (8.17) and (8.20), the velocity potential in the interior region is obtained as

$$\varphi_{rad,1}^{int} = \frac{2H_1^{(1)}(KR)J_1(Kr)e^{-2Ke_1}e^{-Kz}}{KH_1^{(1)'}(KR)J_1(KR)} - \frac{4H_1^{(1)}(KR)e^{-Ke_1}}{\pi KH_1^{(1)'}(KR)} \int_0^{\infty} \frac{I_1(r\xi)L(\xi,z)\sin(\xi e_1)d\xi}{I_1(\xi R)(\xi^2+K^2)}. \tag{8.21}$$

From equations (8.9) and (8.15), the velocity potential in the exterior region is obtained as

$$\varphi_{rad,1}^{ext} = \frac{2H_1^{(1)}(Kr)}{KH_1^{(1)'}(KR)} e^{-Kz}. \tag{8.22}$$

8.4 Hydrodynamic coefficients

Following the similar procedure adopted in Chapter 6, the radiated force on the body due to surge motion in horizontal direction in the interior region can be written as (from equation (1.21))

$$F_{11} = -\rho\,\zeta\,\omega^2 \int_S \varphi^{int}_{rad,1}(R,z)\cos\theta\; n_x ds, \tag{8.23}$$

and the expressions of added mass and damping coefficient for the surge motion of the radiated cylinder in the interior region is given by

$$\mu_{11} + \mathrm{i}\frac{\lambda_{11}}{\omega} = -\rho \int_S \varphi^{int}_{rad,1}(R,z)\cos\theta\; n_x\; ds. \tag{8.24}$$

Using the expression of $\varphi^{int}_{rad,1}$ from equation (8.21) and then simplifying, we get

$$\mu_{11} + \mathrm{i}\frac{\lambda_{11}}{\omega} = \frac{-2\rho\pi a H_1^{(1)}(KR)}{K H_1^{(1)'}(KR)} \left[\frac{e^{-2Ke_1}(1-e^{Ke_1})}{K} - \frac{2e^{-Ke_1}}{\pi}\int_0^\infty \frac{\sin(\xi e_1)(\xi\sin(\xi e_1) + K\cos(\xi e_1) - K)d\xi}{\xi^3 + \xi K^2}\right]. \tag{8.25}$$

The added mass is non-dimensionalized by dividing it by the mass of the water displaced by a semi-immersed sphere with radius R, amounting to $\frac{2}{3}\pi\rho R^3$, and the damping coefficient is non-dimensionalized by dividing it by the same factor but multiplied by the angular frequency ω. Thus the non-dimensionalized added mass $\overline{\mu_{11}}$ and damping coefficient $\overline{\lambda_{11}}$ are given by

$$\overline{\mu_{11}} + \mathrm{i}\overline{\lambda_{11}} = \frac{-3H_1^{(1)}(KR)}{KR^2 H_1^{(1)'}(KR)} \left[\frac{e^{-2Ke_1}(1-e^{Ke_1})}{K} - \frac{2e^{-Ke_1}}{\pi}\int_0^\infty \frac{\sin(\xi e_1)(\xi\sin(\xi e_1) + K\cos(\xi e_1) - K)d\xi}{\xi^3 + \xi K^2}\right]. \tag{8.26}$$

Similarly the non-dimensionalized added mass and damping coefficients in the exterior region are given by

$$\overline{\mu'_{11}} + \mathrm{i}\overline{\lambda'_{11}} = \frac{-3H_1^{(1)}(KR)(1-e^{-Ke_1})}{R^2K^2 H_1^{(1)'}(KR)}. \tag{8.27}$$

The expression of the non-dimensionalized radiated force in the interior region from equation (8.23), after simplification, is given by

$$F_{11} = \frac{-2H_1^{(1)}(KR)}{KR^2H_1^{(1)'}(KR)}\left[\frac{e^{-2Ke_1}(1-e^{-Ke_1})}{K} - \frac{2e^{-Ke_1}}{\pi}\int_0^\infty \frac{\sin(\xi e_1)(\xi\sin(\xi e_1)+K\cos(\xi e_1)-K)d\xi}{(\xi^3+\xi K^2)}\right]. \tag{8.28}$$

8.5 Numerical results and discussion

Having obtained the unknown coefficients $a_1, b_1, A_1(\xi)$ and $B_1(\xi)$ appearing in equations (8.8)–(8.9), we proceed to study the hydrodynamic coefficients, namely added mass and damping coefficient, of the cylinder and the phase angle . We investigate the various effects of different parameters on the hydrodynamic coefficients for this infinite depth problem. Non-dimensional added mass for the interior region is plotted against KR for various values of draft in Figure 8.1. It is observed that in the lower frequency range, higher draft values give rise to higher values of added mass. Further, added mass values, irrespective of the drafts values, are remarkable only in the lower frequency range and they ultimately vanish. The non-dimensional damping coefficient plotted against KR for different draft values, as shown in Figure 8.2, has somewhat different patterns. It begins from zero and is evident only between $KR = 0.2$ to $KR = 3.0$ in which higher draft values give rise to higher values of damping coefficient. Beyond $KR = 3.0$, the values decrease and ultimately all converge to the same value. It is also noticed that the peak values of the coefficient, for all draft values, occur almost at the same value of KR. Figures 8.3 and 8.4, respectively, show the non-dimensional added mass and damping coefficient against wavenumbers in the exterior region with different values of draft. We observe the same patterns as in Figures 8.1 and 8.2, but it is noticed that the values of added mass and damping coefficient in the interior region are greater than the values of added mass and damping coefficient in the exterior region.

In Figure 8.5, we plot added mass against the draft of the cylinder for various wavenumbers. It is clear that the values are higher for lower wavenumbers. Further, as the draft increases, the added mass also increases and after some value of e_1/R, there

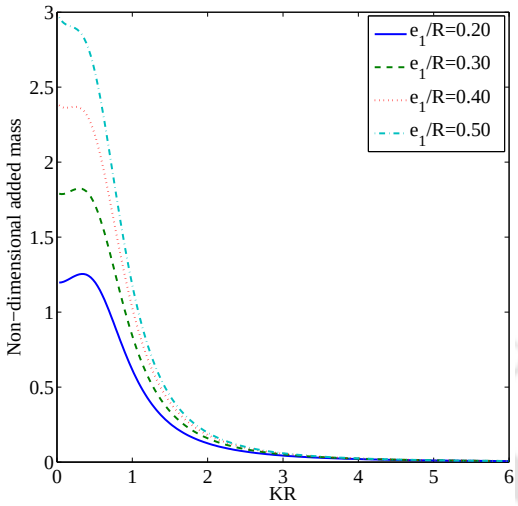

Figure 8.1: Non-dimensional added mass versus KR for different values of draft of the cylinder with fixed radius $R = 3.0$ metre in interior region.

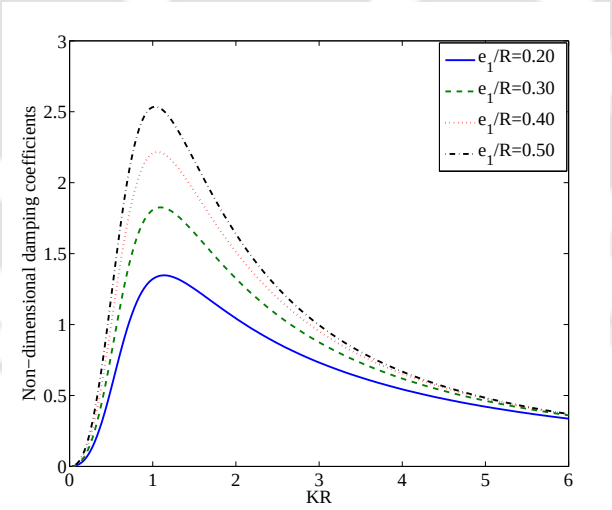

Figure 8.2: Non-dimensional damping coefficient versus KR for different values of draft of the cylinder with fixed radius $R = 3.0$ metre in interior region.

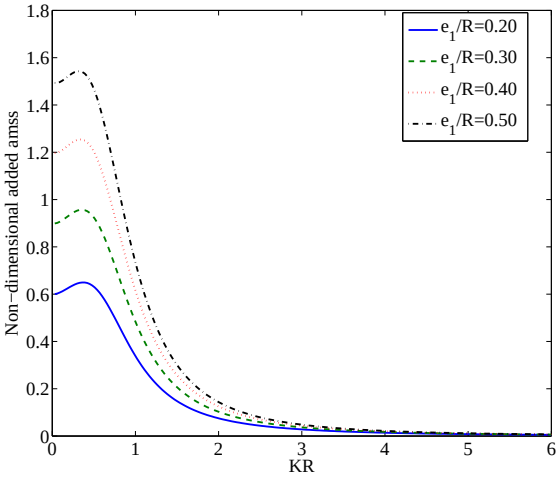

Figure 8.3: Non-dimensional added mass versus KR for different values of draft of the cylinder with fixed radius $R = 3.0$ metre in exterior region.

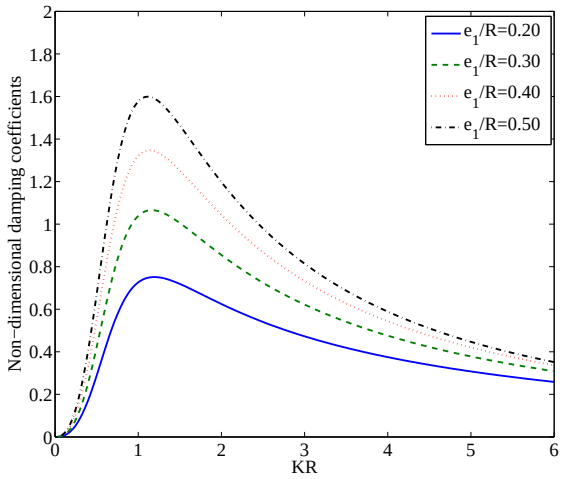

Figure 8.4: Non-dimensional damping coefficient versus KR for different values of draft of the cylinder with fixed radius $R = 3.0$ metre in exterior region.

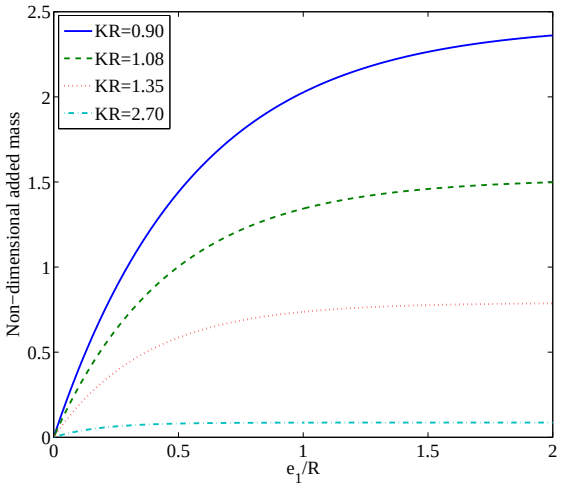

Figure 8.5: Non-dimensional added mass versus draft for different values of wave numbers with fixed radius $R = 3.0$ metre in interior region.

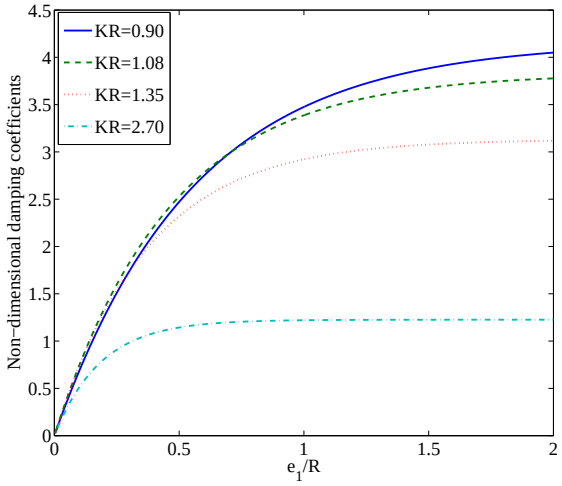

Figure 8.6: Non-dimensional damping coefficient versus draft for different values of wave numbers with fixed radius $R = 3.0$ metre in interior region.

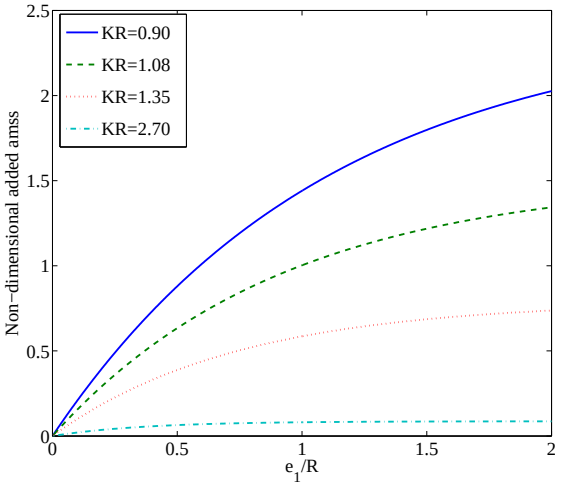

Figure 8.7: Non-dimensional added mass versus draft for different values of wave numbers with fixed radius $R = 3.0$ metre in exterior region.

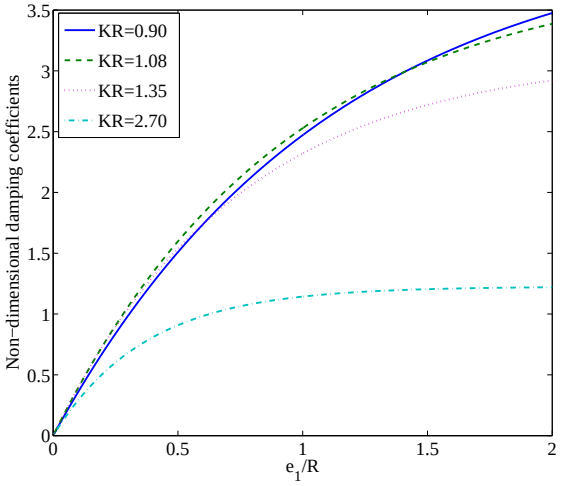

Figure 8.8: Non-dimensional damping coefficient versus draft for different values of wave numbers with fixed radius $R = 3.0$ metre in exterior region.

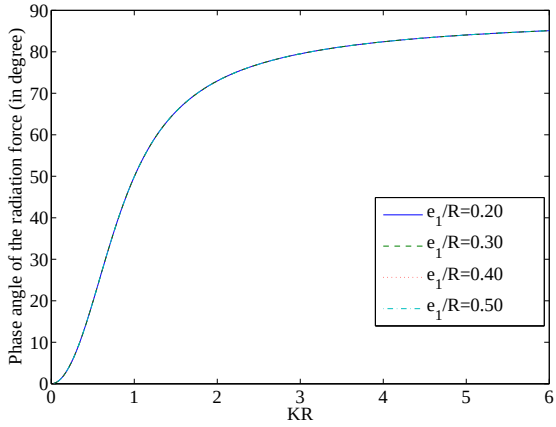

Figure 8.9: Phase angle of non-dimensional radiation force versus wavenumbers in interior region with different drafts for $R = 3\ metre$.

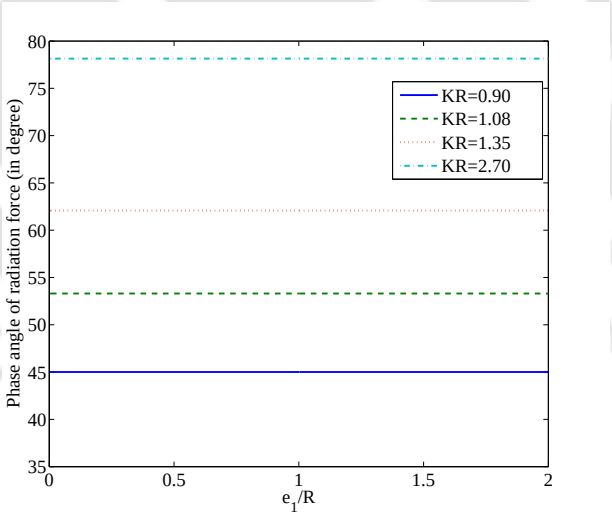

Figure 8.10: Phase angle of non-dimensional radiation force versus drafts in interior region with different wavenumbers for $R = 3\ metre$.

is no change in the added mass values. Figure 8.6 shows that non-dimensional damping coefficient against the draft of the cylinder for the same parameters as in Figure 8.5. Here, the same observation is made as in Figure 8.5 but with the values of the damping coefficient slightly greater than the corresponding values of the added mass. Non-dimensional added mass and damping coefficient are plotted in Figures 8.7 and 8.8, respectively, against the draft of the cylinder in the exterior region with different values of the wavenumbers. We note the same observation as in Figures 8.5 and 8.6. Phase angles are plotted in Figure 8.9 against KR for various values of draft of the cylinder in the interior region. Phase angle begins from zero and increases as the wavenumber increase and tends to the same value for higher wavenumbers. The phase angle does not change even if the draft value is changed for all values of the wavenumbers. Similar observation is made for the exterior region also. In Figure 8.10, where the phase angles are plotted against draft for various wavenumbers in the interior region, we observe that the phase angle does not change for a fixed value of the wavenumber. Also, lower wavenumber gives rise to the lower values of the phase angle.

8.6 Conclusion

The radiation problem of water waves by a semi-submerged hollow cylinder is formulated and solved to analyze the surge motion in water of infinite depth under the assumptions of linearized theory of water waves. The whole fluid domain is divided into two regions: interior and exterior. We derive the expressions for the radiated potentials in each region by using the method of separation of variables and Fourier sine transform. In order to determine the unknown coefficients, which are present in the expressions of radiated potentials, Havelock's expansion theorem and matching conditions along the virtual boundary are utilized. Considering only the surge motion, we derive the corresponding added mass and damping coefficient. These hydrodynamic coefficients are examined for varying drafts and wavenumbers. The added mass is remarkable at low frequencies while the damping coefficient attains higher values in the middle range of frequencies. For fixed wavenumbers, the hydrodynamic coefficient attains higher values for higher

drafts. Phase angle does not change even if draft values are changed in both the exterior and interior regions. Also, the phase angle does not change at all for a fixed value of wavenumber.

Chapter 9

Summary and future work

This chapter is completely devoted to a brief summary of the results highlighting the contributions made by this thesis and also of the techniques used in deriving these. It also provides information for the scope of possible extensions of the present work and future investigations in related problems.

9.1 Summary of the results

In this thesis diffraction and radiation of a train of small amplitude harmonic water waves by two coaxial vertical cylinders is investigated by using linear water wave theory. A brief survey and the preliminaries relevant to our work are given in Chapter 1.

In Chapter 2, using the matched eigenfunction expansion and separation of variables techniques, we solve the diffraction problem of two coaxial vertical cylinders, with the upper one a hollow cylinder and the lower one a solid cylinder, in water of finite depth. The exciting force due to the diffraction problem are derived for both the cylinders. Sets of exciting forces are plotted for different radii of the cylinders and for different gaps between the cylinders. We observe that the higher values of the exciting force occur at lower frequencies of the wave for different values of the radius of lower cylinder. The force diminishes quickly at higher frequencies. If the gap between the cylinders is reduced, then the exciting force increases. While evaluating horizontal force for the lower cylinder, we observe that for reduced values of the radius of the upper cylinder,

the exciting force increases. The force values are remarkable at low frequencies.

Chapter 3 is concerned with the natural extension of the previous work (Chapter 2) for the radiation problem for the same structure. We consider only the surge motion of a floating hollow cylinder placed above a fixed coaxial bottom-mounted cylinder. Using the same methods as in Chapter 2, the analytical expressions for the corresponding radiated potentials in clearly identified regions are obtained. Sets of values of added mass and damping coefficient are obtained for different radii of the fixed cylinder and for different gaps between the cylinders (i.e., also for different drafts of the floating cylinder) for the same fixed radii of the cylinders. We also compute the coefficients due to different gaps between the cylinders with the radii of both taken to be different. The added mass is steady and almost positive at lower frequencies for any gap and for any value of the radius of the lower cylinder. But it exhibits a peculiar behaviour near the non-dimensionalized frequency $\omega\sqrt{(R/g)} = 4.35$. This can be attributed to the resonance situation (Mavrakos [22]; Newman [26]). The added mass exhibits very high values, both positive and negative, in the neighbourhood of the resonant frequency irrespective of the radius ratio. The values of damping coefficient increase when the gap between the cylinders decreases. Here also resonance situation occurs at $\omega\sqrt{(R/g)} = 4.35$ for different radius ratios and for different gaps of the cylinders.

Earlier Miloh [25] and Mavrakos [22] solved the radiation problem by considering a floating solar pond and a floating bottomless cylindrical body, respectively, in water of finite depth. In order to compare the present work with available results presented by other investigators, e.g., Miloh [25], we consider the particular case of a hollow cylinder floating over an even sea bottom with the height of the bottom-mounted cylinder zero, i.e., without the coaxial cylindrical caisson underneath. By solving the boundary value problem of this particular case, the results that are obtained in this case are reasonable to be compared with the work of Miloh [25]. Good agreement is observed from this comparison. This confirms that our model is valid and hence can be employed effectively to investigate various issues related to radiation problems for structures under consideration. A numerical verification is also carried out for the body boundary condition satisfied at the boundary of both the cylinders.

In Chapter 4, the same physical problem as in Chapter 3 is solved for the roll motion of a floating hollow cylinder placed above a fixed coaxial bottom-mounted cylinder. Subsequently we obtain the expressions of added mass and damping coefficient for the structure. This work presents a parametric study of the added mass and damping coefficient on the proposed structure. The added mass is higher at lower frequencies for any value of the radius of the lower cylinder and for any gap between the cylinders. Fluctuations are observed for higher radius ratios ($R_p/R > 2$) in the lower frequency range. The damping coefficient attains higher values only at relatively lower frequencies and diminish steadily as frequency increases. The values of added mass and damping coefficient increase as the gap between the cylinders decreases.

Chapter 5 is concerned with the system consisting of a hollow cylinder floating vertically on the free surface above an immersed solid cylinder. The immersed circular cylinder of greater radius is placed at some finite height above an impermeable horizontal sea-bed. This chapter deals with the diffraction of water waves by this novel coaxial cylinder-circular plate arrangement. By using the similar method as in Chapter 2, we present the exciting force acting on both the cylinders for different radii of the cylinders and for different gaps between the cylinders. Similarly we find the expression of exciting force on the lower cylinder also. We observe fluctuations for higher radius ratios. It is also observed that the fluctuations, in the event of their occurrence, occur only at lower frequencies. We observe that as the gap decreases, the value of the exciting force increases. For higher values of frequency, the force steadily diminishes. The values of the exciting force are significant mainly at lower frequencies. The results that are obtained in this chapter are compared with those of Wu et al. [37] as both the problems bear similarities to a large extent. By considering the particular case that there is no plate arrangement below the floating hollow cylinder, i.e., the case having only the floating cylinder tethered to the sea-bed, comparison of forces for both arrangements is carried out.

Chapter 6 is concerned with the natural extension of the previous work (Chapter 5) for the radiation problem with the same proposed structure. The floating coaxial cylinders are forced to independently oscillate in small surge motion only. By using

the similar method as in Chapter 3, we solve the boundary value problem for the surge motion for both the cylinders and present the expressions of added mass and damping coefficient. We study the hydrodynamic influences of the various parameters on the added mass and damping coefficient for both the cylinders. The added mass and damping coefficient for the upper cylinder show fluctuations for higher radius ratios in the lower range of wavenumbers. We observe that the higher values of the coefficients occur for higher radius ratios within the lower range of wavenumbers. In addition to this, it is also important to analyze how the structure will be moored. Therefore this chapter includes a brief discussion about mooring system. The important observation is that slack chain lines mooring system may be used to moor the structure to the anchor point on the bottom because slack chain lines rely on their weight to provide the necessary horizontal restoring force.

A hollow cylinder alone also captures the most essential feature of an OWC (oscillating water column) which can convert ocean wave energy to electricity. Therefore we consider a hollow cylindrical structure in infinite depth and carry out similar investigation in the next two chapters. Chapter 7 is concerned with the investigation of the diffraction of a train of small amplitude harmonic water waves by a semi submerged hollow cylindrical body in an infinite water depth. Using separation of variables technique, Fourier sine transform and Havelock's expansion theorem, the diffracted potentials in each region are obtained, and consequently the exciting force and its phase angle are evaluated for different draft values and different radius of the cylinder. The free surface elevation for both exterior and interior regions is also discussed. With regard to the effect of the draft of the cylinder, it is observed that the exciting force increases as the draft of the cylinder increases and the peak value occurs only for the lower values of wave numbers. The phase angle of exciting force decreases as the wavenumber increases for a fixed radius.

Chapter 8 is the extension of the physical problem of Chapter 7 for the radiation problem, i.e., we consider the surge radiation of water waves by a semi-submerged hollow circular cylinder in an infinite depth. By applying the same method as in Chapter 7, we evaluate the added mass and damping coefficient, and phase angles of radiated force

for different wavenumbers and different drafts of the cylinder. We observe that mostly the added mass is significant only at lower frequencies while the damping coefficient attains higher values in the middle range of frequencies. For fixed wavenumbers, the hydrodynamic coefficients attain higher values for higher drafts.

This problem of diffraction and radiation by the structure considered in our thesis can be considered as a wave energy device. The energy that is created and transferred by this device finds its use in a number of practical applications. By this system of energy device, the power of ocean waves can be converted to electrical energy. Proper positioning of the device will allow the device to capture waves as large as possible. This type of energy converter assumes immense significance for offshore structures also. The results that are obtained are expected to provide some useful information to the designer/engineer of such devices and also to find an appropriate position for the device so as to extract maximum energy. Taking into consideration the behaviour of the hydrodynamic coefficients under different conditions, our solutions are likely to be helpful in squeezing the maximum benefit out of a properly designed device.

9.2 Scope for future work

We now present some informal observations pertaining to the possible extensions of our results to different problems. We briefly outline some interesting problems which can be taken up in future. Therefore, the possible extensions of this type of problems with the double-cylinder structure can be to:

1. the problems of diffraction and radiation of the same structure in a two-layer fluid: each of the cylinders will be assumed to be located in one of the layers only.

2. the problems of diffraction and radiation by a composite cylinder consisting of a hollow cylinder and a solid cylinder in water of finite depth.

3. the problems of diffraction and radiation of water waves by considering the cylinders as porous.

The possible extension of the problems pertaining to single-cylinder structure can be as follows:

1. We observe that not much work has been carried out regarding diffraction and radiation by a hollow cylinder in a channel of constant width. It can be attempted to solve this problem for a finite depth with channel walls, say, at $y = \pm d$. For some of the channel problems, one can adopt some other method, such as Green's function technique or multipole expansion method.

2. The radiation problem of water waves by considering roll motion of the structure in an infinite water depth.

3. The radiation problem by a single hollow cylinder by assuming some air pressure inside the hollow cylinder while assuming the water region outside the cylinder to be pressure-free.

While carrying out our work, we observe that all the problems that we considered may be extended to the diffraction-radiation problem for the nonlinear case or to take into account the variation of bottom topography. Either of these new directions requires considerable effort.

Bibliography

[1] Abramowitz, M. and Stegun, I. A. *Handbook of Mathematical Functions*, Dover Publicatons, New York, USA (1965).

[2] Berggren, L. and Johansson, M. *Hydrodynamic coefficients of a wave energy device consisting of a buoy and a submerged plate*, Appl. Ocean Res., **14** (1992), 51-58.

[3] Bhatta, D. D. and Rahman, M. *On the scattering and radiation problem for a cylinder in water of finite depth*, Int. J. Eng. Sc., **41** (2003), 931-967.

[4] Bhattacharjee, J. and Soares, C. G. *Wave interaction with a floating rectangular box near a vertical wall with step type bottom topography*, J. Hydrodyn. Ser. B, **22**(5) (2010), 91-96.

[5] Chakrabarti, A. and Sahoo, T. *On the incoming water waves against a vertical cliff*, Proc. Indian Acad. Sci. (Math. Sci.), **107**(1) (1997), 89-93.

[6] Chakrabarti, A. *On the solution of the problem of scattering of surface-water waves by the edge of an ice cover*, Proc. R. Soc. Lond. A, **456** (2000), 1087-1099.

[7] Dong, M., Miao, G., Fan, J. and Zhu, R. *Semi analytical solution for radiation of a hollow sphere with an opening hole in finite depth*, J. Marine Sci. and Tech., **20**(1) (2012), 82-88.

[8] Finnegan, W., Meere, M. and Goggins, J. *The wave excitation forces on a truncated vertical cylinder in water of infinite depth*, J. Fluid Struct., **40** (2013), 201-213.

[9] Garrett, C. J. R. *Bottomless harbours*, J. Fluid Mech., **43**(3) (1970), 433-449.

[10] Garrett, C. J. R. *Wave forces on circular dock*, J. Fluid Mech., **46** (1971), 129-139.

[11] Havelock, T. *Waves due to floating sphere making periodic heaving oscillation*, Proc. R. Soc. Lond. A, **231** (1955), 1-7.

[12] Karmakar, D. and Sahoo, T. *Scattering of waves by articulated floating elastic plates in water of infinite depth*, Mar. Struct., **18** (2005), 451-471.

[13] Kim, C. H. *Nonlinear Waves and Offshore Structures, Advanced Series on Ocean Engineering*, World Scientific Publishing Co. Pvt. Ltd., Singapore (2008).

[14] Lee, J. F. *On the heave radiation of a rectangular structure*, Ocean Eng., **22**(1) (1995), 19-34.

[15] Lovas, S., Mei, C. C. and Liu, Y. *Oscillating water column at a coastal corner for wave power extraction*, Appl. Ocean Res., **32** (2010), 267-283.

[16] MacCamy, R. C. and Fuchs, R. A. *Wave forces on piles: a diffraction theory*, US Army Beach Erosion Board, Tech. Memo, No. 69 (1954), 17 pages.

[17] Manam, S. R., Bhattacharjee, J. and Sahoo, T. *Expansion formulae in wave structure interaction problems*, Proc. R. Soc. Lond. A, **462** (2006), 263-287.

[18] Mandal, B. N. and Chakrabarti, A. *A generalisation to the hybrid Fourier transform and its application*, Appl. Math. Letters, **16** (2003), 703-708.

[19] Martins-Rivas, H. and Mei, C. C. *Wave power extraction from an oscillating water column along a straight coast*, Ocean Eng., **36** (2009), 426-433.

[20] McIver, P. and Evans D. V. *The occurrence of negative added mass in free-surface problems involving submerged oscillating bodies*, J. Eng. Math., **18** (1984), 7-22.

[21] Mavrakos, S. A. *Wave loads on a stationary floating bottomless cylindrical body with finite wall thickness*, Appl. Ocean Res., **7**(4) (1985), 213-224.

[22] Mavrakos, S. A. *Hydrodynamic coefficients for a thick-walled bottomless cylindrical body floating in water of finite depth*, Ocean Eng., **15**(3) (1988), 213-229.

[23] Mavrakos, S. A. *Hydrodynamic coefficients in heave of two concentric surface-piercing truncated circular cylinders*, Appl. Ocean Res., **26** (2004), 84-97.

[24] Mavrakos, S. A. *Hydrodynamic characteristics of floating toroidal bodies*, Ocean Eng. **24**(4) (1997), 381-399.

[25] Miloh, T. *Wave loads on a floating solar pond.* Proc. Int. Workshop on Ship and Platform Motions, Dept of Nav. Arch. and Offshore Eng., Berkeley (USA) (1983), 110-128.

[26] Newman, J. N. *Radiation and diffraction analysis of the McIver toroid*, J. Eng. Math., **35** (1999), 135-147.

[27] Newman, J. N. *Marine Hydrodynamics*, MIT Press, Cambridge, Massachussetts, USA (1977).

[28] Rahman, M. and Bhatta, D. D. *Second order wave forces on a pair of cylinders*, Can. Appl. Math. Q., **1**(3) (1993), 343-382.

[29] Rahman, M. and Bhatta, D. D. *Evaluation of added mass and damping coefficient of an oscillating circular cylinder,* Appl. Math. Model., **17** (1993), 70-79.

[30] Rahman, M. *Water Waves: Relating Modern Theory to Advanced Engineering Applications,* Clarendon Press, Oxford, UK (1995).

[31] Sahoo, T. *On the generation of water waves by cylindrical porous wave-maker*, Acta Mech., **126** (1998), 231-239.

[32] Shen Y. M., Zhang, Y. H. and You, Y. G. *On the radiation and diffraction of linear water waves by a rectangular structure over a sill. Part I. Infinite domain of finite water depth,* Ocean Eng., **32** (2005), 1073-1097.

[33] Siddorn, P. and Taylor, R. E. *Diffraction and independent radiation by an array of floating cylinders,* Ocean Eng., **35** (2008), 1289-1303.

[34] Sabuncu, T. and Calisal, S. *Hydrodynamic coefficients for vertical circular cylinders at finite depth*, Ocean Eng., **8** (1981), 25-63.

[35] Ursell, F. *On the heaving motion of a circular cylinder on the surface of a fluid*, Q. J. Mech. and Appl. Math., **2**(2) (1949), 218-231.

[36] Vicente, P. C., Falcão, A. F. O. and Justino, P. A. P. *Optimization of mooring configuration parameters of floating wave energy converters*, Proc. of the ASME 30th Int. Conference on Ocean, Offshore and Arctic Eng. (OMAE 2011), June 19-24, 2011, Rotterdam, The Netherlands, 7 pages.

[37] Wu, B. J., Zhang, Y. H., You, Y. G, Sun, X. Y. and Chen, Y. *On diffraction and radiation problem for a cylinder over a caisson in water of finite depth*, Int. J. Eng. Sci., **42** (2004), 1193-1213.

[38] Wu, B. J., Zhang, Y. H., You, Y. G, Jie, D. S. and Chen, Y. *On diffraction and radiation problem for two cylinders in water of finite depth*, Ocean Eng., **33** (2006), 679-704.

[39] Yeung, R. W. *Added mass and damping of a vertical cylinder in finite-depth water*, Appl. Ocean Res., **3**(3) (1981), 119-133.

[40] Zhang, Y. H., Shen, Y. M., You, Y. G, Wu, B. J. and Rong, L. *Hydrodynamic properties of two vertical truncated cylinders in waves*, Ocean Eng., **32** (2005), 241-271.

[41] Zheng, Y. H., Shen, Y. M., You, Y. G., Wu, B. J. and Rong, L. *Scattering of linear water waves by a fixed and infinitely long rectangular structure parallel to a vertical wall in oblique seas,* J. Waterw. Port Coast. Ocean Eng., **132**(2) (2006), 106-113.

[42] Zheng, Y. H., Shen, Y. M. and Tang, J. *Radiation and diffraction of linear water waves by an infinitely long submerged rectangular structure parallel to a vertical wall*, Ocean Eng., **34** (2007), 69-82.

[43] Zhou, H. W., Wu, G. X. and Zhang, H. S. *Wave radiation and diffraction by a two-dimensional floating rectangular body with an opening in its bottom*, J. Eng. Math., **83** (2013), 1-22.

[44] Zhu, S. P. and Mitchell, L. *Diffraction of ocean waves around a hollow cylindrical shell structure*, Wave Motion, **46** (2009), 78-88.

The following are the outcomes of the work carried out in this thesis.

List of Published/Accepted/Communicated Papers

1. **M. Hassan** and S. N. Bora, Exciting forces for a pair of coaxial hollow cylinder and bottom-mounted cylinder in water of finite depth, *Ocean Engineering*, 50, (2012): 38-43, (DOI:10.1016/j.oceaneng.2012.05.013).

2. **M. Hassan** and S. N. Bora, Exciting forces for a wave energy device consisting of a pair of coaxial cylinders in water of finite depth, *Journal of Marine Science and Application*, 12, (2013): 315-324, (DOI: 10.1007/s11804-013-1207-9).

3. **M. Hassan** and S. N. Bora, Rotational motion due to the interaction of water waves with a pair of coaxial cylinders in water of finite depth, *Journal of Advanced Research in Applied Mathematics*, 6(1), (2014): 48-65, (DOI: 10.5373/jaram.1682.012713).

4. **M. Hassan** and S. N. Bora, Hydrodynamic coefficients for a radiating hollow cylinder placed above a coaxial cylinder at finite ocean depth, **In Press: Accepted on July** 5, 2014**,** *Journal of Marine Science and Technology,* doi: 10.1007/s00773-014-0280-3.

5. **M. Hassan** and S. N. Bora, Diffraction of water waves by a finite circular hollow cylinder in water of infinite depth, Communicated to *International Journal of Applied Mechanics*.

6. **M. Hassan** and S. N. Bora, Surge motion coefficients of a finite circular hollow cylinder radiating in water of infinite depth, Accepted on Sept 15, 2014 in *International Journal of Fluid Mechanics Research*.

7. **M. Hassan** and S. N. Bora, Surge hydrodynamic coefficients by a pair of two coaxial vertical cylinders in water of finite depth, Accepted on June 20, 2014 in *Development and Applications of Oceanic Engineering*.